Track-based Alignment of a CMS Tracker Endcap

von

Daniel Sprenger

Diplomarbeit in Physik

vorgelegt der

Fakultät für Mathematik, Informatik und Naturwissenschaften

der RWTH Aachen University

im Juli 2008

angefertigt im

I. Physikalischen Institut B

Prof. Dr. Lutz Feld

Abstract

This year, 2008, a new hadron accelerator, the Large Hadron Collider (LHC), is being finalised at the European Organization for Nuclear Research (CERN). It will be important for studies of new physics and the current standard model. The Compact Muon Solenoid (CMS), an experiment at the LHC, is a multi purpose detector designed to allow a large variety of high-energy physics studies. The central CMS tracking device consists entirely of silicon detectors and is made up of a barrel part and two endcaps.
In total, the CMS tracker consists of more than 15 000 detector modules. Due to limited mounting accuracy, these are expected to be spread around their ideal positions on the support structure. For track reconstruction and momentum measurement of charged particles, it is necessary to know the actual deviations of sensor position and orientation as precisely as possible. Therefore, hardware alignment systems and track-based alignment are used to determine an alignment – the current module positions and orientations – of the tracker. For track-based alignment, tracks of charged particles, for example cosmic muons, are used to estimate an alignment by minimising the χ^2 of all available tracks as a function of module positions and orientations.
This work presents studies of track-based alignment for the CMS tracker endcap TEC+, that was integrated at RWTH Aachen University. The goal of this work is to determine and validate an alignment of this endcap.
First, an overview of the LHC and the CMS experiment with focus on the tracker is given in Chapter 1. Then, track-based alignment and an alignment algorithm based on a Kalman Filter are discussed in Chapter 2.
During two periods, data of particle tracks crossing the TEC+ were recorded. During the endcap integration, data were taken with all sensors active, and after integration of the entire CMS tracker, tracks were recorded with about 25% of TEC+ being active. Chapter 3 describes the experimental setup for both data-taking periods. After that, the data processing procedure and the implementation of the Kalman Filter Alignment Algorithm are detailed in Chapter 4. For each data set, an alignment is calculated at the level of the largest endcap substructures, the TEC+ discs, as well as at the level of the next smaller substructures, the TEC+ petals. The results are discussed in Chapters 5 and 6.
Chapter 7 contains interpretation of the results described in the previous chapters including studies to validate them. Here, comparisons to optical survey measurements of the TEC+ and results of the Laser Alignment System are made and good agreement is found. A comparison to an alignment determined by another alignment algorithm is made to prove the correct functionality of the used algorithm. The tracker temperature has been varied during the data taking after tracker integration. The agreement of alignments determined using data sets at different temperatures

indicates a good stability of the TEC+ with respect to temperature. Comparing the results of the endcap integration data (Aachen) with that of the tracker integration data (CERN), the TEC+ is found to be mechanically stable considering the tilting, the transport from Aachen to Geneva, the integration into the tracker, and several thermal cycles which took place between the two data-taking periods.

Contents

Title **i**

Abstract **iii**

1 Introduction **1**
1.1 Large Hadron Collider . . . 1
1.2 Compact Muon Solenoid . . . 2
1.2.1 Coordinate System . . . 3
1.2.2 Muon Systems . . . 4
1.2.3 Hadronic Calorimeter . . . 5
1.2.4 Electromagnetic Calorimeter . . . 6
1.2.5 Tracker . . . 7
CMS tracker endcap . . . 8
Laser Alignment System . . . 9
1.2.6 Trigger . . . 11

2 Track-based Alignment **13**
2.1 Motivation . . . 13
2.2 Alignment Algorithms . . . 13
2.2.1 Kalman Alignment Algorithm . . . 14
2.2.2 MillePede . . . 15
2.3 Weak Modes . . . 17
2.4 Sensitivity to Torsion . . . 17
2.5 Selection of Coordinate System . . . 18

3 Data Taking **21**
3.1 Sector Tests . . . 21
3.1.1 Experimental setup . . . 21
3.2 Tracker Slice Test . . . 22
3.2.1 Experimental setup . . . 23

4 Data Processing **25**
4.1 Calibration and Detection of Sensor Defects . . . 25
4.2 Estimation of Track Parameters . . . 27
4.2.1 Clustering . . . 28
4.2.2 Track seeding and reconstruction . . . 29
4.2.3 Saving track and alignment information . . . 29
4.3 Alignment Algorithm Implementation . . . 30
4.3.1 Deterministic Annealing . . . 31

4.3.2 Outlier rejection 31

5 Sector Test Data **33**
5.1 Data Characteristics 33
5.2 Disc Alignment 33
5.2.1 Alignment in ϕ 34
5.2.2 Alignment in x, y, ϕ 34
5.2.3 Alignment in x, y, z, ϕ 35
5.3 Petal Alignment 36
5.3.1 Alignment in ϕ 38
5.3.2 Alignment in x, y, ϕ 38

6 Slice Test Data **43**
6.1 Data Characteristics 43
6.2 Disc Alignment 43
6.2.1 Temperature dependence 44
6.2.2 Alignment in ϕ 45
6.3 Petal Alignment 46
6.3.1 Alignment in ϕ 46

7 Result Interpretation and Comparison **49**
7.1 Comparison of Sector and Slice Test Results 49
7.2 Sensitivity to torsion 50
7.3 Comparison to Laser Alignment System Results 52
7.3.1 Sector test disc alignment 52
7.3.2 Sector test petal alignment 53
7.3.3 Slice test disc alignment 54
7.4 Comparison to Survey Measurements 56
7.4.1 Sector test disc alignment 56
7.5 Comparison to MillePede Results 56
7.5.1 Slice test disc alignment 57

8 Summary **59**

A Results from Petal Alignment with Sector Test Data **61**

B Configuration files **71**

Bibliography **79**

1. Introduction

In the following, an overview on the Large Hadron Collider, the currently most powerful particle accelerator, and one of its experiments, the CMS detector, is given with a focus on the CMS tracker and especially the tracker endcaps.

1.1 Large Hadron Collider

The Large Hadron Collider (LHC) is a synchrotron at the European Organization for Nuclear Research (CERN), designed to create proton-proton collisions at a centre of mass energy of 14 TeV as well as heavy ion collisions. It is located in a 27 km long tunnel about 100 m below the border of France and Switzerland north west of Geneva.
There are four experiments located at the beam interaction points of the LHC (Fig. 1.1): ATLAS and CMS are multi-purpose detectors, designed for a broad programme of physics studies. The ALICE experiment will investigate heavy ion collisions, and LHCb concentrates on studying b quark physics.

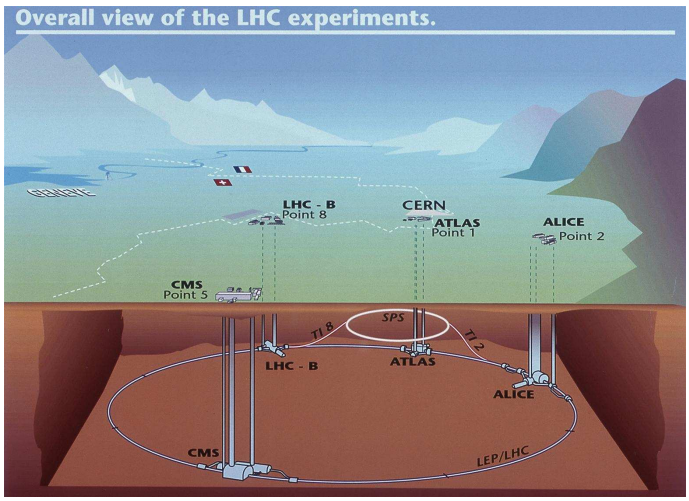


Figure 1.1: Overview on the Large Hadron Collider and its experiments.

With a centre of mass energy of 14 TeV, the LHC will supersede the Tevatron, which is a proton-antiproton synchrotron at Fermilab near Chicaco with a centre of mass energy of 1.96 TeV, as the most sophisticated particle accelerator. The design luminosity of the LHC is $10^{34}\,\mathrm{cm}^{-2}\mathrm{s}^{-1}$.

At the LHC, the validity of the Standard Model at an energy scale of 1 Tev as well as a broad programme of theories about new physics will be investigated. A prime goal is the elucidation of the nature of electroweak symmetry breaking, for which the Higgs mechanism is assumed to be responsible. Due to the significantly increased centre of mass energy at the LHC, the cross section for Higgs production is multiple magnitudes higher than it is at the Tevatron. Figure 1.2 gives an overview of cross sections and event rates for Higgs production and various other processes at the LHC as well as the Tevatron.

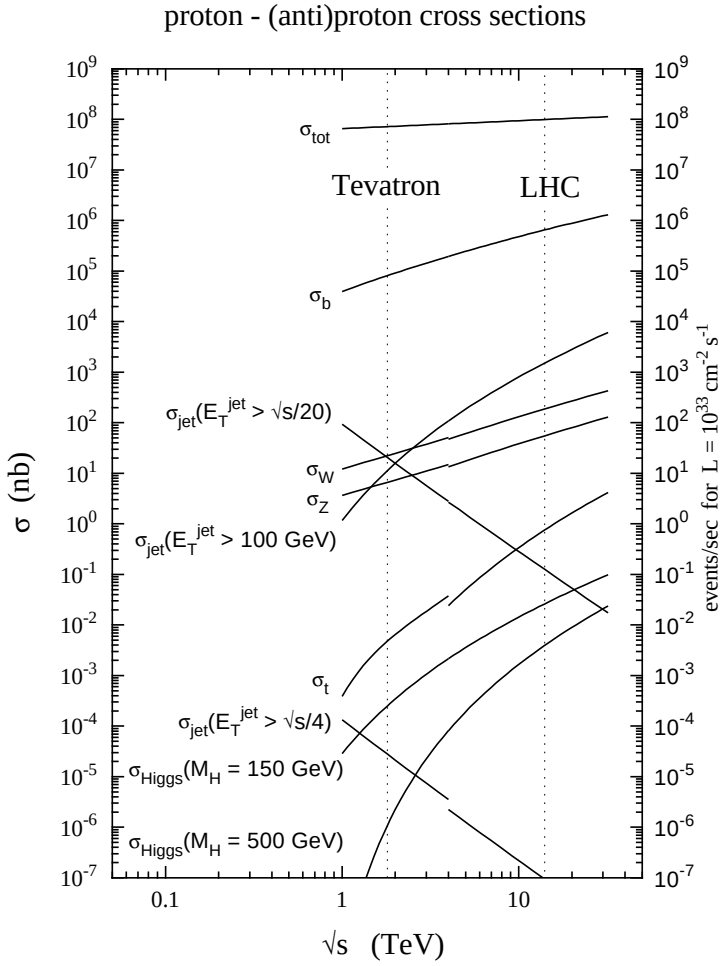


Figure 1.2: Cross sections for various processes at the LHC and the Tevatron.

1.2 Compact Muon Solenoid

The Compact Muon Solenoid (CMS) is a multi-purpose detector at the LHC. A detailed description of CMS and all of its subdetectors is given in [1].

The CMS detector consists of multiple layers of subdetectors arranged in a barrel region and two endcaps (Fig. 1.3). The innermost detector is a pixel detector necessary for determining starting vertices of charged particles. The tracks of these particles are precisely measured inside the next layer, the silicon strip tracker. Particle energies are measured with the electromagnetic and the hadronic calorimeters which represent the next two detector layers. Both calorimeters are placed inside the superconducting solenoid coil, which creates an almost homogeneous magnetic field of 4 T over a cylindrical volume of 6 m diameter and 12.5 m length. The outermost detector layers consist of four muon stations interlaced in the iron flux return yokes.

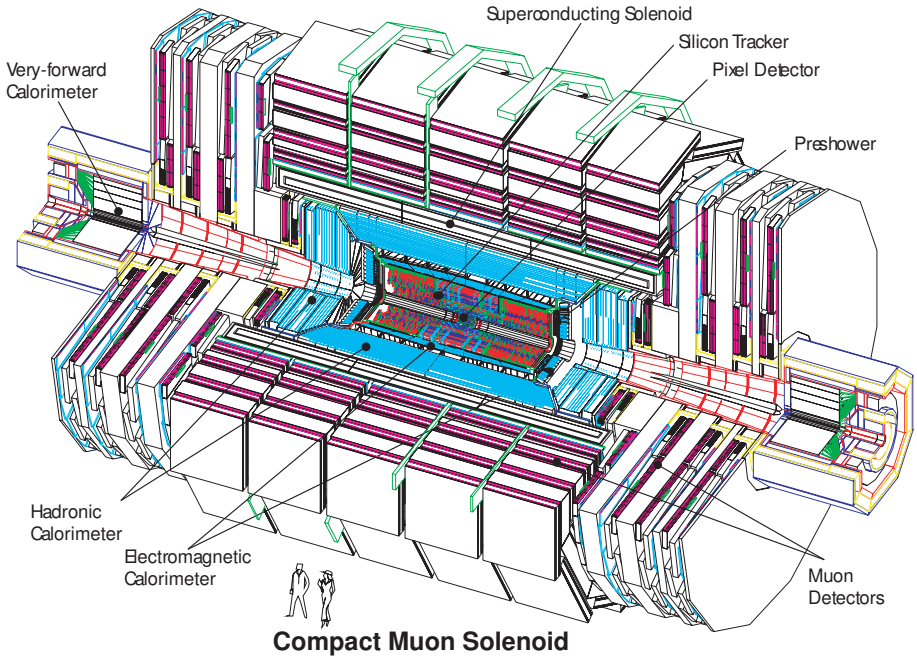


Figure 1.3: The CMS detector [1].

1.2.1 Coordinate System

To avoid confusing conventions regarding the coordinate system, CMS has agreed on the following coordinate definitions: The y-axis points upwards, the x-axis points radially to the centre of the LHC ring, and the z-axis points in direction of the beam line, completing a right-handed coordinate system. The azimuthal angle ϕ describes the angle to the x-axis in the x-y-plane, and hence rotations around the z-axis, and the polar angle θ the angle to the z-axis.
The polar angle can also be specified by the pseudo-rapidity η, which is defined as

$$\eta = -\ln\left(\tan\frac{\theta}{2}\right).$$

The pseudo-rapidity is positive at the plus side ($\theta < \frac{\pi}{2}$).

Apart from the global coordinate system, local coordinates are used to describe displacements and rotations of individual sensor modules. Here, positions are given by u, v, and w and rotation are specified by α, β, and γ. For silicon strip modules, the v-axis always points in direction of the silicon strips, away from the readout

electronics, and the w-axis in direction of the silicon sensor surface normal. The u-axis lies in the sensor plane, perpendicular to the silicon strips, creating a right-handed coordinate system. The angles α, β, and γ describe right-handed rotations around the u, v, and w-axis, respectively (Fig. 1.4).

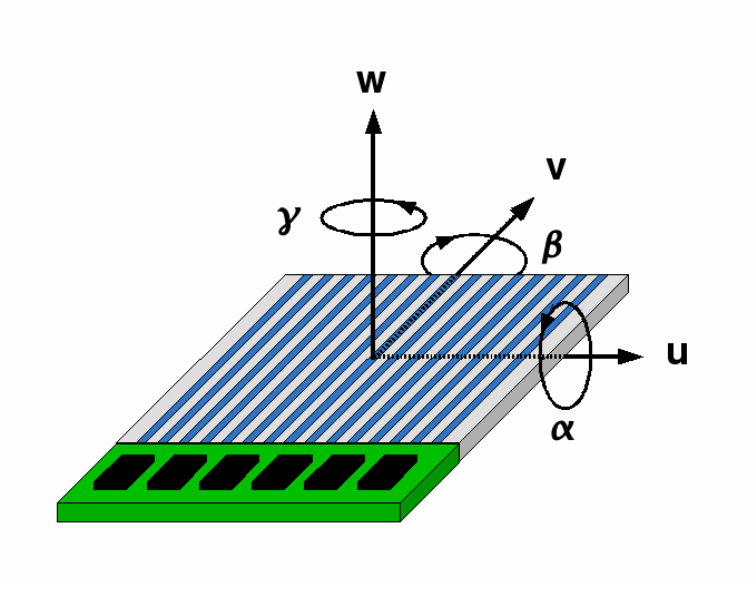


Figure 1.4: Positions and rotations in the local coordinate system of a silicon strip module.

1.2.2 Muon Systems

The purpose of the muon systems [2] is the identification, triggering, and momentum measurement of muons. An acceptance of nearly 100% is demanded to ensure the hermeticity of the detector. Therefore, the system is designed with high redundancy by complementing high precision muon detectors with sensors dedicated for fast muon triggering.

In the barrel part of the CMS muon detector, a lower magnetic field and also lower occupancy is expected. Here, four stations of aluminium drift tubes (DT) are used for precision measurements, covering the range of $|\eta| < 1.3$. The stations consists of 250 DT chambers, which are 2.5 m long. There are 12 layers of drift tubes inside each chamber, four of them measuring the z coordinates of crossing muons, while the others are sensitive in ϕ direction. The $r\phi$ precision of a single DT layer is about 250 μm providing a total accuracy of about 100 μm per chamber.

Cathode strip chambers (CSC), which allow precision measurements in space and time in the presence of a high and varying magnetic field, are used in the endcaps and cover the region between $|\eta| = 0.9$ and $|\eta| = 2.4$. These chambers have a faster response time, which is needed due to higher muon rates in these parts of the detector. Separated by iron discs of the flux return yoke, there are four CSC stations consisting of trapezodial shaped chambers arranged in concentric rings in each endcap. The chambers contain six layers of wires between cathode strip panels. Non-muon background is rejected and detected muons are matched with tracks in the CMS tracker by a robust pattern recognition.

The CSCs are designed to fit the accuracy requirements of 75 μm in the innermost and 150 μm in the remaining stations. In total, the endcaps are made up of 540 CSC chambers with about 1000 readout channels each.

In addition to the precision measurement muon detectors, resistive plate chambers (RPC) are integrated both into the barrels and endcaps of the CMS detector, covering a range of $|\eta| < 2.1$. There are six RPC layers in the barrel region and four layers in each endcap. The RPCs are dedicated muon trigger detectors, which allow unambiguous assignment of a detected muon to a bunch crossing, with a very fast response time of about 3 ns. An RPC consists of parallel plates of phenolic resin, which is coated with a conductive graphite paint, with a distance of about 3 mm to each other. The sensors are readout by aluminium strips outside the resin plates.
Due to high segmentation, the RPCs can measure the transverse momentum p_T at trigger time with an accuracy of about 50 GeV.

The total momentum resolution of the muon systems can be described as

$$\frac{\delta p}{p} = 4\% \cdot \sqrt{p/TeV} \tag{1.1}$$

for muons with p greater than 70 GeV.

To monitor positions and deformations of the muon chambers, an optical alignment system is installed. It can also determine the position of the tracker in relation to the muon systems. The precision of this alignment system is comparable to the resolution of the muon chambers.

1.2.3 Hadronic Calorimeter

CMS has a hadronic sampling calorimeter [1, 3], consisting of brass and stainless steel absorbers and plastic scintillators. Its dynamic energy range of 5 MeV to 3 TeV allows the observation of single muons as well as the measurement of the highest possible particle energies.
The hadronic calorimeter is arranged in a central calorimeter, which covers the range of $|\eta| < 3$, containing the Hadronic Barrel (HB), the Hadronic Endcaps (HE), and the Outer Hadronic calorimeter (HO), complemented by the forward and backward calorimeters (HF) in the range of $3 < |\eta| < 5$.

The HB is divided into two half barrels, each containing 18 identical wedges. The wedges are made of absorber plates, complemented by 17 layers of plastic scintillators. The innermost and outermost absorber plates consist of stainless steel for stability reasons, the others are made of brass to maximise the hadronic interaction length. Due to its location inside the magnet coil, the thickness of the HB is restricted to 100 cm. The granularity of the scintillators in the barrel part is $\Delta\eta \times \Delta\phi = 0.087 \times 0.087$.
Each of the Hadronic Endcaps consists of absorber plates and scintillators arranged in 10 °-sectors. There are 18 absorber layers of 80 mm thickness, each. As in the barrel part, the innermost and outermost layer is made of stainless steel, while the others consist of brass. The scintillator granularity is the same as in the barrel part, except for the highest η-regions. Here, the granularity matches that of the electromagnetic calorimeter (see below).

The HO is placed outside the solenoid, enveloping the first iron absorber layer of the muon system. It contains one sampling layer in the endcap region, two layers in the barrel region and an additional layer in the range of $|\eta| < 0.4$. The Outer Hadronic Calorimeter is essential for the full containment of hadron showers.
The total absorber thickness of the hadronic calorimeter corresponds in the barrel to 5.15 hadronic interaction lengths λ at $\eta = 0$ up to $9.1\,\lambda$ at $\eta = 1.3$ and averages at about $10.5\,\lambda$ in the endcap regions.

The HF calorimeters, positioned at a distance of about 11 m from the interaction point, are needed for identification and reconstruction of very forward jets. Due to the high radiation field in this region, quarz fibres were chosen as active material, which emit Cherenkov light, detected by photodiodes. The fibres are placed between 5 mm thick steel absorber plates with a total thickness of 10 hadronic interaction lengths λ.

During test beam studies, the energy resolution of the CMS calorimeter system (including the electromagnetic calorimeter) for hadrons in the energy range $30\,\text{GeV} < E < 1\,\text{TeV}$ was found to be

$$\left(\frac{\sigma_E}{E}\right)^2 = \left(\frac{100\%}{\sqrt{E}}\right)^2 + (4.5\%)^2 \qquad (E \text{ in GeV}). \tag{1.2}$$

1.2.4 Electromagnetic Calorimeter

The electromagnetic calorimeter [4] is a high-resolution, high-granularity detector made of lead tungstate ($PbWO_4$) crystals. Lead tungstate is a fast scintillator providing a small Molière radius and short radiation length.

Precision energy measurements are possible for tracks with $|\eta| < 2.6$, but the geometrical crystal coverage extends up to $|\eta| = 3.0$. The front face area of $22 \times 22\,\text{mm}^2$ matches the Molière radius of lead tungstate (21.9 mm). This area corresponds to a granularity of $\Delta\eta \times \Delta\phi = 0.0175 \times 0.0175$ in the barrel region and 0.0175×0.0175 up to 0.05×0.05 in the endcaps.
The crystals in the barrel section are 23 cm thick, which corresponds to 26 radiation lengths. In the endcap region, 22 cm thick crystals are complemented by preshower detectors, that consist of lead/silicon detector layers and cover a range of $1.65 < |\eta| < 2.6$. These allow the identification of neutral pions and improve the position determination of electrons and photons.
In total, the electromagnetic calorimeter consists of 82728 crystals, 61200 of them in the barrel part, summing up to a volume of $11.18\,\text{m}^3$.

The scintillation signals are detected by photodetectors. In the calorimeter barrel, avalanche photodiodes, which provide gain even within high transverse magnetic fields, are used. Vacuum phototriodes have been chosen for the endcaps, since they are able to resist the higher integrated radiation dose in these regions.
The photodetectors are readout by a 16 bit readout chain. The corresponding energy range extends from about 30 MeV in the barrel part and about 150 MeV in the endcaps up to about 2 TeV per crystal.

A parametrisation of the energy resolution can be given by

$$\left(\frac{\sigma_E}{E}\right)^2 = \left(\frac{2.8\%}{\sqrt{E}}\right)^2 + \left(\frac{0.12}{E}\right)^2 + (0.30\%)^2 \qquad (E \text{ in GeV}). \tag{1.3}$$

Here, $a = 2.8\%$ is a stochastic term including fluctuations in the shower containment and photostatistics, $\sigma_n = 0.12$ describes noise caused by electronics or pileup energy, and $c = 0.30\%$ is a constant characterising energy leakage and intercalibration errors. These coefficients were found to be typical values for electrons with momenta between 20 GeV and 250 GeV during a test beam in 2004 [1].

1.2.5 Tracker

The CMS tracker [1] is entirely based on silicon detector technology. It covers the range up to $|\eta| = 2.5$ and can be divided into five subsystems (Fig. 1.5): Pixel detector (PIXEL), tracker inner barrel (TIB), tracker outer barrel (TOB), tracker inner discs (TID), and tracker endcaps (TEC).

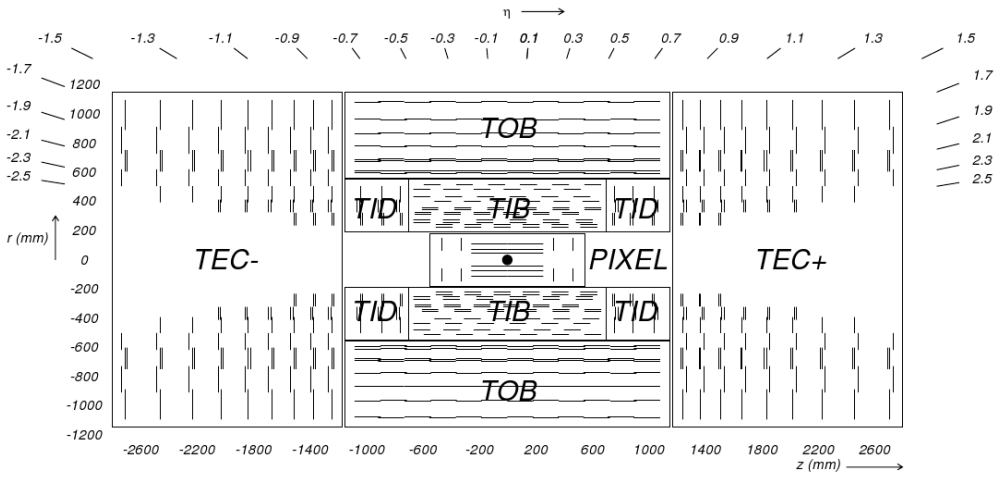


Figure 1.5: View of the CMS tracker in the rz-plane [1]. Each line represents a silicon strip or pixel detector. Stereo modules are indicated by double lines.

The pixel system is not only essential for secondary vertex reconstruction, but also for track seeding, which is important for the outer track reconstruction and high level triggering. It surrounds the interaction point with hybrid pixel detectors arranged in three cylindrical layers in the barrel region and two discs in each forward region. The cylinders have radii of 4.4, 7.3, and 10.2 cm and a length of 53 cm. The pixels have a dimension of $100 \times 150\ \mu\text{m}^2$ and consist of n^+ implants on n substrates. This pixel size leads to a spatial resolution of the pixel detector of 15-20 μm. In total, there are about 66 million pixels covering an active silicon area of about $1\,\text{m}^2$ in the pixel detector.

The remaining tracker subsystems form the silicon strip tracker. Its inner part consists of TIB with four barrel layers of silicon modules and TID representing two endcaps containing three discs each. The inner part is surrounded by the TOB containing six cylindrical strip detector layers. The inner strip tracker and the TOB are complemented in the forward regions by the TECs, two endcaps, that are each formed by nine discs with up to seven rings of silicon modules on them. In total, the strip tracker has an active silicon area of $198\,\text{m}^2$ covered by 9.3 million strips. The strip tracker consists of single sided p-on-n type silicon micro-strip sensors, made of 6 inch wafers. The modules are rectangular in the barrel part and wedge shaped in the endcaps. On the wafer front sides, strip shaped p^+ implantations into the n

bulk form diodes. There is a uniform n^+ implantation, covered by aluminium, on the back sides to create ohmic contact to the positive voltage. The strip dimensions in the inner part of the strip tracker (20 cm $< r <$ 55 cm) are 10 cm $\times$ 80 μm and 25 cm $\times$ 180 μm in the outer part (55 cm $< r <$ 110 cm). These longer strips are formed by two wafers, connected by bonding wires. While, in the inner part, the wafers have a thickness of 320 μm, at higher radii, 500 μm thick wafers are used to compensate higher noise due to increased strip length with a higher signal.
To allow 2-dimensional hit measurements, stereo modules are formed by mounting additional modules back-to-back onto some of the detector modules. These extra modules are rotated by 100 mrad with respect to the original module, allowing the determination of the hit positions in z direction with a precision of 230 μm in TIB and 530 μm in TOB. In the endcap sections, the accuracy of r measurements varies due to different module specifications in different TEC rings. Stereo modules are placed in layers 1 and 2 of TIB and TOB, rings 1 and 2 of each disc in TID, and rings 1, 2, and 5 in the TECs.

The p_T resolution of the CMS tracker is between 1% and 2% for high momentum tracks (100 GeV) in the range of $|\eta| < 1.6$. The resolution of the transverse impact parameter for this kind of tracks is about 10 μm. The tracking efficiency is degraded by multiple scattering, caused by the material inside the tracker. Thus, the material budget of the tracker has been kept as low a possible. However, a non-negligible amount of support material is necessary to provide electrical powering of about 60 kW, cooling of the resulting heat, and mechanical stability. The CMS tracker will be operated at a temperature of -10 °C to reduce the effects of radiation damage to the silicon detector modules.

CMS tracker endcap

The abbreviation TEC is used as well for the tracker subsystem consisting of the two endcaps TEC+ and TEC- (the sign represents the sign of the endcap's z-coordinate) as for one of the endcaps itself. This thesis deals with the alignment of the TEC+, which was integrated at Aachen University.

Each TEC consists of nine discs (Fig. 1.6) carrying 16 wegde-shaped substructures called petals, on which the sensor modules are mounted with the strips in radial direction. Discs and petals are made of carbon fibre to provide sufficient stability while having a low mass. The modules are arranged in seven rings on the petals with rings 1, 2, and 5 consisting of stereo modules. Each disc has eight petals mounted on the side facing the interaction point (front petals) and eight on the far side (back petals) (Fig. 1.7). By grouping the neighbouring front and back petals that are linked by the readout control loops, the discs are divided into eight sectors with IDs from 1 to 8 (Fig. 1.8).

Due to geometrical reasons, the sensor modules for each TEC ring have different, basically trapezoidal shapes. The length of the silicon strips increases from 87.2 mm for modules on ring 1 to 205.7 mm for those on ring 7. There are 512 strips on each single sided module and 768 strips on each silicon strip sensor in the stereo modules. The strip pitch of the modules also varies among the rings. The modules on ring 1 have the smallest pitch with 81 μm at the bottom side and 112 μm at the top side while the ones on ring 6 have a pitch of 163 μm up to 205 μm, which is the largest one (Tab. 1.1).

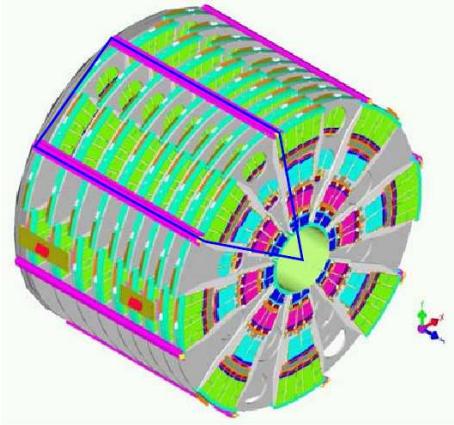


Figure 1.6: Sketch of a tracker endcap [1].

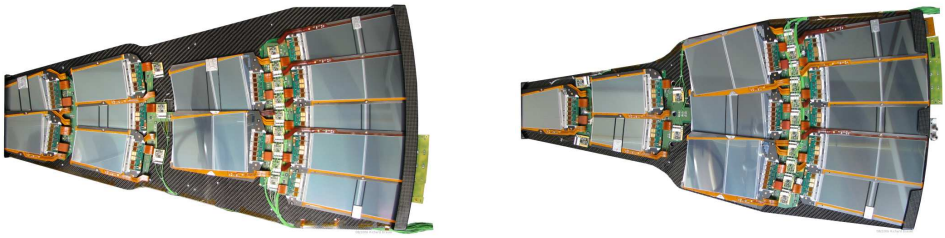


Figure 1.7: A TEC front petal (left) and a back petal (right) [5].

The acceptance of the tracker extends up to $|\eta| < 2.5$. Therefore, the innermost module rings are left out on the discs far away from the interaction point. Also the spacing between the discs increases from disc 1 to disc 9. The z-coordinates and ring configurations of the TEC discs are shown in Table 1.2.

Laser Alignment System

To measure diplacements of the tracker subsystems and the TEC discs with respect to each other, the CMS tracker has an internal alignment system. The Laser Alignment System [1] (LAS) measures the piercing points of laser beams with a wavelength of λ =1075 nm with some of the silicon strip modules in the tracker. By comparing the position of these piercing points to their nominal position, it deter-

Table 1.1: Properties of the sensor modules on the various rings [5].

Ring number	r_{in} [mm]	r_{out} [mm]	Strip length [mm]	Pitch [μm]	Modules per front petal	Modules per back petal	Stereo modules
1	233.0	320.2	87.2	81 - 112	2	1	yes
2	323.0	411.1	88.1	113 - 143	2	1	yes
3	392.1	502.7	110.6	123 - 158	3	2	no
4	504.1	619.2	115.1	113 - 139	4	3	no
5	603.2	750.4	147.2	126 - 156	2	3	yes
6	727.0	910.9	183.9	163 - 205	4	3	no
7	888.4	1094.1	205.7	140 - 172	5	5	no

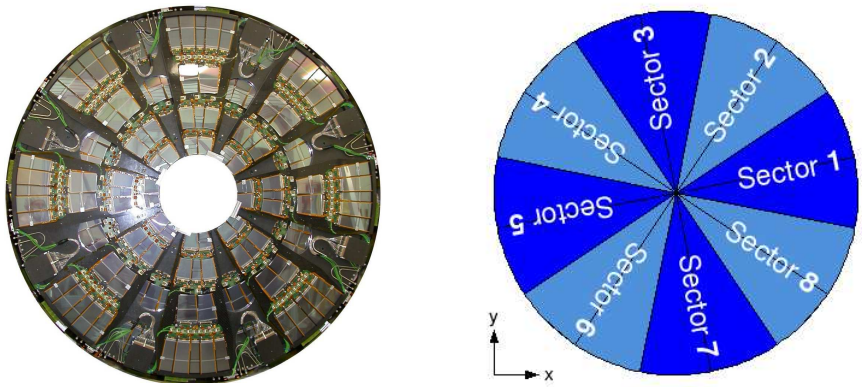


Figure 1.8: A photo of a TEC disc is shown on the left. One the right, the numbering scheme of the TEC sectors each consisting of a front and a back petal is displayed.

mines the relative positions of the tracker substructures with a precision of about 100 μm providing the initial alignment needed for successful track reconstruction.

There are three classes of laser beams inside the CMS tracker (Fig. 1.9). Two of them are used to determine positions and orientations of the TEC discs, and the other one is used to estimate displacements of the subsystems TIB, TOB and TEC with respect to each other. Special sensor modules are used in the TEC at places where the laser beams cross the discs. These have an antireflective coating and a hole in their backside metalization to increase the transmission of the module and allow the laser beam to pierce all modules with sufficient high intensity. With a fourth beam class on the outside of the tracker its position and orientation relative to the muon systems can be estimated.

Both TEC internal LAS beam classes are integrated eight times in each endcap, equally distributed in ϕ. There are eight beams of the class connecting the tracker subsystems in the central part of the tracker. Due to incompatible azimuthal segmentation of the barrel and tracker endcaps, these beams could not be distributed equally and hence are positioned with $\Delta\phi$ between 32.2° and 51.4° [7].

Table 1.2: Configuration of the nine TEC discs [5, 6].

Disc number	z-coordinate [mm]	Module rings mounted on the disc
1	1360	1 - 7
2	1500	1 - 7
3	1640	1 - 7
4	1780	2 - 7
5	1920	2 - 7
6	2095	2 - 7
7	2285	3 - 7
8	2490	3 - 7
9	2705	4 - 7

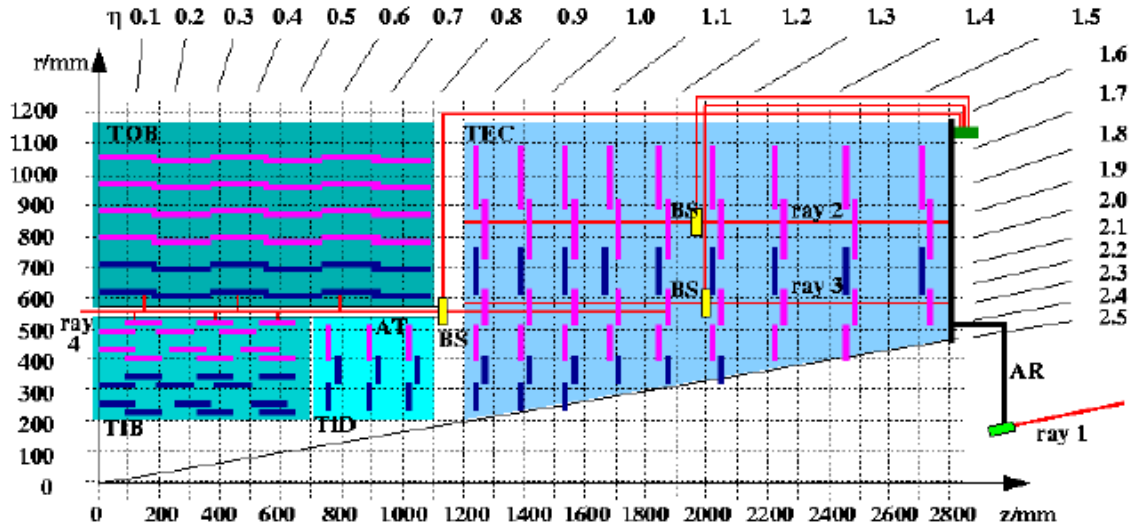


Figure 1.9: Overview of LAS laser beams in the CMS tracker [1]. Ray 1 connects the tracker with the Myon system. Ray 2 crosses a sensor module in ring 6 on each TEC back petal, ray 3 a module in ring 4. The positions and orientations of TIB, TOB and TEC with respect to each other can be determined with ray 4.

1.2.6 Trigger

At design luminosity of the LHC ($10^{34}\,\mathrm{cm^{-2}s^{-1}}$), a proton-proton interaction rate of about 10^9 Hz is expected. The mass storage systems are able to write the event data to tape at a maximum sustained rate of about 300 Hz [8] (corresponding to 450 MB/s), though. Therefore, a trigger system [9] is needed to filter events down to this rate. At CMS, this is done in two steps: The Level-1 Trigger (L1), implemented by custom electronics, reduces the event rate to about 100 kHz. The remaining filtering is done by the High Level Trigger (HLT), which is a farm of commercial processors.

The Level-1 trigger has to reduce the event rate by a factor of about 10^4. It is designed as deadtime-less electronic pipelines, that perform every calculation for each bunch crossing. The event data are held in a pipeline for about 3.2 μs (128 bunch crossings). After this time, the trigger decision whether or not to keep the event and to transport its data to the HLT has to be available. Therefore, only promptly available data can be used for the trigger decision, which excludes information from the tracker and the preshower detectors. The trigger decisions are based upon pre-defined thresholds for instance for particle counts, p_T, or missing transverse energy $\not\!\!E_T$.

The HLT reduces the event rate by a factor of about 10^3 writing the remaining 150 Hz (corresponding to 225 MB/s) event stream [8] to a mass storage system. A series of filters is applied to select interesting events. The large volume of tracker data is used only, if an event passes the initial filters, which are based on calorimeter and muon data. Eventually, the full event data is used for the final HLT filter algorithms.

2. Track-based Alignment

2.1 Motivation

Due to limited mounting precision of the sensor modules, their positions and orientations differ from the ideal positions. Deviations from the ideal geometry are called *misalignment*. Misalignment occurs not only on module level, but also on the level of higher substructures, for example the CMS tracker endcap petals. Movements[1] of these substructures result in correlated displacements of the affected modules.
There are more causes for misalignment than the mounting precision: For example, there can be time-dependent deformations of a tracker due to external forces caused by movements of other detector systems. Further, varying temperatures or humidity can cause changes in the geometry due to contracting or expanding material.
Misalignment has a negative effect on track reconstruction and momentum measurement. Therefore, it is important to know the deformations of the tracker as precisely as possible. The process of finding out the current tracker geometry and the result itself is called *alignment*. The tracker substructures to be aligned are named *alignables*.

2.2 Alignment Algorithms

Before a tracker is integrated into the detector, there are several possibilities to measure deviations from the ideal geometry. External measurements such as photogrammetry are possible at this time. After insertion into the detector, access to the tracker is limited and only internal methods can be used to determine an alignment. There are basically two categories of internal alignment: The measurement of displacements of the tracker and its substructures with an installed alignment system, like the Laser Alignment System of the CMS tracker, or the usage of track-based alignment. For the latter one, track data are needed, that are processed by alignment algorithms.
These algorithms basically change the geometry of the tracker to minimize the χ^2

[1] In this work, the terms "movement" and "displacement" are used synonymously and refer to changes of position and orientation.

of the given tracks. Important advantages of the track-based alignment are the high precision and that no installed alignment systems are needed to estimate the current deviations from ideal geometry.
For the alignment of the CMS tracker, three different algorithms are used: MillePede, Kalman Alignment Algorithm, and HIP. The Kalman Alignment Algorithm and MillePede are described in the following.

2.2.1 Kalman Alignment Algorithm

For the studies described in this work, an alignment algorithm based on a Kalman filter is used. It is a sequential algorithm, meaning that the alignment parameters (current positions and orientations of the detector units) are updated after each track. These updates are not restricted to the detector units crossed by the track, which makes the algorithm a global method.

Table 2.1: Notation used in this section.

d	Current alignment parameters
D	Current covariance matrix
d'	Updated alignment parameters
D'	Updated covariance matrix
f	Track model
p	Track prediction
m	Track measurements
M	Covariance matrix of measurements
x	Track parameters
T	Track derivatives
A	Alignment derivatives

It is assumed that alignment parameters d with a covariance matrix D are given. These shall be updated using information of a track in the form of hit measurements m with covariance matrix M and a vector p containing the track prediction from the track fitter.

The track measurements m can be parameterised as function of the track parameters x, the alignment parameters d, and effects of observation error and multiple scattering ϵ. Applying a linear Taylor approximation in x_0 and d_0, the track measurements yield

$$\begin{aligned} m &= f(x,d) + \epsilon \\ &= f(x_0,d_0) + T \cdot (x - x_0) + A \cdot (d - d_0) + \epsilon \\ &= c + T \cdot x + A \cdot d + \epsilon \end{aligned}$$

with c being a constant. The track predictions are represented by the track model f, evaluated at the expansion point ($p = f(x_0, d_0)$). Track derivatives T and alignment derivatives A are given by

$$\begin{aligned} T &= \frac{\partial f}{\partial x}(x_0,d_0) \\ A &= \frac{\partial f}{\partial d}(x_0,d_0). \end{aligned}$$

Typically, for x_0, the parameters of the track fit are used, and for d, the expansion point is set to the ideal geometry ($d_0 = 0$).

The χ^2 of the track is given by

$$\chi^2 = (m - f(x,d))^T \cdot M \cdot (m - f(x,d)). \tag{2.1}$$

It has to be minimised by finding the ideal vector of alignment parameters d. The Kalman filter is used to calculate an update of the alignment parameters and their covariance matrix using track predictions p, measurements m, and the derivatives T and A [10, 11]:

$$\begin{aligned} d' &= d + DA^T \cdot W \cdot (p - m - Ad) && (2.2)\\ D' &= D - (DA^T)^T \cdot W \cdot DA^T && (2.3) \end{aligned}$$

Here, W and V are auxiliary matrices, given by

$$\begin{aligned} W &= -(V^{-1})^T \cdot T^T \cdot (T^T V^{-1} T)^{-1} \cdot T \cdot V^{-1} + V^{-1} \\ V &= M + ADA^T. \end{aligned}$$

Using these formulae, the alignment parameters are updated track by track until the optimal alignable displacements regarding the entire data set are estimated.

Large startup uncertainties are set to the alignment parameters to prevent the results from being biased by starting values. To fix the position of certain detector units for definition of the reference system, small prior uncertainties can be assigned to these detector units.

Deterministic annealing can be applied to avoid local minima in the parameter space and hence to more likely find the global minimum. This is done by increasing track uncertainties for measurements which are not on reference detector units. For calculation of the updates,

$$M_{ii}^{anneal} = M_{ii} \cdot c(k) \tag{2.4}$$

is used instead of M with k being the current iteration number. For $c(k)$, various models can be applied. The deterministic annealing model used in this work is described in Section 4.3.1.

2.2.2 MillePede

Another common alignment algorithm is MillePede [12]. It chooses a different mathematical ansatz to solve the χ^2 minimisation problem than the Kalman algorithm.

After linearising the problem as it is done in the previous section, the problem is transformed into a system of linear equations.

$$\left(\begin{array}{c|ccc} \sum C_j & \dots & G_j & \dots \\ \hline \vdots & \ddots & 0 & 0 \\ G_j^T & 0 & \Gamma_j & 0 \\ \vdots & 0 & 0 & \ddots \end{array}\right) \cdot \left(\begin{array}{c} d \\ \hline \vdots \\ \delta x_j \\ \vdots \end{array}\right) = \left(\begin{array}{c} \sum b_j \\ \hline \vdots \\ \beta_j \\ \vdots \end{array}\right) \tag{2.5}$$

This system contains the information of all available tracks. It is not gathered track by track as in the Kalman algorithm. Thus, the matrix in (2.5) has a huge size for a large number of tracks:

$$size = (n_{par} + 5 \cdot n_{tracks})^2$$

with the number of alignment parameters n_{par} and the number of tracks n_{tracks}.

Defining

$$z_i = \frac{m - f(x, d)}{M_{ii}}$$

and using the notation of the previous section with matrix entry IDs as subscripts, the submatrices are given by

$$\begin{aligned}
(C_j)_{kl} &= \frac{\partial z}{\partial d_k} \cdot \frac{\partial z}{\partial d_l}, \\
(G_j)_{kl} &= \frac{\partial z}{\partial d_k} \cdot \frac{\partial z}{\partial x_l}, \\
(\Gamma_j)_{kl} &= \frac{\partial z}{\partial x_k} \cdot \frac{\partial z}{\partial x_l}, \\
(b_j)_k &= \frac{\partial z}{\partial d_k} \cdot z, \\
(\beta_j)_k &= \frac{\partial z}{\partial x_k} \cdot z
\end{aligned}$$

with z and x of track j in each case.

The structure of (2.5) can be exploited to transform into an equation system with reduced matrix size. Defining the matrix C' and the vector b' as

$$\begin{aligned}
C' &= \sum_j C_j - \sum_j G_j \Gamma_j^{-1} G_j^T \\
b' &= \sum_j b_j - \sum_j G_j (\Gamma_j^{-1} \beta_j),
\end{aligned}$$

the equation system can be significantly reduced in its size to

$$C' \cdot d = b' \tag{2.6}$$

with C' having a size of n_{par}^2. This final equation system now only contains the global alignment parameters d.

MillePede is split into two parts: *Mille* is run first and creates the needed matrices with given track information. Afterwards, the second part, *Pede*, solves the equation system (2.6). Various methods can be used to solve the equation system in the Pede step. The recommended method is GMRES [13], which is a numerical method, that considers the given matrices as sparse and hence saves memory and CPU time. The equation system can also be solved by matrix diagonalisation. For large numbers of alignables, this is a very CPU time intensive process, but provides also the uncertainties of the alignment parameters.

2.3 Weak Modes

Deformations of a tracker that do not change the χ^2 of tracks are called *weak modes*. Weak modes cannot be determined when making only the assumption that the recorded tracks are straight (or describable by a helix model, considering a non-zero magnetic field). Additional information is needed: For instance, if the origin of a set of tracks is known to be the beam spot or a displaced vertex, a corresponding *vertex constraint* can be applied to estimate weak modes.

Considering the Kalman Alignment Algorithm, weak modes correspond to eigenvectors of the covariance matrix D with large eigenvalues. Eigenvalues represent the uncertainty of correlated alignable movements described by eigenvectors, and hence the largest eigenvalues indicate the least well determined modes of the detector.

Known weak modes of the TEC+ are shifts in x, y, or z direction which increase linearly with the z coordinate. Shifts of this kind are interpreted as additional inclinations of the particle tracks and hence cannot be determined with cosmic track data.
To first order, a linear increasing torsion of the TEC+ is also a weak mode. However, considering second order effects, a straight track crossing the TEC+ will not only change its inclination, but will also bend by applying this kind of torsion. In the following, it is examined if this effect is sufficient to detect the torsion with track-based alignment and cosmic tracks.

2.4 Sensitivity to Torsion

A torsion that increases linearly with the z coordinate causes bending of tracks in the TEC+. These bendings grow to second order with the magnitude of the torsion and basically allow a detection of this kind of distortion with track based alignment. The quantitative effect of a TEC+ torsion on crossing particle tracks is examined and compared to the precision of the integrated sensor modules.

Assuming that the TEC+ is symmetric under rotations around the beam axis, any track can be parameterised by

$$\begin{pmatrix} x(z) \\ y(z) \end{pmatrix} = \begin{pmatrix} 0 \\ y_0 \end{pmatrix} + (z - z_0) \cdot a \cdot \begin{pmatrix} \cos(\delta) \\ \sin(\delta) \end{pmatrix}. \tag{2.7}$$

By varying y_0 correspondingly, z_0 can be set to the z-coordinate of the first TEC+ disc. Thus, the coordinate of the track hit on disc 1 is $\left(\begin{smallmatrix} 0 \\ y_0 \end{smallmatrix}\right)$. The track inclination is specified by its magnitude a and the direction angle δ.

When applying a torsion $\gamma(z)$ to the TEC+, the following corrections need to be applied to the hit coordinates:

$$\begin{pmatrix} \Delta x(z) \\ \Delta y(z) \end{pmatrix} = \sqrt{x(z)^2 + y(z)^2} \cdot \begin{pmatrix} \sin\left(\arctan\left(\frac{y(z)}{x(z)}\right) + \gamma(z)\right) \\ \cos\left(\arctan\left(\frac{y(z)}{x(z)}\right) + \gamma(z)\right) \end{pmatrix} - \begin{pmatrix} x(z) \\ y(z) \end{pmatrix} \tag{2.8}$$

Because the exact origin of the detected particles is generally not known, the track-fit algorithm just assumes that the track is straight. Therefore, linear terms in the

calculated hit corrections are interpreted as an inclination of the track. By calculating a linear fit to the corrections and considering the residuals, only higher order corrections are regarded.

Residuals are calculated for tracks that have a radial inclination direction, and for those that are inclined tangentially (Fig. 2.1, 2.2). A linear torsion of the TEC+ with a total magnitude of $\gamma_{total} = 0.5$ mrad is simulated and the track inclination scale a is variated between 0.0 and 0.5. The maximum order of magnitude of disc rotations measured by optical survey method is 0.5 mrad. Therefore, no larger torsion of the TEC+ is expected. The maximum track inclination is chosen as an approximation of the highest possible inclination of a track which still hits all nine discs within one TEC+ sector.

The residuals in r-direction reach about 50 μm for tangential inclinations, the ϕ-residuals go up to 0.1 mrad for tracks that are inclined radially.
In the r-direction, a measurement precision between 250 μm and 450 μm is reached by the TEC+ stereo-modules. Thus, the applied torsion cannot be detected using a track, which is inclined tangentially. The ϕ-resolution of the TEC+ modules varies between 0.05 mrad and 0.10 mrad, depending on the ring onto which the module is mounted. Accordingly, a detection of a linear torsion with the applied magnitude is theoretically possible using a radially inclined track. However, the sensitivity is expected to be small due to the low number of hit position deviations per track that are larger than the sensor precision.
If more than one track is considered, the sensitivity increases with the number of processed tracks. Thus, a large set of inclined tracks is needed to determine the linear torsion.

In general, the mode $\Delta\phi = a_\phi \cdot z$ like other linear modes is set to zero by subtracting a corresponding fit from results. This mode it will be dealt with in Section 7.2.

2.5 Selection of Coordinate System

Displacements can only be determined with respect to a reference. Thus, a part of the tracker needs to be considered as reference and its alignment parameter fixed to estimate an alignment.
To set weak modes to zero, other parts of the tracker can be fixed. Alternatively, these modes can be set manually to zero by subtracting a corresponding fit from the determined alignment results. Here, if not stated otherwise, the mean and slope (as a function of z) of all aligned parameters are fixed to zero, eliminating the modes

$$\begin{aligned} \Delta x &= a_x + b_x \cdot z \\ \Delta y &= a_y + b_y \cdot z \\ \Delta z &= a_z + b_z \cdot z \\ \Delta\phi &= a_\phi + b_\phi \cdot z. \end{aligned}$$

This is done by, at first, determining an alignment of the selected alignables with respect to the fixed detector part. After that, the alignment parameters d and the

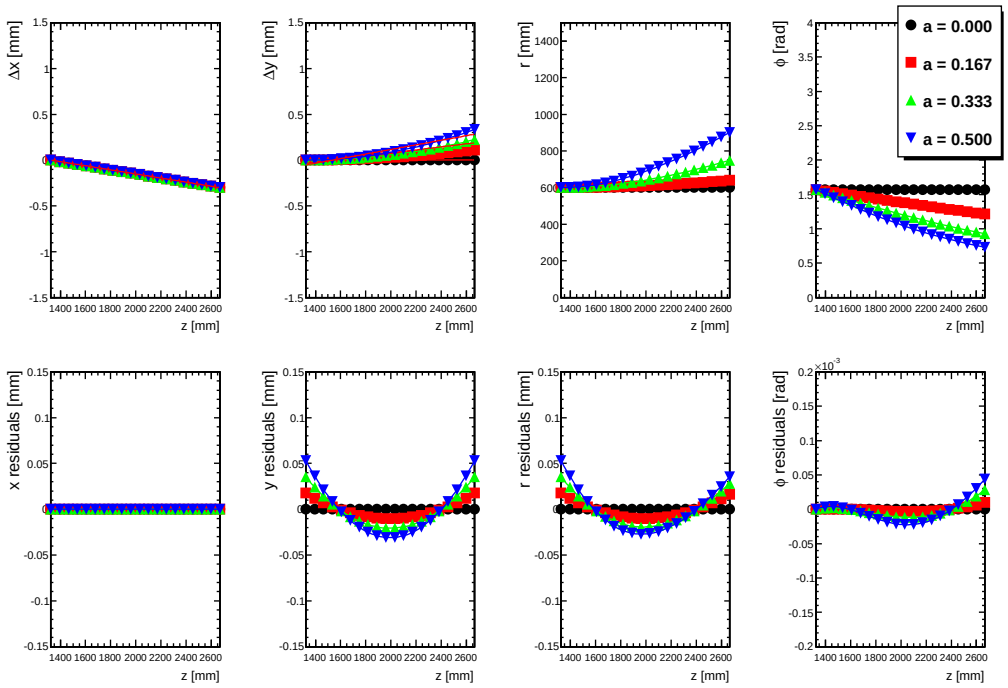


Figure 2.1: Hit positions and residuals for tracks with a tangential inclination ($\delta = 0$). The inclination magnitude a is variated between 0.0 and 0.5.

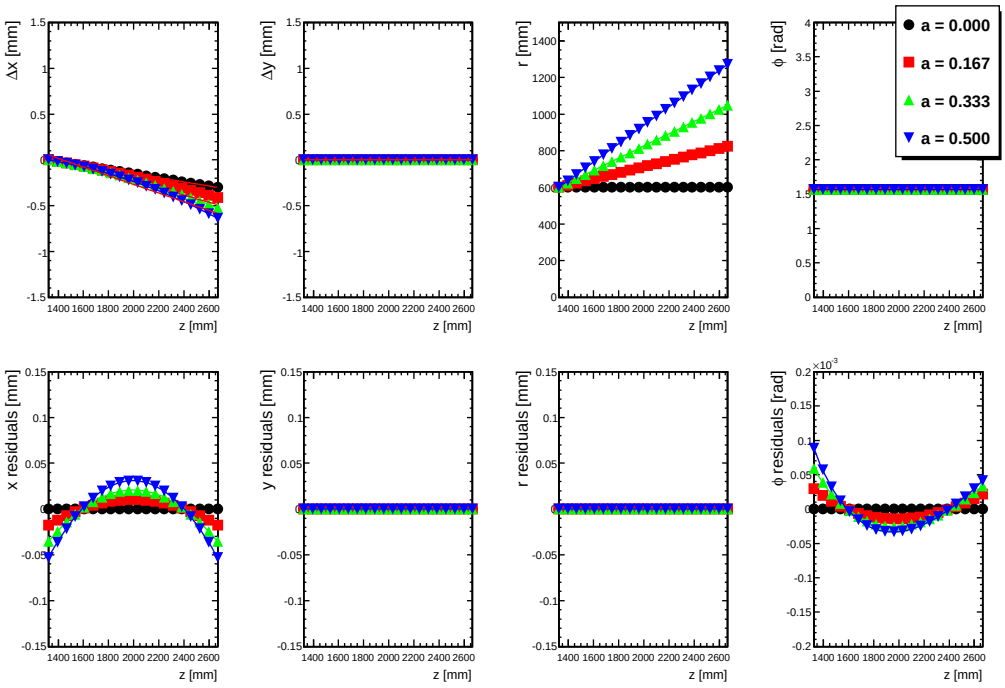


Figure 2.2: Hit positions and residuals for tracks, that are inclined radially ($\delta = \frac{\pi}{2}$). The inclination magnitude a is variated between 0.0 and 0.5.

covariance matrix D are split into subvectors d^X and submatrices D^X corresponding to the different degrees of freedom ($X = x, y, z, \phi$). These are transformed into

$$\begin{aligned} d^{X\prime} &= d^X - \frac{1}{n_{ali}} \sum_{j=1}^{n_{ali}} d_j^X \\ D^{X\prime} &= (I - \left\{ \frac{1}{n_{ali}} \right\}) \cdot D^X \cdot (I - \left\{ \frac{1}{n_{ali}} \right\}) \end{aligned}$$

to set the mean of each d^X to zero. Here, I denominates the identity matrix and n_{ali} the number of alignables. Eventually, considering the alignable z-positions, a linear fit in $d^{X\prime}(z)$ is created and subtracted from the alignment parameters. For the fit calculation, all parameters are regarded with the same weight.

3. Data Taking

This chapter describes the data taking of cosmic muons crossing the TEC+. After integration of each TEC+ sector, a set of muon tracks in this sector was recorded. The fully integrated TEC+ was transported to CERN, where it was inserted into the tracker. Further data were taken after finishing the tracker integration.

3.1 Sector Tests

The petals were integrated into the endcap sectorwise (integration procedure, the following tests, and the data taking is described in detail in [5]). To keep the mass distribution of the TEC+ balanced, the order of the integrated sectors was not in order of their IDs (Fig. 1.8). At first, sector 1 was integrated, then the sectors 5 and 3. After that, the petals of sector 1 were replaced due to defects. Integration of the sectors 7, 2, 6, 4, and 8 followed thereafter in this order.
After finishing integration and testing of each sector, cosmic muons passing the TEC+ were triggered and their tracks readout and stored. The first data were taken in March, the last in October 2006.

3.1.1 Experimental setup

During data taking, the TEC+ was in a vertical position (disc planes horizontal). Two square scintillators with edge length of 80 cm, that each consisted of four scintillator panels, were positioned below and above the tested sector (Fig. 3.1). Each scintillator panel was read out by two photo multiplier tubes.
A signal from one of the upper scintillator panels and one of the lower panels was demanded to trigger a readout of the TEC+ sector. Both photo multipliers needed to deliver a signal above an adjustable threshold to create a signal from one of the scintillator panels. That way, there was a reduced chance of triggering due to noise in the photo multiplier tubes.
Between the lower scintillators and the bottom of the TEC+, a 10 cm thick shielding of lead bricks was placed to absorb low energy muons and prevent them from triggering a readout. Considering a lead mass density of $11.34\,\mathrm{g/cm^2}$, muons with momentum lower than 250 MeV were stopped before reaching the lower scintillators [14].

After integration of the odd-numbered sectors, the trigger setup was modified: By optimising the thresholds needed for a signal from the photo multiplier tubes, the trigger efficiency increased [6]. The number of tracks recorded for each sector is shown in Table 3.1.

Table 3.1: Sector test data sets in chronological order [6].

Runs	Sector	Number of triggers in good runs[a]	Number of tracks
20613 - 20725	0[b]	180131	14854
20944 - 20952	5	87400	6961
21136 - 21163	3	122058	5821
21238 - 21269	1	88591	5807
21428 - 21448	7	83772	8502
21512 - 21530	2	82139	62650
21592 - 21617	6	87258	68210
21666 - 21670	4	58248	42260
21713	8	73227	61159

[a]Some runs have been marked as "bad" and sorted out for instance due to hardware problems, DAQ crashes, or wrong latency settings.
[b]later replaced by sector 1.

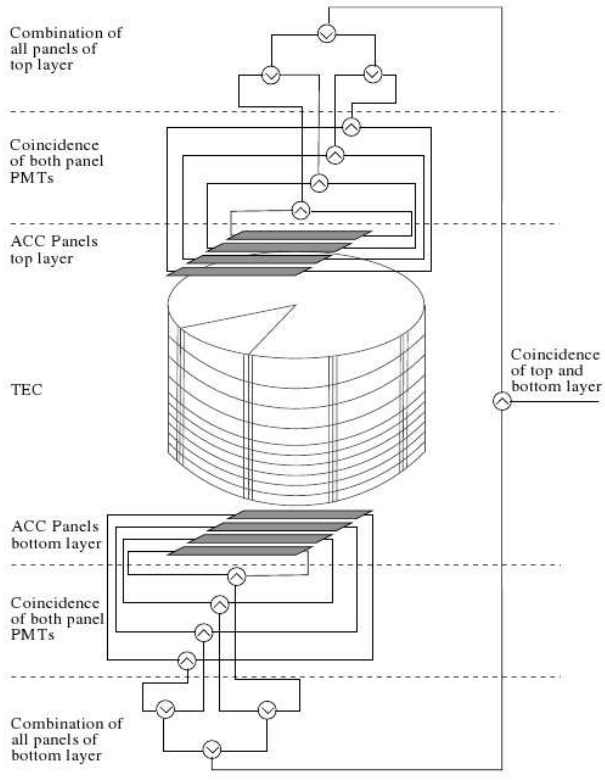


Figure 3.1: Cosmic trigger setup during TEC+ sector tests [5].

3.2 Tracker Slice Test

After successfully completing its integration, the TEC+ was transported from Aachen to Geneva in October 2006 to be inserted into the CMS tracker at CERN.

After integration of the full tracker, tracks of cosmic muons crossing the tracker were recorded at different temperatures and various scintillator configurations in March 2007.
Between the transport to CERN and the starting of the slice test, two petals of the TEC+ were replaced because of defects which had already been found in Aachen, but could not be fixed due to time constraints [5]. These were the back petal on disc 3 and the front petal on disc 4, both in sector 2.

3.2.1 Experimental setup

During the slice test, about 13% of the whole silicon tracker was powered and read-out. This included sectors 2 and 3 of TEC+. These were the upper sectors of the endcap, considering that the TEC+ was in its final horizontal position inside the tracker (its disc planes perpendicular to the beam axis).
Cosmic muons passing the tracker were detected using scintillators below and above the tracker. Tracks were recorded using three different scintillator configurations called A, B, and C (Fig. 3.2). Above the lower scintillators, lead bricks were placed to absorb low energy muons. The thickness of the shielding was 5 cm hence muons with a momentum lower than 180 MeV were stopped in it [14]. To trigger a readout of the active tracker parts, a signal from one of the upper scintillators and one of the lower scintillators was demanded.
During data taking with scintillator configuration C, the temperature of the tracker was altered. Tracks were recorded at a chiller coolant temperature of 15 °C, 10 °C, -0.5 °C, -10 °C, -15 °C, and 14 °C. There was not enough cooling power to cool the active tracker parts to -15 °C. Therefore, some parts of the tracker had to be switched off in order to reach this temperature. Amongst others, the TEC front petals were deactivated, so only the backpetals were readout in this run.

Table 3.2 shows the number of events recorded with the various scintillator and temperature settings [15].

Table 3.2: Slice test data sets [15].

Runs	Active detectors	Scintillator configuration	T [°C]	Number of good events	Number of tracks in TEC+
6203 - 6930	TIB TOB	A	15	665409	0
7277 - 7296	TIB TOB TEC	A	14	189925	not determined
7635 - 8055	TIB TOB TEC	B	15	177768	not determined
9255 - 9341	TIB TOB TEC	C	15	496635	5201
10145 - 10684	TIB TOB TEC	C	10	535533	21287
10848 - 11274	TIB TOB TEC	C	-0.5	886801	33844
11316 - 11915	TIB TOB TEC	C	-10	902863	35861
12045 - 12585	TIB TOB TEC	C	-15	655298	5229
12599 - 12656	TIB TOB TEC	C	14	112139	4335
12934 - 12982	TIB TOB	C	14	46568	0

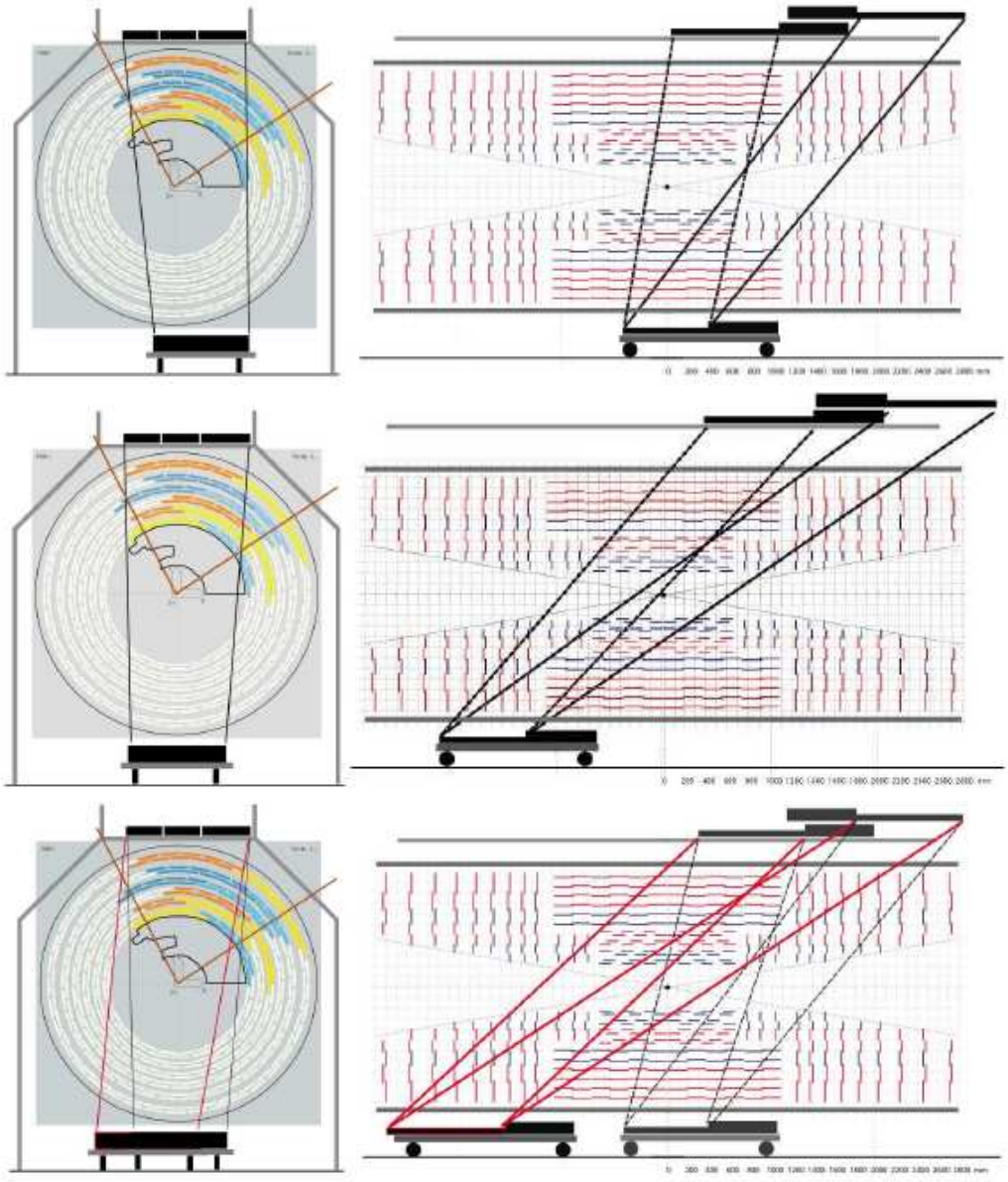


Figure 3.2: Scintillator configurations A (top), B (middle) and C (bottom) during the slice test [15]. On the left, the xy-plane of the setup is shown. The right side displays the yz-plane of the setup. A readout of the active detector parts was triggered if a cosmic muon was detected in one of the scintillators above the tracker and in the scintillator below it (in case of configuration C, one of the two scintillators below it).

4. Data Processing

4.1 Calibration and Detection of Sensor Defects

Before recording physics data, the detector needs to be calibrated. This has been done in a special calibration run [5]. The output of the silicon strip sensors without particles crossing the TEC+ has been recorded by applying a random trigger. Even without traversing particles, the sensor modules provide a non-zero signal, which fluctuates around a mean, the *pedestal*. The pedestal is different for each strip and needs to be known to distinguish between signal and background.
From the pedestal run events, the pedestal p_i of each strip i is computed as the mean of all recorded signals of this strip. The standard deviation is called the *raw noise*, σ_i^{raw}, and expresses the size of the signal fluctuations around the pedestal without particles crossing the silicon.

$$p_i = \frac{1}{N}\sum_{j=1}^{N} r_{i,j} \tag{4.1}$$

$$\sigma_i^{raw} = \sqrt{\frac{1}{N-1}\sum_{j=1}^{N}(r_{i,j}-p_i)^2} \tag{4.2}$$

The signal of strip i in event j is denoted by $r_{i,j}$.

The output of the 128 strips which are connected to the same readout chip (APV) contains a highly correlated component caused for instance by power supply noise. Thus, for each event, the mean deviation of the signal from the pedestal of all strips belonging to the same APV is calculated and subtracted from the raw signals. The standard deviation of the thus adjusted signals (for strip i) is called *common mode subtracted noise*, σ_i^{CMS}.
These calculated noise characteristics are then used to evaluate and cut on strip and signal qualities.

In order to improve track reconstruction and hence alignment with the sector test data, sensor defects need to be detected and marked. At first, the number of hits

per module in the entire data set is counted and compared to the other modules of the same sector. Here, some modules are found to be hit far more often than the average. Examining the hit distribution on these "hot" modules, most hits are found to be detected on the same strips (Fig. 4.1). Often, these are strips at the edges of the module.

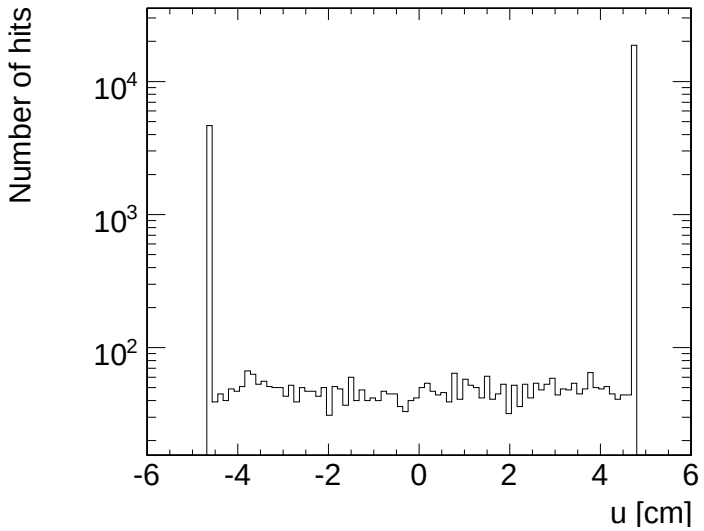


Figure 4.1: Total number of hits on a "hot" module in TEC+ sector 8 against the local u coordinate of these hits. Most of the hits are detected in the strips at the edge of the module and are expected to be fake hits.

Irregularities in the hits distributions are most likely due to noisy or dead strips. These can cause fake hits, that deteriorate the track reconstruction. Dead and noisy strips cause large deviations in the noise distribution of the module. Thus, they can be detected by searching the common mode subtracted noise for strips that are five standard deviations away from the common mode subtracted noise distribution of the same APV.
The sector test calibration data has been searched for strip defects using a standard procedure of the CMS software framework. Now it is reprocessed using this 5σ criterion to mark dead (common mode subtracted noise 5σ or more below APV average) and noisy strips (common mode subtracted noise 5σ or more above APV average). All previously known defects [6] are found and, in addition, 8833 strips that have been flagged as okay, before, are now considered as dead or noisy (Tab. 4.1).

Table 4.1: Number of strips flagged previously and with 5σ criterion as okay, dead, or noisy. In addition to strips that were previously flagged as damaged, more dead and noisy strips are found using the new criterion.

Strips marked	Strips previously marked as		
with 5σ criterion as	okay	dead	noisy
okay	2160724	0	0
dead	939	595	0
noisy	7894	0	2776

The calibration data (pedestal, raw noise, common mode subtracted noise, and strip flags) for a module on which strip defects are found during the data reprocessing are displayed in Figure 4.2.

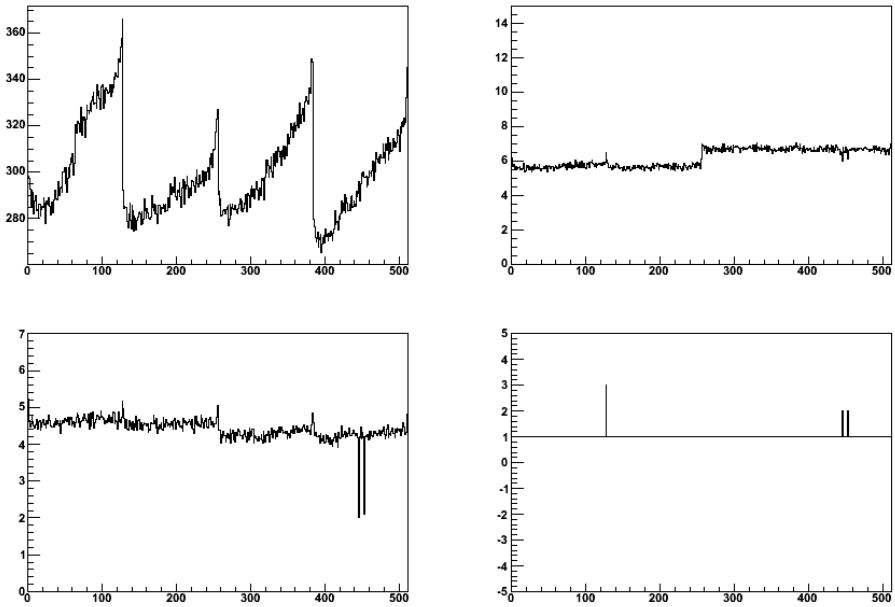


Figure 4.2: Calibration data for a module after the reprocessing of the sector test data with the 5σ criterion for detection of damages strips. The pedestal (upper left), the raw noise (upper right), the common mode subtracted noise (lower left), and the strip flags (lower right) are shown. A strip flag of 1 marks a strip as being okay, a flag of 2 declares it as a dead strip, and a value of 3 indicates a noisy strips. Deviations in the noise distribution of the module indicate damaged strips. The strip flags show, that these are identified as such.

Figure 4.3 shows a visualisation of all modules of TEC+ sector 4, color-coded with their total number of hits in the sector test track data divided by the sensor area, before (left) and after reprocessing the data (right).

The calibration of the slice test data has been done by other members of the CMS collaboration and is not part of this work [15].

4.2 Estimation of Track Parameters

The Kalman Alignment Algorithm needs information on tracks and alignables in a format which is independent of the original data set. For clustering, track reconstruction, and estimation of track and alignment derivatives, the object-oriented CMS software framework is used.
Between the data-taking phases referred to in this thesis, CMS has changed its object-oriented software framework. Correspondingly, the first data, taken in 2006, are processed with the ORCA software framework [16], whereas for the second set of data, taken in 2007, the CMSSW framework [17] is used. Due to the different frameworks, each data set is processed by an independent program. These programs write the information needed by the alignment algorithm for each track into

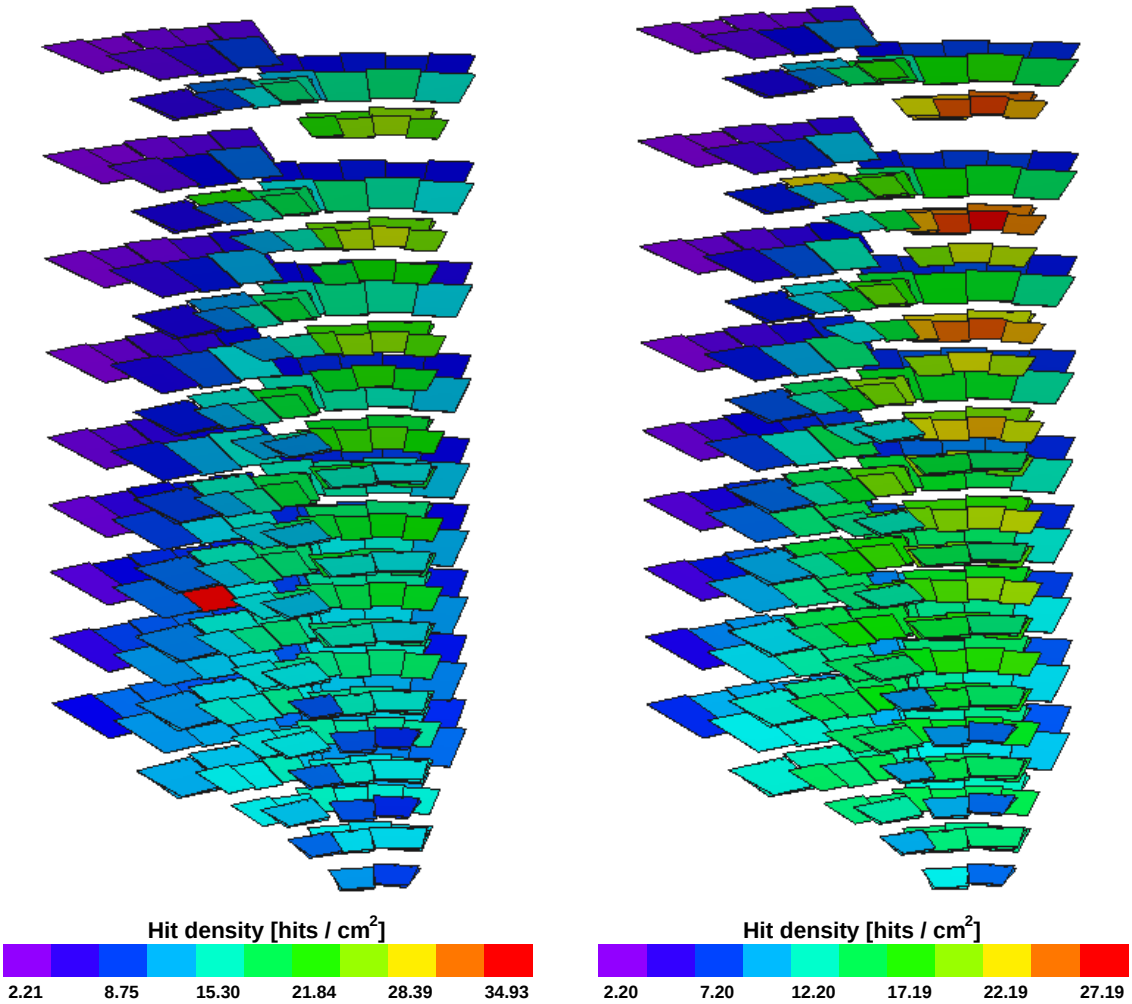


Figure 4.3: Visualisation of all modules of TEC+ sector 4, color-coded with their hit density in the slice test track data, before reprocessing the data (left) and after it (right). After the reprocessing, the hit distributions is more continuous – there are no outliers any more.

ROOT [18] files. The configuration of these programs and the framework is specified using *configuration files*, which can be found in Appendix B.
Eventually, the alignment corrections are computed by one program for both data sets.

4.2.1 Clustering

The first step of track reconstruction is the cluster finding. A cluster is created by a particle traversing the detector silicon and depositing charge in one or more strips, depending on the track inclination.
Strips with a signal-over-noise ratio (S/N) above the *SeedThreshold* (= 8 in ORCA and = 5 in CMSSW) form cluster seeds. Adjacent strips are added to the cluster if their S/N exceeds the *StripThreshold* (= 3). Eventually, a cluster is accepted if it has a cluster signal

$$S_{cluster} = \frac{\sum S_i}{\sqrt{\sum N_i^2}}$$

(S_i Strip signals, N_i Strip noise values)

higher than the *ClusterThreshold* (= 8 in ORCA), = 5 in CMSSW).

After the clustering, a RecHit is created from a cluster by calculating the local u coordinate of the signal mean in case of a single-sided module. In case of a stereo module, a pair of u and v coordinates is estimated from the signal means of the clusters of both affected sensor modules.

4.2.2 Track seeding and reconstruction

Due to different experimental setups, the track seeding and reconstruction with the sector test data and the slice test data differ from each other.

During the sector tests, the TEC+ has been placed in a vertical orientation with disc 9 on top. For this data set, track seeds are created from all possible combinations of the RecHits on disc 9 and disc 8. Using these seeds, tracks are fitted through the detected RecHits by the Combinatorial Track Fitter (CTF) [19]. The CTF recursively evolves a track by following the projection of RecHits which are already considered part of the track to the next detector surface. There it searches for further hit candidates until it reaches the last detector layer. The final fitting of the track through the collected RecHits is done by a Kalman filter.
Eventually, a track selection is applied: A minimum number of four hits is demanded on each track. Otherwise, the track is rejected.

During the recording of the slice test data, about 13% of the entire tracker have been active (see Section 3.2). With these data, track seeds are created in the two outermost layers of the tracker barrel and in each pair of adjacent TEC+ discs [20]. The track fitting is also done using the CTF, here, but with the improved version of an updated framework. The final track selection also differs from the sector test data processing: To adapt the selection to the common track selection that has been agreed on by the CMS Tracker Alignment Team [21], a minimum number of five hits in TEC+ is demanded.

4.2.3 Saving track and alignment information

Only details relevant for the alignment process need to be known about each track. After the track reconstruction and selection, this information is gathered and written into a ROOT file, which can be readout by the alignment algorithm program.

Using a configuration file, it can be specified which parts of the TEC+ shall be aligned in which parameters. The type of substructures considered as alignables (discs, petals, or modules) as well as an alignable selection by specifying coordinate ranges can be picked. With these settings, an ID table is created for all selected alignables.

The program loops over all selected tracks, rejecting events containing multiple tracks, and stores

- track χ^2,
- the number of hits,
- a vector containing the hit measurements (RecHits),
- the measurement covariance matrix,
- a vector of hit predictions estimated by the track fitter,
- the IDs of the alignables, hit by the track,
- track derivatives, and
- the alignment derivatives matrix

for each track in the ROOT file. After looping over all tracks, the file is closed, ready to be processed by the alignment algorithm itself.

4.3 Alignment Algorithm Implementation

The Kalman Alignment Algorithm is implemented as a C++ program, which uses the ROOT Data Analysis Framework. It reads the needed track information from ROOT files which are created by the ORCA and CMSSW programs, described in the previous section.
The program initialises a vector of alignment parameters and the corresponding covariance matrix with configurable starting values. Then, track by track, the parameters and the covariance matrix are updated as specified in Equations (2.2) and (2.3). This process is sped up by reducing the alignment derivatives matrix to non-zero rows and columns, which correspond to the alignables hit by the current track.

During each step, the current alignment parameters and their uncertainties, given by the covariance matrix, are stored in histograms. After all tracks have been processed, another histogram is created containing the final parameters and uncertainties. These histograms are written into a ROOT file together with additional information on the alignment process like the number of hits for each alignable.

The tracks contained in the sector test data set are ordered by their sector ID. To avoid a bias of the determined alignment due to the track ordering, a random map can be created to change the track positions in the processing sequence. This random map is created with the random seed 8071984 for all alignments which are determined in this work.

For each alignment parameter, zero is used as the starting value. The covariance matrix is initialised with startup errors of 10 (rad, cm) to avoid biasing the alignment results by the starting values. To fix alignables that are used as reference, a startup error of 10^{-5} (rad, cm) is applied.

4.3.1 Deterministic Annealing

As described in Section 2.2.1, deterministic annealing can be used to prevent the alignment algorithm from getting stuck in local minima of the parameter space. The convergence behaviour of the alignment parameters depends on the function $c(k)$ in Equation (2.4), by which the diagonal covariance matrix entries of all alignables are multiplied that are not fixed to define the reference system. A fast and well-behaved convergence is achieved using [11]

$$c(k) = 10000^{\frac{n-k}{n}}. \tag{4.3}$$

Here, n is the number of tracks which are processed until deterministic annealing stops, and hence should be a value between 1 and the number of tracks in the data set.
Using this annealing model, the uncertainty of the first track is largely increased, reducing its impact on the alignment parameters. The weights of the following tracks then are increased with each step, and eventually after processing n tracks, the annealing stops and all remaining tracks are regarded using their full weight.
Depending on the size of the data set, the annealing is applied to the first 100 - 5000 processed tracks. Unless stated otherwise, the standard annealing configuration with $n = 100$ is used.

4.3.2 Outlier rejection

To prevent bad measurements from having a large impact on the alignment results, outlier rejection is implemented. Tracks with a high χ^2 are rejected if the probability P for the track does not exceed a threshold value. The standard threshold is 0.5. The track probability calculation[1] is based on the incomplete gamma function Γ_{inc} using the track χ^2 and its number of degrees of freedom n_{dof}:

$$P(\chi^2, n_{dof}) = 1 - \Gamma_{inc}\left(\frac{n_{dof}}{2}, \frac{\chi^2}{2}\right) \tag{4.4}$$

$$\Gamma_{inc}(a, x) = \frac{1}{\Gamma(a)} \int_0^x t^{a-1} e^{-t} dt \tag{4.5}$$

with the gamma function Γ.

An additional outlier rejection is implemented by sorting out tracks that move the alignment parameters beyond their uncertainties. Tracks with this effect are assumed to result from noise clusters in the track reconstruction. Considering the fact, that the current alignment parameters combine the information of all previously processed tracks, one additional track should not have an impact that large on the results. This threshold can be adjusted, too, but the standard value is one times the parameter uncertainty.
Unless stated otherwise, all alignments are estimated using both rejection methods and the standard thresholds.

[1] The probability function "TMath::Prob(chi2,ndf)" of the ROOT framework [18] is used.

5. Sector Test Data

This chapter covers analysis of the data taken during the sector tests (see Section 3.1). After describing the basic characteristics of the data, the performed alignment studies are specified. These are classified into studies on disc level and studies on petal level.

5.1 Data Characteristics

Each of the eight TEC+ sectors has been tested separately. Therefore, there is no data set containing tracks that connect two sectors; and hence, a part of each sector has to be used as reference to define eight sector specific coordinate systems.

For each sector with an odd sector ID, there are beetween 4000 and 6000 tracks available after the χ^2 cut. Due to a better trigger configuration, which was applied after integration of the odd-ID sectors, sectors with an even sector ID have a larger data set. For these, between 35 000 and 60 000 tracks have been collected that fulfil the χ^2 requirements. In total, the sector test data contain about 220 000 tracks which can be used for alignment.
All collected data were merged to a global data set to make disc level alignment with tracks of more than one sector possible. For each of the following studies, this set of tracks is used.

5.2 Disc Alignment

The largest substructures inside the TEC+ are the nine discs. The first alignment studies examine movements of these substructures, while the petals (and modules) are fixed to their nominal positions on the discs. The most important contributions are the corrections Δx, Δy, and $\Delta\phi$, which are displacements perpendicular to the z-axis and rotations around it.

The coordinate system is defined by fixing the mean and slope of the deviations as a function of z to zero (as described in Section 2.5). At first, disc 1 is fixed and movements of the other discs are determined with respect to it. After running the algorithm, the evaluated alignment parameters are converted into the mentioned coordinate system by subtracting a linear fit from them.

5.2.1 Alignment in ϕ

To get familiar with the data set, it is reasonable to begin with a small set of alignables and one degree of freedom per alignable. Therefore, the most simple alignment, a disc level alignment in ϕ, is determined.

The parameter evolution (Fig. 5.1) shows convergence after a settling phase of about 40 000 tracks. The first disc is fixed during the alignment procedure to define the coordinate system. Therefore, its parameter is not moving.
For all non-fixed discs, the shape of the parameter evolution looks similar. These common movements of the free parameters are a sign of high (mathematical) correlation among the discs and corresponds to the weak mode of a linearly increasing torsion of the TEC+, which is subtracted from the final alignment parameters.

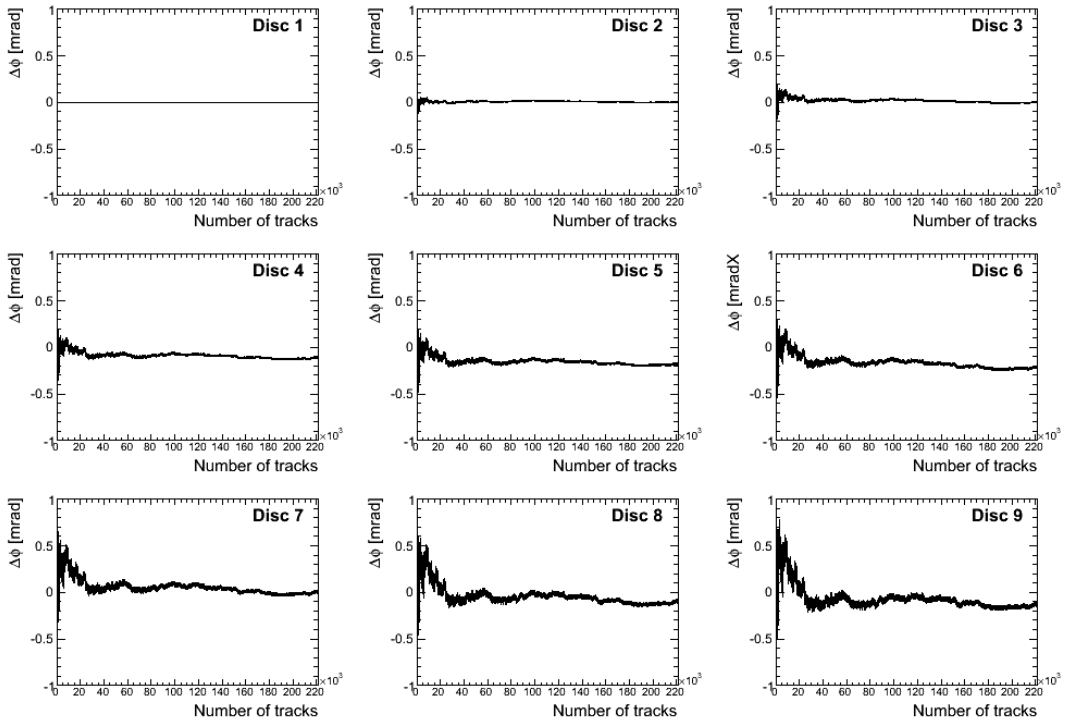


Figure 5.1: Evolution of alignment parameter $\Delta\phi$ during disc alignment in ϕ: The estimated disc rotation is plotted against the number of tracks processed by the alignment algorithm. The width of the band indicates the error of the parameter.

The results of the alignment algorithm (Tab. 5.1, Fig. 5.2) are corrections to the disc rotation angles ϕ of up to about 0.1 mrad. These corrections can be determined with a precision of about 0.005 mrad. A rotation of 0.1 mrad corresponds approximately to a movement of 100 μm at the disc margin. This is consistent with the mounting accuracy of the TEC+.

5.2.2 Alignment in x, y, ϕ

It is expected that the actual disc placement inside the TEC+ differs not only in the orientation ϕ from the ideal geometry. An alignment is done to determine the disc displacements Δx and Δy in addition to corrections $\Delta\phi$.

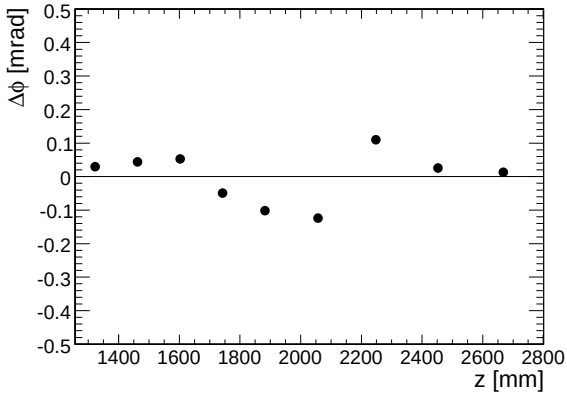


Figure 5.2: Alignment parameters for disc alignment in ϕ. Error bars are displayed, but are smaller than the symbol size.

The magnitude of the obtained displacements (Tab. 5.2, Fig. 5.3) is up to 150 μm, which is compatible to the size of movements at the disc margin due to estimated corrections of ϕ alone. The mounting precision of the TEC+ discs is of the same order of magnitude.

The displacements are determined with an accuray of about 5 μm. Compared to the alignment in ϕ only, there is no significant difference in the corrections $\Delta\phi$. Thus, fixing the parameters x and y does not seem to bias the calculated corrections of the disc orientations.

5.2.3 Alignment in x, y, z, ϕ

For corrections to the three remaining degrees of freedom z, α, and β, a lesser sensitivity is expected because these parameters describe corrections to position and rotations of the discs that do not lie inside the silicon sensor planes and can hence not be detected in first order. Nevertheless, these corrections can be determined with a sufficiently large set of tracks by second order effects.
In order to test the algorithm's sensitivity to displacements in z with the current data set and to detect major dislocations orthogonal to the disc planes, an alignment in x, y, z and ϕ is evaluated. The evolution of Δz during the alignment process (Fig. 5.4) shows movements of a few millimeters during the settling phase. These

Table 5.1: Alignment parameters obtained from disc alignment in ϕ

Disc number	$\Delta\phi$ [mrad]
1	0.0298 ± 0.0073
2	0.0439 ± 0.0056
3	0.0525 ± 0.0041
4	-0.0492 ± 0.0027
5	-0.1016 ± 0.0017
6	-0.1235 ± 0.0019
7	0.1100 ± 0.0037
8	0.0254 ± 0.0062
9	0.0127 ± 0.0091

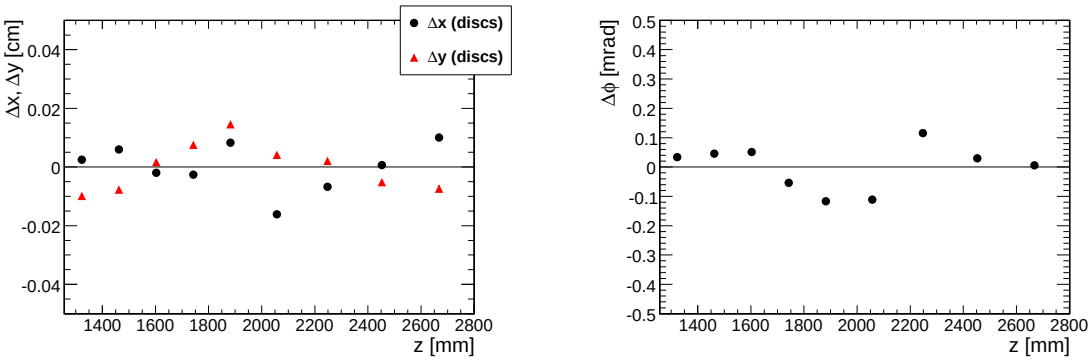


Figure 5.3: Alignment parameters for disc alignment in x, y, ϕ. Error bars are displayed, but are smaller than the symbol size.

are considerably larger than those of Δx during the pevious alignment study. This and the larger error bars indicate the expected lesser sensitivity to this parameter.

The calculated alignment parameters Δx, Δy and $\Delta\phi$ (Tab. 5.3, Fig. 5.5) show no significant differences from the previously determined results. It is concluded that fixing z also does not significantly bias the determination of the other parameters. There is a slight increase of the error estimates, though, due to the fact that more parameters are being estimated with the same amount of track input.
Displacements of up to 150 μm along the beam axis are being determined. They are of the same order of magnitude as the disc displacements in x and y, which is reasonable. Unlike position corrections in the disc planes, Δz can only be calculated with an accuracy of about 50 μm with this data set.
A similarity between the corrections Δz and Δy can be observed. The empirical correlation coefficient of Δy and Δz for the nine discs yields 0.87. There is no obvious reason for a correlation between displacements in those directions so the correlation is assumed to be a coincidence.

5.3 Petal Alignment

The 16 petals on each disc are not expected to be perfectly mounted but to be distributed around the ideal positions within the bounds of their mounting accuracy. Two alignments of the 144 petals have been determined to measure the displacements of the petals and to get an estimate for the precision with which the petals were

Table 5.2: Alignment parameters obtained from disc alignment in x, y, ϕ

Disc number	Δx [mm]	Δy [mm]	$\Delta\phi$ [mrad]
1	0.024 ± 0.008	-0.099 ± 0.008	0.0336 ± 0.0073
2	0.060 ± 0.006	-0.077 ± 0.006	0.0453 ± 0.0056
3	-0.020 ± 0.004	0.017 ± 0.004	0.0512 ± 0.0041
4	-0.026 ± 0.003	0.076 ± 0.003	-0.0536 ± 0.0027
5	0.083 ± 0.002	0.146 ± 0.002	-0.1170 ± 0.0017
6	-0.162 ± 0.002	0.042 ± 0.002	-0.1114 ± 0.0019
7	-0.067 ± 0.004	0.021 ± 0.004	0.1158 ± 0.0037
8	0.007 ± 0.006	-0.051 ± 0.007	0.0299 ± 0.0062
9	0.100 ± 0.010	-0.074 ± 0.010	0.0062 ± 0.0092

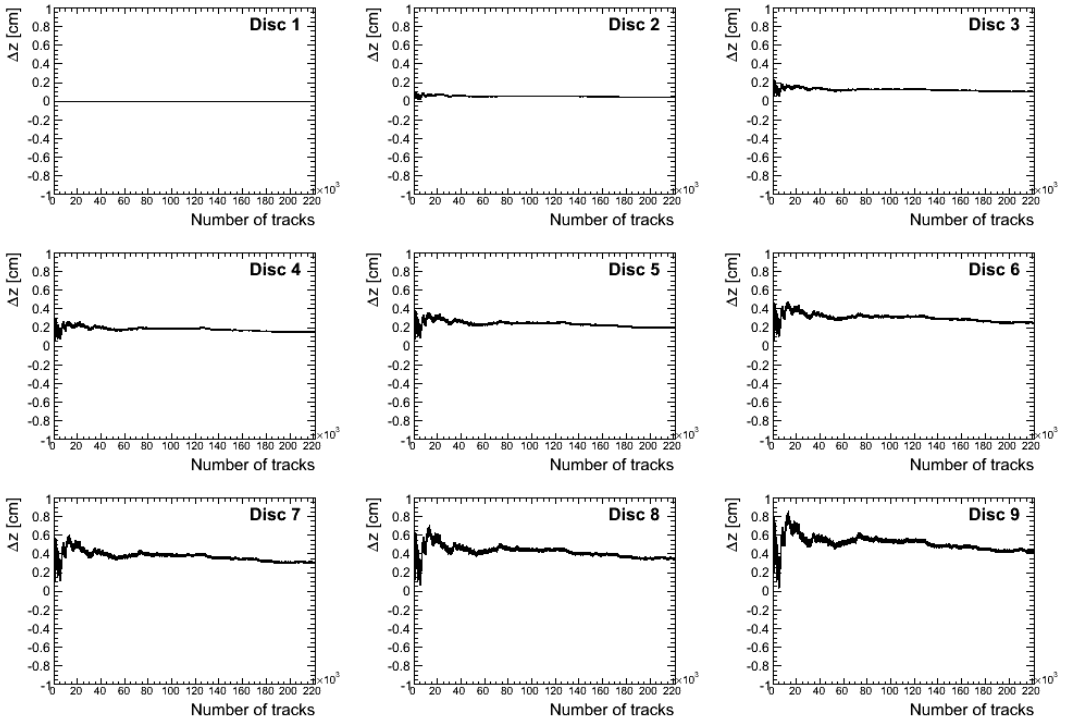


Figure 5.4: Evolution of alignment parameter Δz during disc alignment in x, y, z, ϕ: The estimated disc displacement is plotted against the number of tracks processed by the alignment algorithm. The width of the band indicates the error of the parameter.

mounted onto the discs. These alignments will be discussed below.
Because of having no tracks in the data set which connect two sectors with each other, a separate coordinate system has to be defined for each sector. Therefore, for each sector, the front petal on disc 1 is fixed during the alignment process. Afterwards, the coordinate system for each sector is defined by setting the mean and slope (as a function of the petal z coordinates) of the deviations to zero, and the estimated parameters are being transformed into these coordinate systems.

For petal alignment, more tracks are needed to update all alignables than for a disc alignment. Thus, the number of tracks until the deterministic annealing stops is increased to 5000 ($n = 5000$ in (4.3)).

Table 5.3: Alignment parameters obtained from disc alignment in x, y, z, ϕ

Disc number	Δx [mm]	Δy [mm]	Δz [mm]	$\Delta\phi$ [mrad]
1	0.020 ± 0.009	-0.097 ± 0.010	-0.120 ± 0.047	0.0464 ± 0.0123
2	0.060 ± 0.007	-0.077 ± 0.008	-0.111 ± 0.036	0.0573 ± 0.0095
3	-0.019 ± 0.005	0.018 ± 0.006	0.057 ± 0.027	0.0468 ± 0.0069
4	-0.024 ± 0.003	0.074 ± 0.004	0.087 ± 0.018	-0.0625 ± 0.0045
5	0.086 ± 0.002	0.146 ± 0.002	0.117 ± 0.012	-0.1288 ± 0.0025
6	-0.161 ± 0.002	0.040 ± 0.003	0.118 ± 0.013	-0.1259 ± 0.0030
7	-0.065 ± 0.005	0.020 ± 0.005	0.062 ± 0.024	0.1078 ± 0.0063
8	0.008 ± 0.008	-0.051 ± 0.009	-0.163 ± 0.040	0.0426 ± 0.0105
9	0.095 ± 0.012	-0.073 ± 0.013	-0.046 ± 0.062	0.0163 ± 0.0153

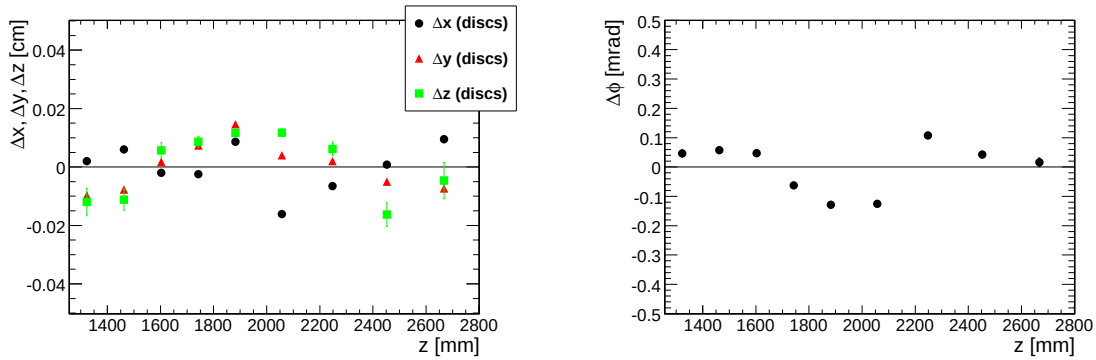


Figure 5.5: Alignment parameters for disc alignment in x, y, z, ϕ. Error bars for Δx, Δy, and $\Delta\phi$ are displayed, but are smaller than the symbol size.

5.3.1 Alignment in ϕ

At first, the most simple alignment on petal level, an aligment with just ϕ as a free parameter, is estimated. Here, ϕ is defined as rotation of the petal centre of mass around the disc center rather than of the petal around its own center. This allows a comparison of the petal alignment results to the already determined disc alignment.

There are less tracks and hence less updates for the parameters of petals in odd-ID sectors available. The parameter evolution of these petals (Fig. 5.6) points out, that the algorithm barely reaches the end of the settling phase, while the evolution of corrections to the other petals show a good convergence towards a stable limit.

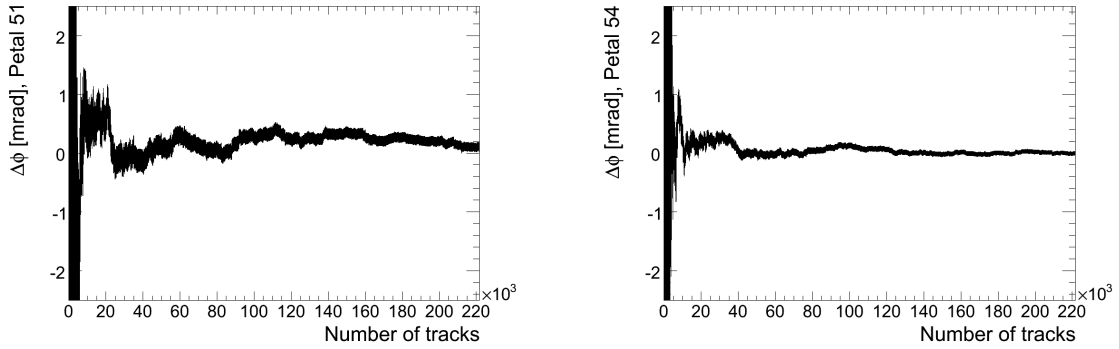


Figure 5.6: Evolution of $\Delta\phi$ for petal alignment in ϕ for two petals. On the left, the evolution for the disc 4 front petal in sector 1 is displayed. On the right, the correction for the corresponding petal in sector 4 is shown.

The determined petal corrections $\Delta\phi$ are distributed around the previously estimated disc orientations (Fig. 5.7, App. A). Most petals agree with the disc corrections within their errors, but there are also some deviations of up to 0.2 mrad visible. These are compatible with the mounting precision of the TEC+. Due to the lower track rate in TEC+ sectors with odd ID, the uncertainties on the alignment in these sectors are significantly larger.

5.3.2 Alignment in x, y, ϕ

After the alignment in ϕ alone, now a petal alignment with three free parameters, x, y, and ϕ, is determined. For the displacements x and y, the global coordinate

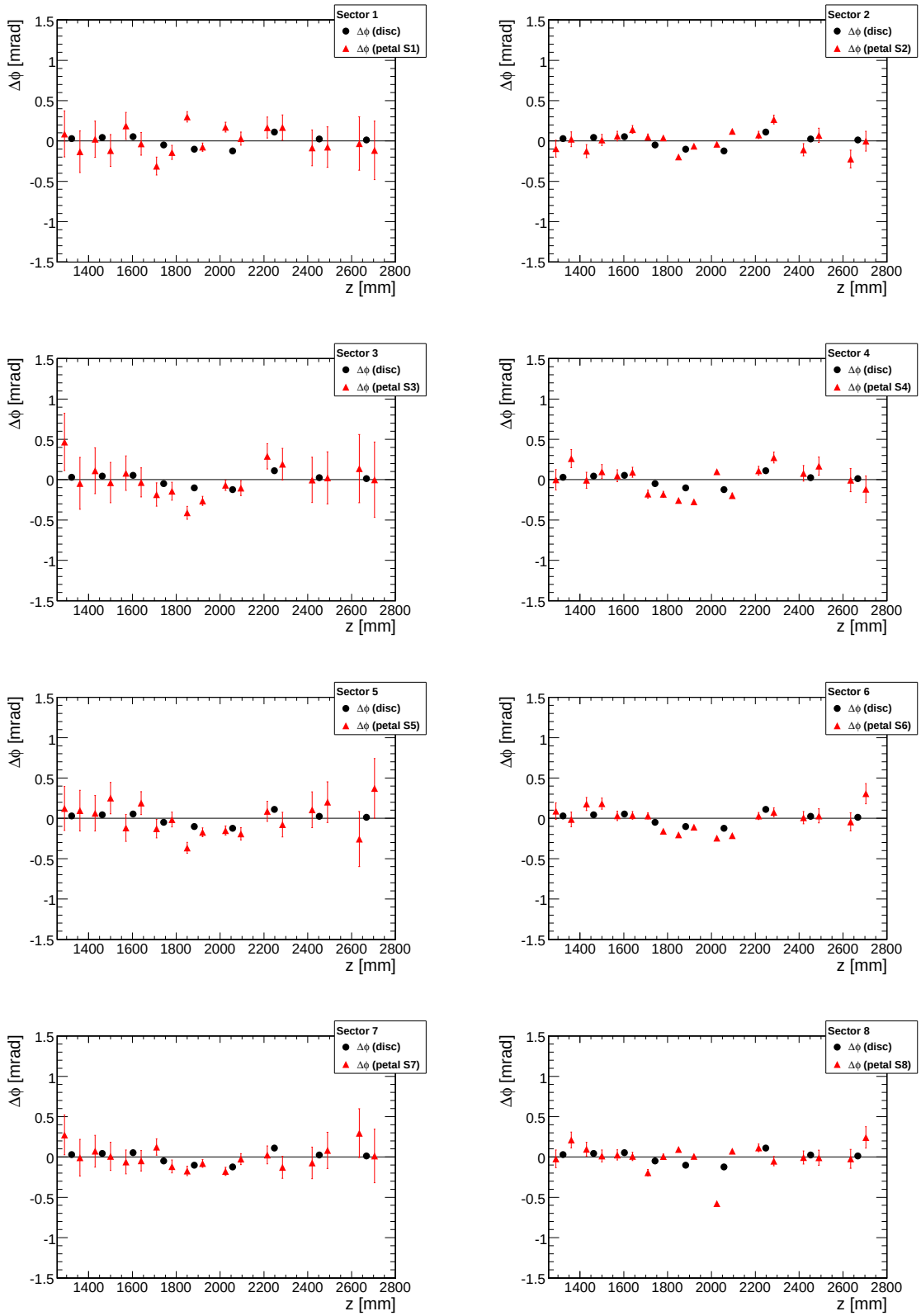


Figure 5.7: Alignment parameters for petal alignment in ϕ for the eight TEC+ sectors.

system is used, meaning that the corrections Δx and Δy are defined similarly to those in the disc alignment and can hence be directly compared to these.
The parameter evolution (Fig. 5.8) shows large error values even after all tracks have been processed. These errors are especially large in odd-ID sectors. The alignment results for an odd-ID and an even-ID sector are shown in the Figures 5.9 and 5.10. The alignment parameters for the remaining sectors can be found in Appendix A.
The estimated petal parameters are distributed around the disc corrections, but with a rather large spread of up to about 0.5 mrad in ϕ and 0.5 mm in the x and y direction. This spread, however, is compatible with the large correction uncertainties.

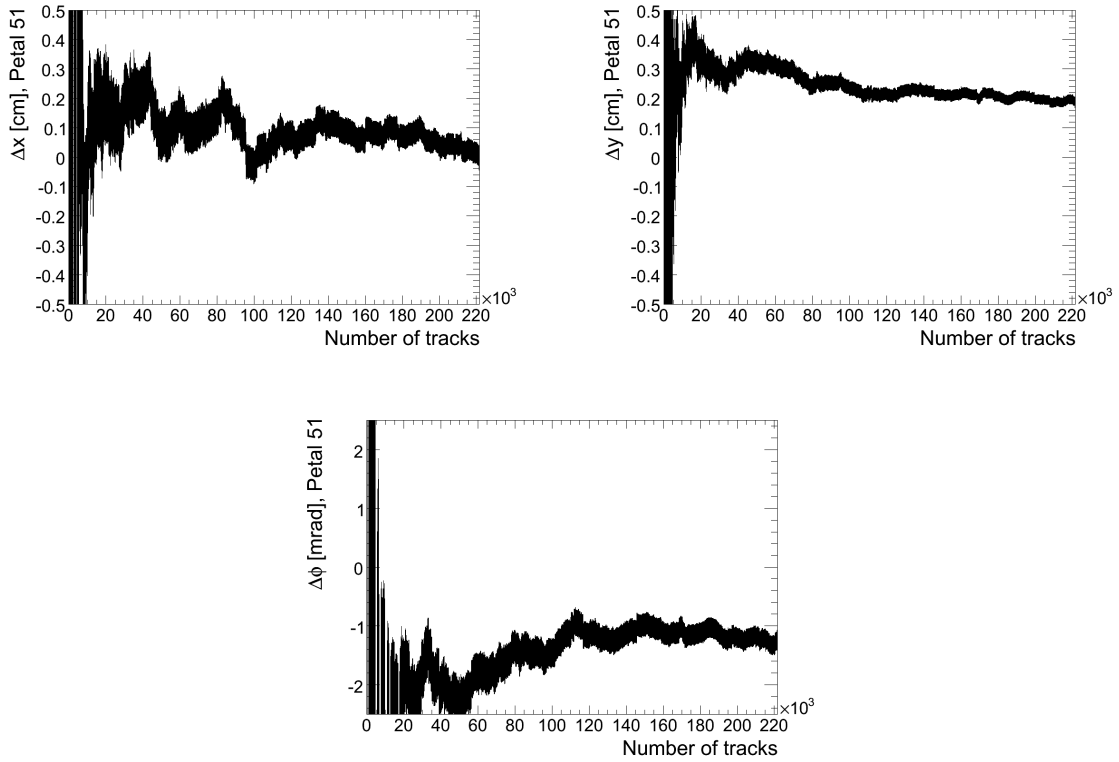


Figure 5.8: Evolution of Δx, Δy, and $\Delta\phi$ for petal alignment in x, y, ϕ for the front petal in sector 1 of disc 4.

The petals have different silicon strip orientations in relation to the global coordinates x and y. The modules are mounted on the petals such that the strips run radially outwards. Due to significantly higher measurement precision perpendicular to the strip direction, the sensitivity to corrections in x and y varies with the petal orientation and hence the regarded TEC+ sector.
In sector 1, the direction of the strips is predominantly along the global x axis. Therefore, Δy can be determined with smaller uncertainties than Δx (Fig. 5.9). In sector 4, the strips run predominantly diagonal to x and y axis, and hence the errors on both corrections, Δx and Δy, are of equal magnitude (Fig. 5.10).

A sketch of the TEC+ petals and their displacements is shown in Figure 5.11. The corrections are scaled to a visible order of magnitude. The errors, which strongly variate in size for different sectors and discs, are not considered in this sketch.

Considering the alignment precision, most estimated petal displacements in x, y, and ϕ are not significant. At this point, the limit of the data set is reached. Far more

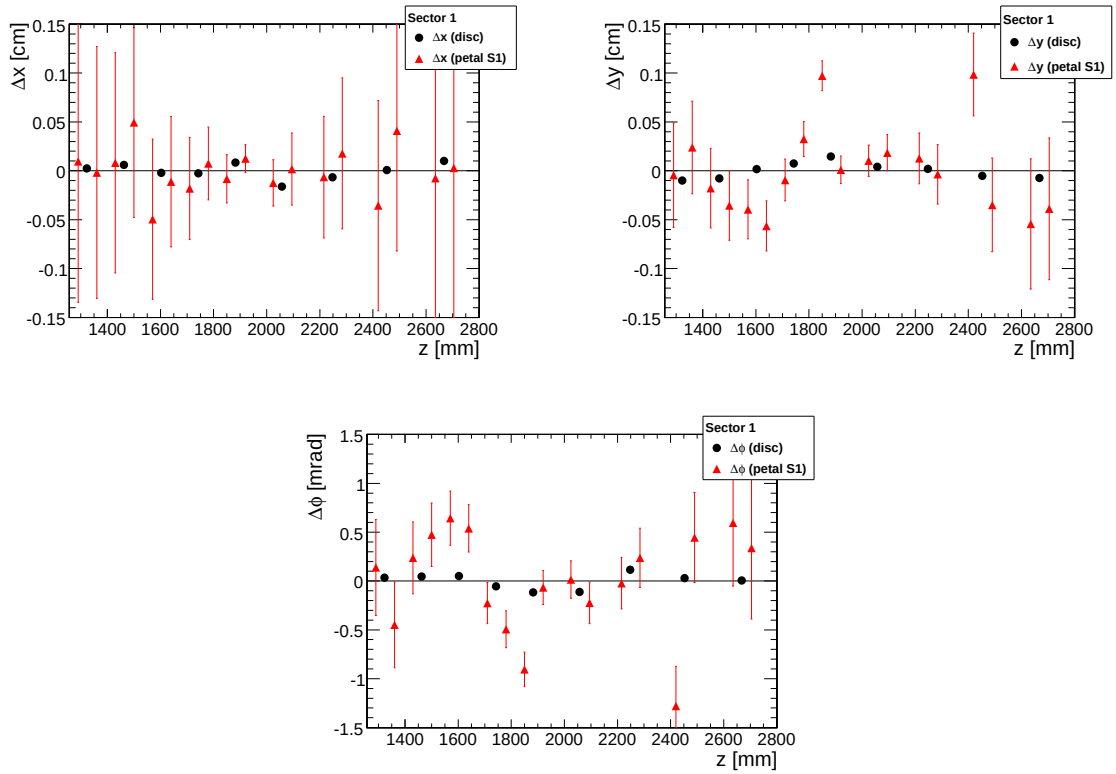


Figure 5.9: Alignment parameters for petal alignment in x, y, and ϕ for TEC+ sector 1

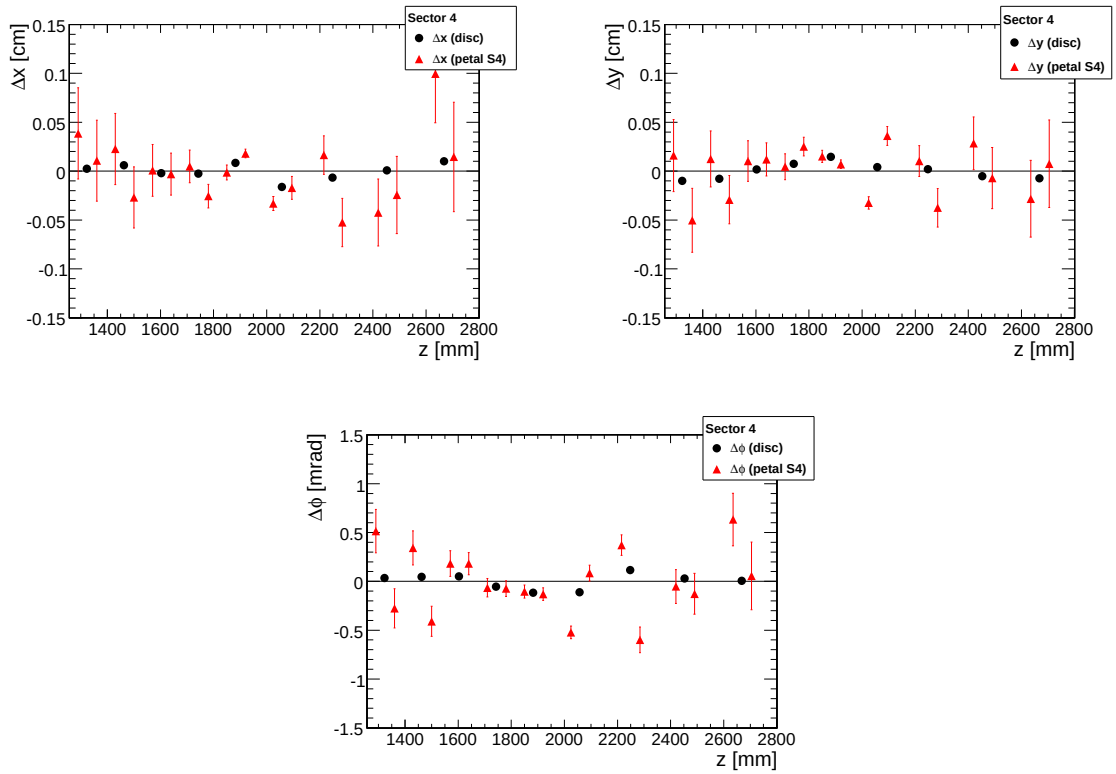


Figure 5.10: Alignment parameters for petal alignment in x, y, and ϕ for TEC+ sector 4.

tracks are needed to determine an accurate petal alignment in three parameters. In general, the petal corrections agree with the disc correction within the accuracy that can be reached with the current track sample. But there are some outliers, for example $\Delta\phi$ for the front petal on disc 6 and the back petal on disc 7, both in sector 4. These outliers differ from the disc alignment up to 0.5 mrad with uncertainties of about 0.2 mrad. In Δx and Δy, there are outliers as well. These differ from the disc alignment up to 0.8 mm with an uncertainty of about 0.2 mm (for example the front petal on disc 5 in sector 1).

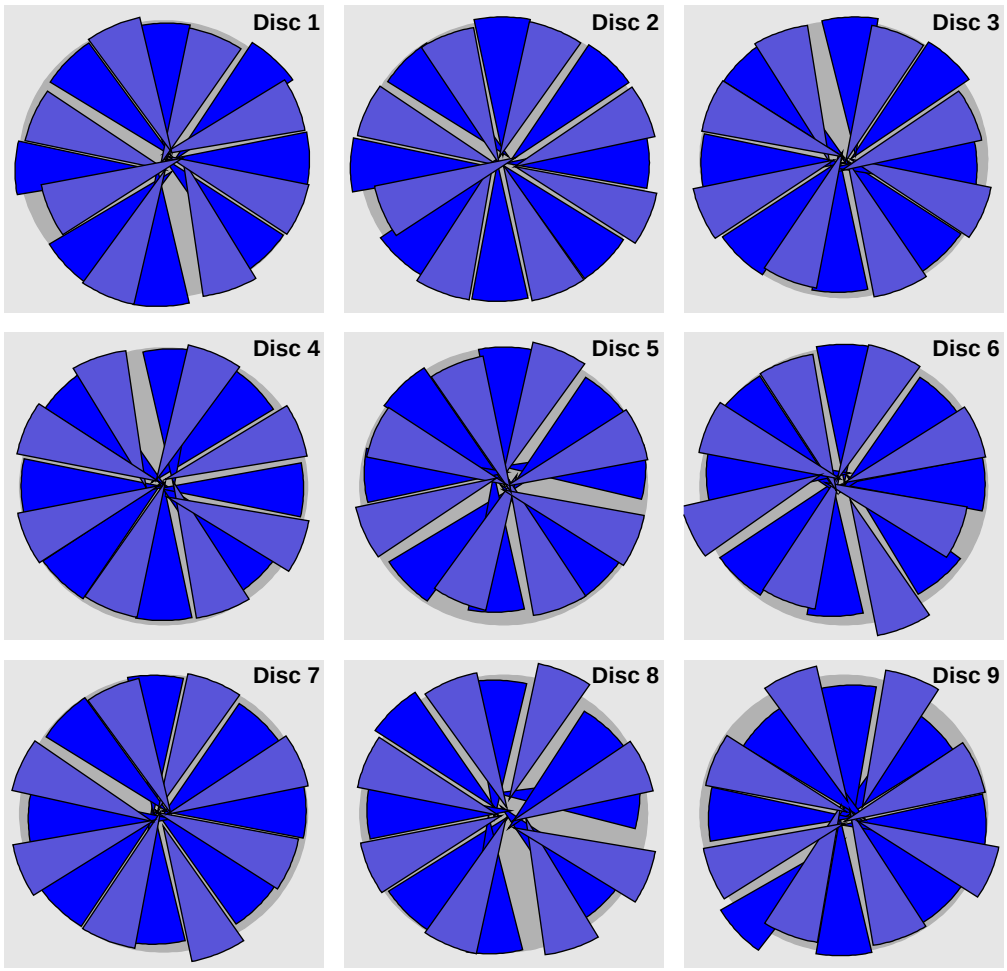


Figure 5.11: Sketch of petal corrections at petal alignment in x, y, and ϕ. Position and orientation corrections of the petals are scaled by a factor of 150.

6. Slice Test Data

This chapter covers alignment studies based upon data from the slice test. Slice test setup and data taking have been detailed in Section 3.2. First, characteristics of the data and their impact on the alignment studies are specified. After that, the results from a disc level alignment are detailed and their dependence on tracker temperature is examined. Finally, an alignment study on petal level is discussed.

6.1 Data Characteristics

Less than 10% of the events which have been recorded with TEC+ active have been taken with scintillator configuration A or B. Therefore, very few tracks are reconstructed in scintillator configuration A and B, while a large set of tracks is available in configuration C. Thus, the configuration C data is used for the following alignment studies.

Muon tracks were recorded with both, sectors 2 and 3 of the TEC+, operational. Thus, there are tracks in the sample which connect the two sectors with each other. Accordingly, to define the coordinate system, it is sufficient to fix one disc for disc level alignments and one petal for petal level alignments. An exception is data taken at -15 °C: Due to cooling limitations, all front petals had been deactivated. Thus, no connection between the two active back petal towers can be established using the available tracks because these cross the tracker essentially vertically. For these data, a coordinate system has to be defined for each petal tower separately.

For each temperature level, there are between 700 and 6000 tracks available which fulfil the χ^2 and hit number requirements and can be used for alignment. The hits of these tracks are not distributed uniformly in the TEC+. Due to the position of the scintillators, there are more hits on discs which are closer to the interaction point (Fig. 6.1). Thus, alignment parameters of these discs should be determined more precisely than those of the other discs.

6.2 Disc Alignment

In the following, a disc alignment study using slice test data is described. The coordinate system is defined by fixing the first TEC+ disc. Therefore, the alignment

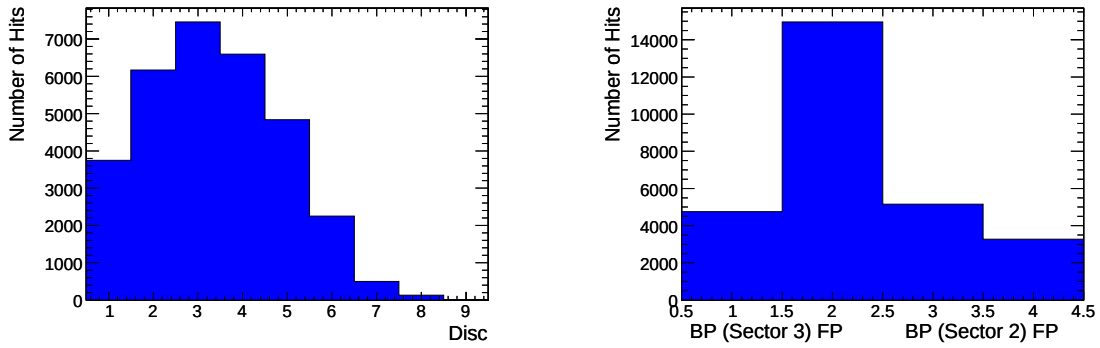


Figure 6.1: The number of hits per disc for the -10 °C data is shown on the left. On the right, the number of hits per petal tower in these runs is displayed.

algorithm estimates displacements of the other discs relative to the mean of the sensor module positions in sectors 2 and 3 of disc 1.
Because there are less than 6000 usable tracks per temperature level and only data from two sectors, there is no sensitivity to more than one alignment parameter. Therefore, the only aligned parameter is ϕ.

6.2.1 Temperature dependence

To examine temperature stability of the TEC+, a disc alignment in ϕ is determined for all available temperature levels. No correction can be calculated for disc 9 at $T = -15$ °C and $T = 14$ °C because this disc is never hit in these data sets. Comparing the results for the different tracker temperatures, good agreement is found (Fig. 6.2).

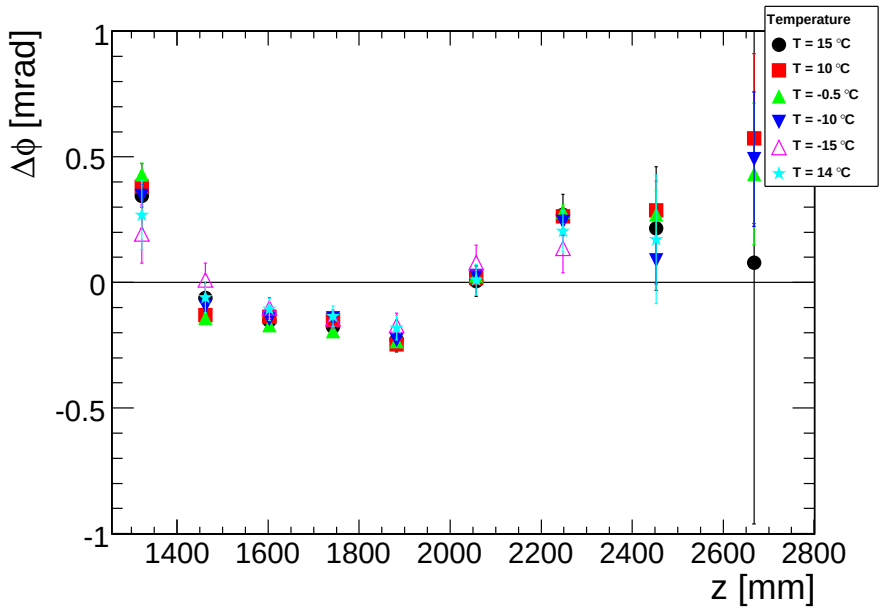


Figure 6.2: Alignment parameters for disc alignment in ϕ for different temperatures.

Figure 6.3 displays the parameter evolution for the largest data set (tracker temperature of -10 °C). It shows a good convergence; but, due to the low number of hits, a very large error on the correction $\Delta\phi$ of disc 9.
To increase the precision of the alignment results, the available data sets are merged excluding the -15 °C set because of the different experimental setup. The agreement among the determined corrections implies a good stability of the TEC+ with temperature. Therefore, a merging of the data taken at different tracker temperatures to increase alignment accuracy is reasonable.

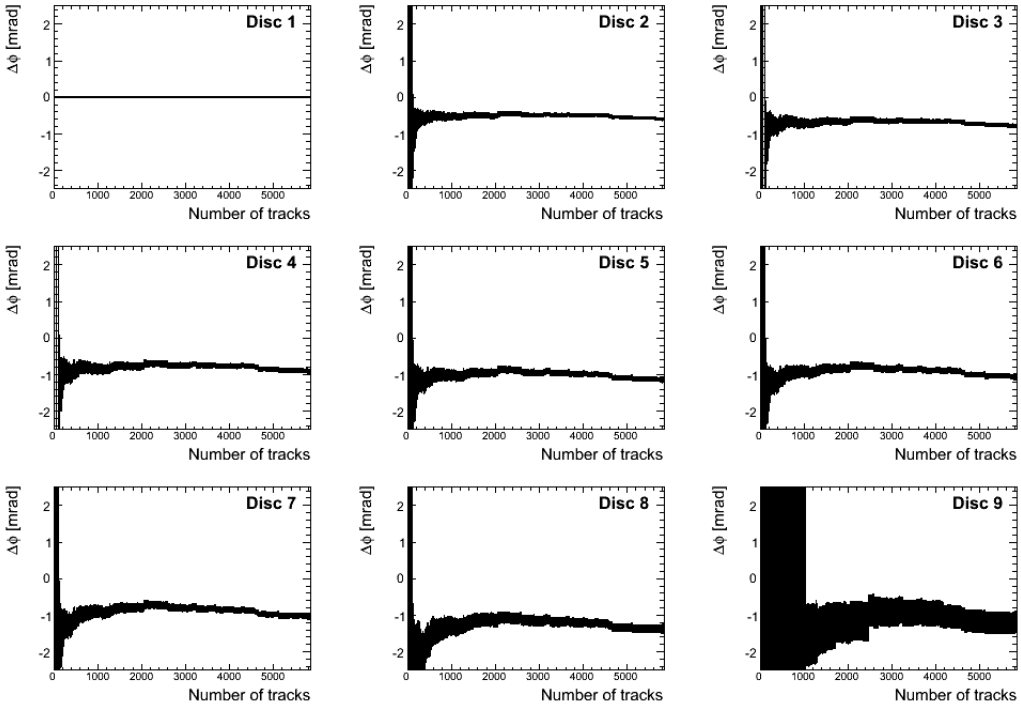


Figure 6.3: Evolution of alignment parameters for disc alignment in ϕ with data taken at a tracker temperature of $T = -10$ °C.

6.2.2 Alignment in ϕ

A disc alignment in ϕ is estimated with data from different tracker temperatures (except $T = -15$ °C) merged (Tab. 6.1, Fig. 6.4).

Table 6.1: Alignment parameters obtained from disc alignment in ϕ

Disc number	$\Delta\phi$ [mrad], merged T	$\Delta\phi$ [mrad], $T = -10$ °C
1	0.5322 ± 0.0317	0.4288 ± 0.0545
2	-0.0705 ± 0.0244	-0.0435 ± 0.0408
3	-0.1549 ± 0.0226	-0.1290 ± 0.0375
4	-0.2367 ± 0.0219	-0.1592 ± 0.0362
5	-0.3171 ± 0.0217	-0.2793 ± 0.0358
6	-0.0795 ± 0.0215	-0.0675 ± 0.0355
7	0.1182 ± 0.0228	0.1014 ± 0.0379
8	0.0043 ± 0.0356	-0.1015 ± 0.0607
9	0.2041 ± 0.1432	0.2499 ± 0.2297

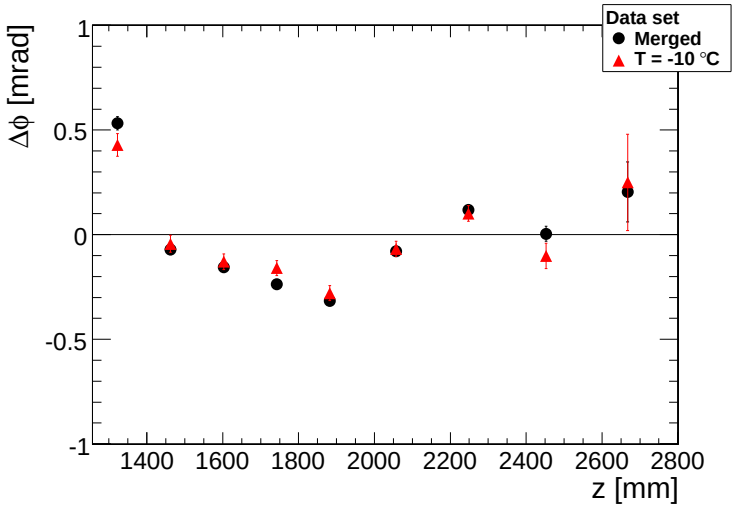


Figure 6.4: Alignment parameters for disc alignment in ϕ for $T = -10$ °C data and data merged from all temperature runs (except $T = -15$ °C).

The calculated orientation corrections have a reasonable order of magnitude. While the correction to disc 1 is slightly off with about 0.5 mrad, $\Delta\phi$ is up to 0.3 mrad for the remaining discs. These corrections correspond to movements of up to about 300 μm at the outer disc circumference.

6.3 Petal Alignment

As already mentioned in the previous section, there is no sensitivity to more than one parameter; hence, the TEC+ petals are aligned just in ϕ. The reference system is defined by fixing the front petal in sector 3 of disc 1 to ideal position, and hence the mean of its sensor area. This petal is chosen because it covers the ϕ range with the highest hit density (Fig. 6.1).

6.3.1 Alignment in ϕ

A petal alignment in ϕ is determined and shown in Table 6.2. Figure 6.5 displays the calculated petal corrections $\Delta\phi$ in comparison to the previously estimated disc corrections. Two petals on disc 9 have never been hit in this data set. Thus, they still carry the large startup error and differ from zero only due to the transformation of the parameters into the correct reference system (mean and slope fixed to zero).

The petal corrections are distributed around the disc corrections with a spread of up to 0.2 mrad. This spread is of the same order of magnitude that has already been observed in the petal alignment with the sector test data. Due to the lower number of tracks, the orientations of the petals of discs 8 and 9 cannot be determined as precisely as those of the other petals. However, within their uncertainty, they also agree with a range of 0.2 mrad around the disc positions.
The petals of disc 1 are distributed around the disc alignment parameter with a very large spread of about 0.8 mrad. These unusually large petal corrections yield an explaination for the unusually large correction $\Delta\phi$ determined for disc 1: Basically, since the alignment parameter for a disc is the mean of the petal parameters weighted

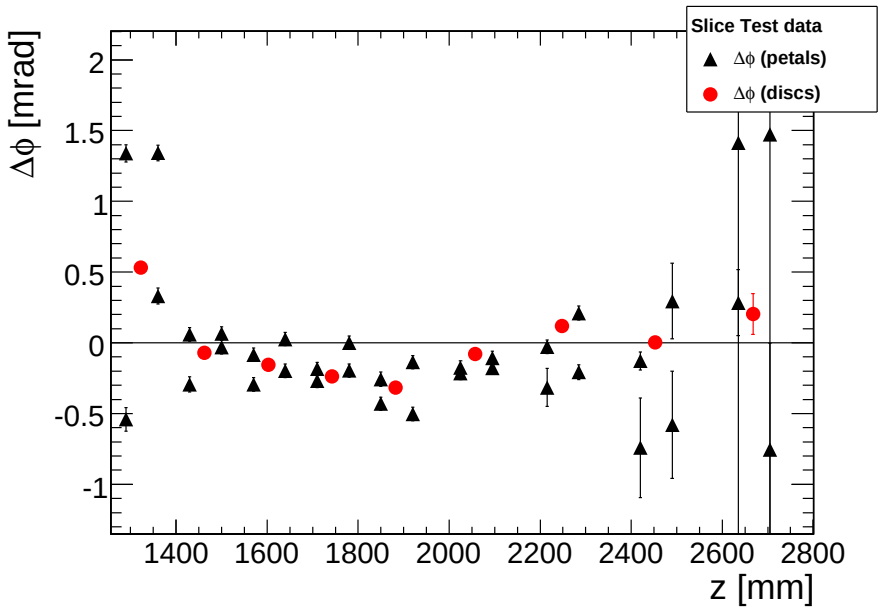


Figure 6.5: Alignment parameters for petal alignment in ϕ estimated with slice test data. For comparison, the disc alignment results are also displayed.

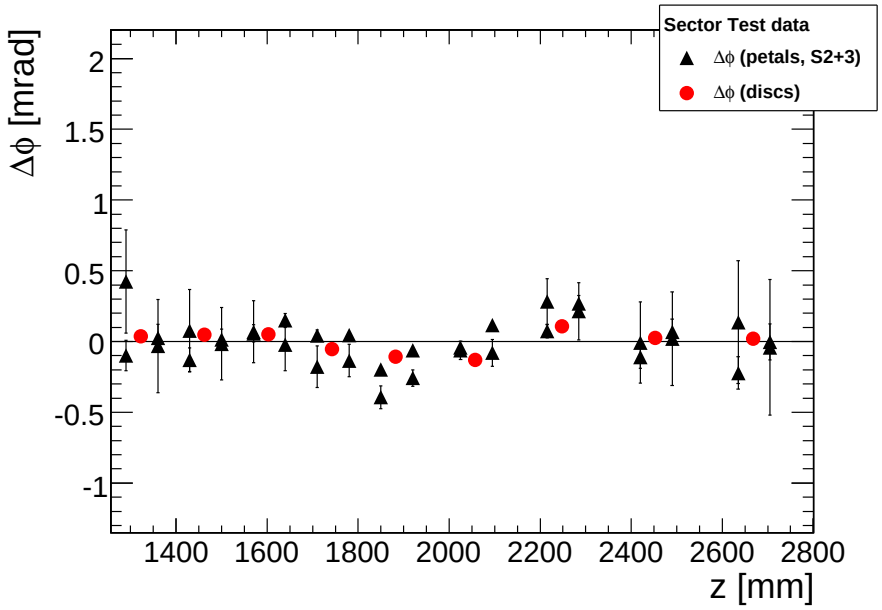


Figure 6.6: Alignment parameters for petals in TEC+ sectors 2 and 3 obtained from petal alignment in ϕ with sector test data. The disc alignment in ϕ (estimated with the entire sector test data set) is also displayed for comparison.

by the number of hits on the petals, the disc parameter can take each value in the interval created by the petal parameters depending on the petal hit distribution. Still, an explaination for the large petal alignment parameters of disc 1 with the slice test data has to be found. Figure 6.6 displays the petal alignment for sectors 2 and 3 estimated with the sector test data. Here, the alignment parameters for the petals of disc 1 do not show a spread of that magnitude. More information on this and the comparison of the data sets is given in the context of comparison studies detailed in Chapter 7.

Table 6.2: Alignment parameters $\Delta\phi$ for the 4 active petals on each disc

Disc number	S2FP $\Delta\phi$ [mrad]	S3FP $\Delta\phi$ [mrad]	S2BP $\Delta\phi$ [mrad]	S3BP $\Delta\phi$ [mrad]
1	-0.718 ± 0.080	1.161 ± 0.052	0.186 ± 0.047	1.197 ± 0.044
2	-0.407 ± 0.042	-0.054 ± 0.034	-0.114 ± 0.034	-0.018 ± 0.033
3	-0.344 ± 0.034	-0.134 ± 0.031	-0.217 ± 0.032	0.008 ± 0.031
4	-0.256 ± 0.033	-0.171 ± 0.030	-0.152 ± 0.032	0.046 ± 0.031
5	-0.181 ± 0.036	-0.354 ± 0.030	-0.028 ± 0.032	-0.395 ± 0.032
6	-0.020 ± 0.033	-0.058 ± 0.031	0.010 ± 0.032	0.081 ± 0.032
7	-0.075 ± 0.135	0.214 ± 0.033	0.066 ± 0.041	0.483 ± 0.037
8	-0.406 ± 0.387	0.206 ± 0.057	-0.213 ± 0.416	0.660 ± 0.280
9	1.844 ± −	0.715 ± 0.239	-0.291 ± 0.793	1.935 ± −

7. Result Interpretation and Comparison

7.1 Comparison of Sector and Slice Test Results

For TEC+ stability validation, a comparison of the sector test and slice test results is made. Two equivalent data sets are needed for a comparison. The first set is created by merging the tracks of all slice test temperature runs (excluding the tracks recorded at $T = -15\,°\mathrm{C}$ because of the different experiment setup). The sector test data of sectors 2 and 3 are merged to create the second set.
With both sets a disc level alignment in ϕ is determined (Fig. 7.1). Track reconstruction and alignment are done using the same geometry. The sector test data are processed with a backport of the CMSSW_1_3_6 geometry. Thus, CMSSW_1_3_6 is also used for processing of the slice test data.

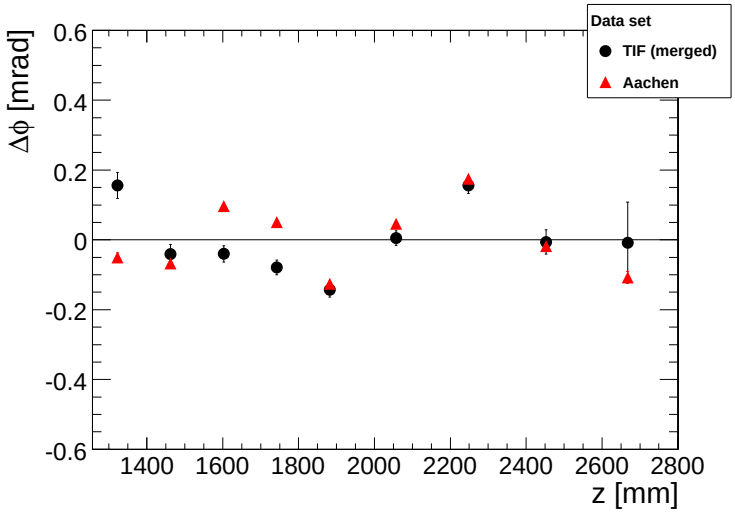


Figure 7.1: Corrections $\Delta\phi$ calculated with equivalent sets of slice test and sector test data.

Considering that they have been determined with two completely independent data sets, the corrections agree very well with each other except for the corrections of disc 1, 3, and 4, which show a difference of up to 0.2 mrad.
After performing the sector test and before the slice test, the TEC+ has been tilted from vertical into horizontal position, transported in a truck a distance of about 800 km from Aachen to Geneva, integrated into the tracker, and subject to multiple temperature cycles between 15 °C and -15 °C. In sectors 2 and 3, two petals have been replaced at CERN before integration of the TEC+ into the tracker: One on discs 3 and one on disc 4, which explains a difference in the estimated alignment parameters.
The alignment estimated with the sector test data set does not confirm the large correction to disc 1 in the alignment determined with the other data set. The anomalous $\Delta\phi$ value is caused by unusually large corrections to the petal orientations on this disc (see Section 6.3), but this seems to be a data set specific effect.

The conclusion drawn from this comparison is that the TEC+ (at least concerning discs 2 to 9) has endured its transport without significant deformations – its mechanical stability is very good.
Not only have the compared track data been recorded independently from each other, the two parts of the result calculation are also done with two independent computer programs. While the sector test data are being processed with an ORCA program, the slice test results are being estimated using a CMSSW program. The good agreement among the results indicates that these programs do not bias the determined alignment.

7.2 Sensitivity to torsion

To test the algorithm's sensivity to a torsion of the TEC+ which increases linearly with z, a comparison of the sector test and the slice test disc level alignment is made, without subtracting the slope of the deviations (Fig. 7.2). Assuming that a linearly increasing torsion is a weak mode to which the algorithm is not sensitive, the results are expected to differ in a linear component because of using two independent data sets.

Ignoring the differences that already have been observed in the previous comparison of the two alignments, the corrections determined from the different data sets match each other very well. This agreement is not a sufficient criterion to proove the sensitivity of the algorithm to this kind of deformations. However, it is a necessary criterion indicating that this sensitivity is likely to be existing.

The parameters x and y cannot be aligned with the slice test data. Therefore, disc shiftings in x and y are transformed by the algorithm into corrections of the free parameter ϕ. When subtracting the slope of the deviations, no significant changes of $\Delta\phi$ can be seen between a disc alignment in ϕ and one in x, y, and ϕ (see Section 5.2). When only subtracting the mean of the corrections, there are considerable differences visible (Fig. 7.3). Accordingly, displacements of the alignables along fixed parameters are converted into linear components in the corrections of the free parameters, to which the algorithm (with the current data set) is less sensitive. Therefore, it is necessary to align not only ϕ, but also x and y if the linear component of the TEC+ torsion is to be determined.

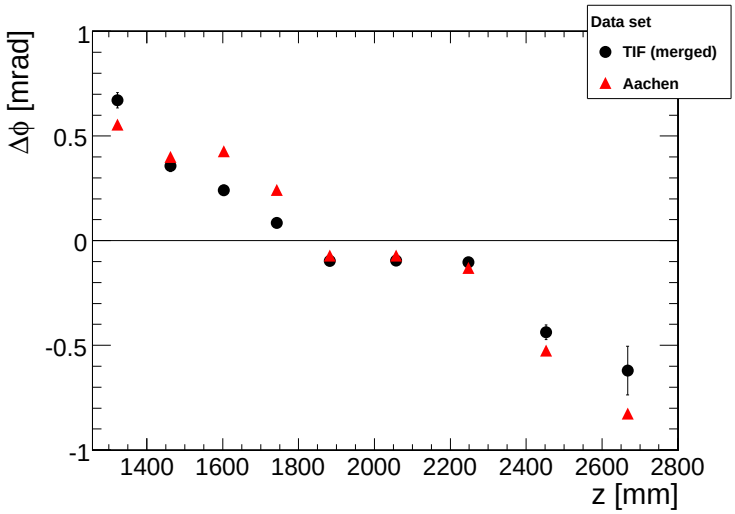


Figure 7.2: Corrections $\Delta\phi$, calculated with equivalent sets of slice test and sector test data without subtracting the slope of the deviations.

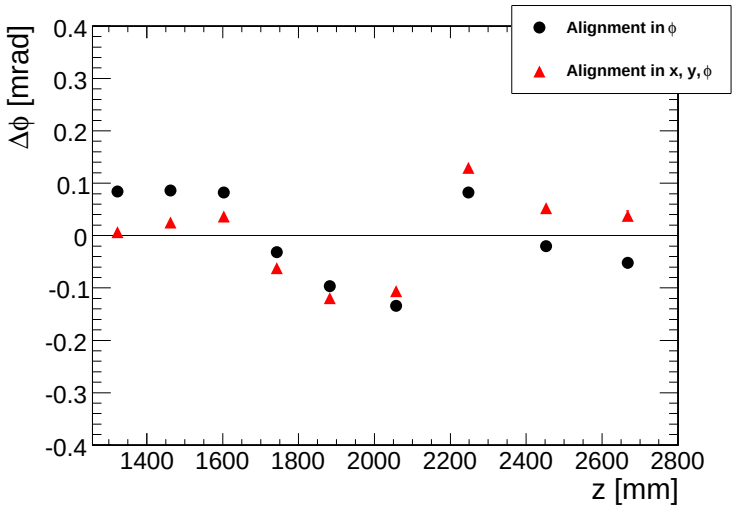


Figure 7.3: Corrections $\Delta\phi$ without fixing the slope of the deviations to zero, determined for disc alignment in ϕ and disc alignment in x, y, and ϕ with the entire sector test data set.

Another sign for a sensitivity to the regarded mode is given by the movement of alignment parameters despite their fixation when applying a fixation in ϕ to more than one disc. Basically, the mode $\Delta\phi = a_\phi \cdot z + b_\phi$ can be set to zero by fixing two alignables. However, if a disc alignment with the sector test data and a fixation of discs 1 and 9 is estimated, the algorithm changes the parameters of these discs by about 0.06 mrad in opposing directions, though the prior uncertainty is set to 0.01 mrad. This indicates, that fixing both discs is not compatible with the estimated alignment; the system is overdetermined.

Accordingly, fixing disc 1 is sufficient to define the reference system in this alignment procedure because a linear torsion can be detected. With enough tracks per alignable, as for a sector test disc alignment, the mode $\Delta\phi = a_\phi$ can be determined.

The global, linearly increasing torsion of the TEC+ is estimated from disc alignment in x, y, and ϕ with sector test data: Table 7.1 displays the alignment parameters $\Delta\phi$ without subtracting the slope of the deviations. The slope of the parameters, as a function of z, corresponds to the size of a linearly increasing endcap torsion per mm in z. Applying a linear fit, a total linear torsion component of 0.059 mrad over 1.35 m, the full length of the TEC+, is calculated.

Table 7.1: Alignment parameters $\Delta\phi$ obtained from disc alignment in x, y, ϕ without subtracting the slope as a function of z

Disc number	$\Delta\phi$ [mrad]
1	0.0068 ± 0.0073
2	0.0247 ± 0.0056
3	0.0366 ± 0.0041
4	-0.0621 ± 0.0027
5	-0.1194 ± 0.0017
6	-0.1061 ± 0.0019
7	0.1292 ± 0.0037
8	0.0524 ± 0.0062
9	0.0379 ± 0.0092

7.3 Comparison to Laser Alignment System Results

During the TEC+ sector tests and the tracker slice test, the Laser Alignment System has been active and laser beam residuals have been recorded. Residuals of all 16 TEC+ laser beams are available from the sector tests. After the tracker integration, four of these beams have been active during the slice test. In the following, the LAS results are compared to the displacements determined with the track based alignment.

7.3.1 Sector test disc alignment

The LAS has been fully activated during the sector tests. From the residuals of all 16 beams the most probable corrections to positions and orientations of the nine discs can be calculated [22] (Tab. 7.2). Figure 7.4 displays the comparison of the determined corrections Δx, Δy, and $\Delta\phi$ with the disc alignment which was estimated with the sector test track data.

The LAS corrections are estimated with measurements on 16 sensor modules per disc. Front petals are completely neglected. Because the alignment parameters of the track-based alignment correspond to the mean displacement of the active silicon area of an entire disc, misalignment on module and petal level could cause differences between the two results.
Both results match each other with a few differences of the order of 100 μm and 0.1 mrad. This shows, that deviations at disc level are the main source of misalignment and that the LAS modules are, on average, positioned precisely on the TEC+ discs.

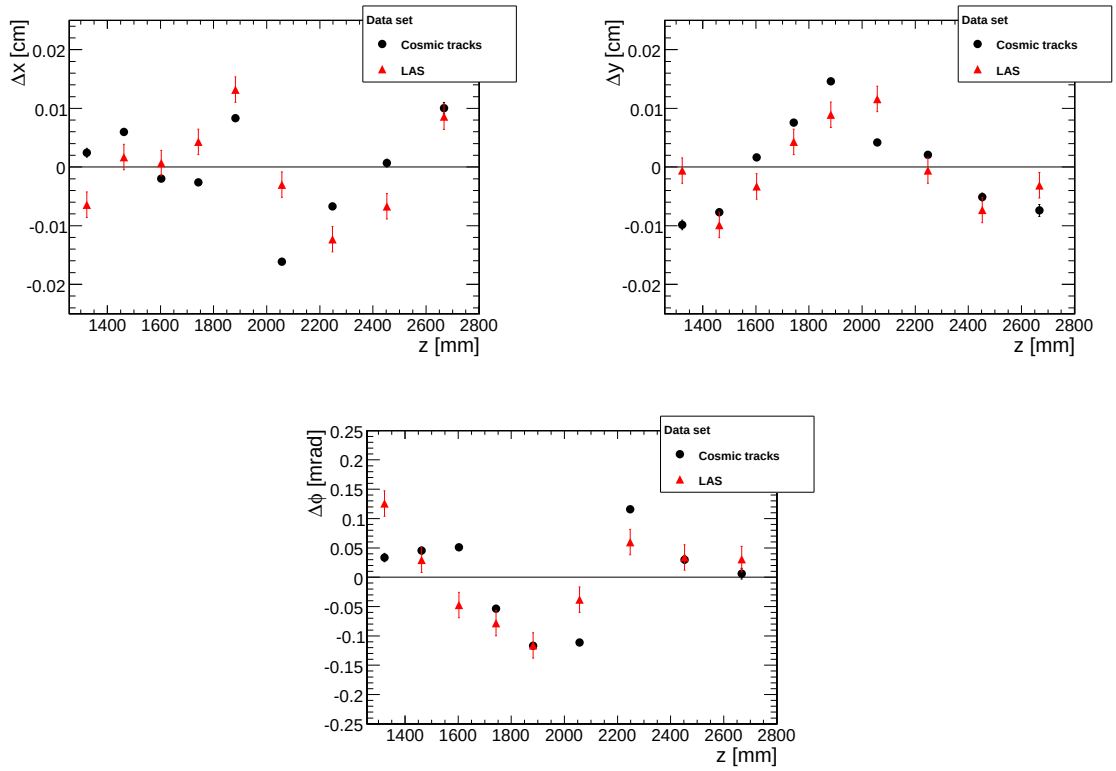


Figure 7.4: Comparison of Laser Alignment System [22] and track-based alignment results.

7.3.2 Sector test petal alignment

Assuming that disc and petal rotations in ϕ are the most significant contributions to the deformation of the TEC+ and neglecting effects due to translation of discs, the sector test laser beam residuals can, considering the radial positions of the laser beam spots $r_{R4} = 564$ mm and $r_{R6} = 840$ mm, directly be converted into corrections $\Delta\phi$ of the TEC+ back petals.
Considering the mounting precision of LAS sensor modules on the TEC+ petals, the LAS residuals can be determined with an accuracy of 47 μm [22]. This corresponds to an uncertainty in ϕ of 0.083 mrad for residuals measured on ring 4 modules and

Table 7.2: Displacements Δx, Δy, $\Delta\phi$ of TEC+ discs determined with LAS residuals. The precision of the position corrections Δx and Δy is 0.023 mm, and $\Delta\phi$ is determined with an accuracy 0.023 mrad.

Disc number	Δx [mm]	Δy [mm]	$\Delta\phi$ [mrad]
1	-0.064	-0.006	0.126
2	0.017	-0.099	0.030
3	0.007	-0.033	-0.047
4	0.043	0.043	-0.078
5	0.132	0.089	-0.116
6	-0.030	0.116	-0.038
7	-0.123	-0.006	0.060
8	-0.067	-0.073	0.034
9	0.086	-0.031	0.031

0.056 mrad for those from modules on ring 6.
To validate the petal alignment in ϕ, which was estimated using the sector test data, the LAS corrections are compared to this petal alignment (Fig. 7.5).

The number of hits per petal in the sector test data is not very high. Thus, the error on the petal corrections $\Delta\phi$ are relatively large compared to the alignment at disc level. In general, there is a good agreement of LAS results and the track based alignment within the errors. Differences can be interpreted as misalignment of the LAS sensor modules on the TEC+ petals or by shifts of the discs and petals in x and y, which affect the track-based alignment and the LAS residuals in different ways.

7.3.3 Slice test disc alignment

Since only four laser beams have been active during the slice test, positions and orientations of the TEC+ discs cannot be determined in the usual way. The measured laser residuals are assumed to be caused only by rotations of the discs and are directly transformed into corrections of the disc orientation using the radii of the laser beam spots (Tab. 7.3).

Table 7.3: LAS residuals in the different sectors and rings, transformed into corrections $\Delta\phi$ of TEC+ discs using the radial laser beam positions.

Disc number	S2R4 $\Delta\phi$ [mrad]	S2R6 $\Delta\phi$ [mrad]	S3R4 $\Delta\phi$ [mrad]	S3R6 $\Delta\phi$ [mrad]
1	0.505	0.080	0.328	0.306
2	0.041	0.022	0.093	0.053
3	-0.256	0.049	-0.006	-0.105
4	-0.365	-0.275	-0.117	-0.242
5	-0.304	-0.044	-0.722	-0.057
6	-0.038	0.083	0.148	-0.262
7	0.270	0.174	0.007	0.085
8	0.141	-0.100	0.163	0.141
9	0.006	0.011	0.107	0.082

There are four values $\Delta\phi$ for each disc estimated by the LAS because two TEC+ sectors have been active during the slice test (two laser beam residuals for each active back petal). They do not match each other perfectly, but are spread by about 0.4 mrad. The mean of the four values and their standard deviation, compared to the alignment results determined by the Kalman algorithm, are shown for each disc in Figure 7.6.

The results from the track-based alignment and the LAS values show a good agreement considering their spread. While the LAS measurements are being performed on module level, the alignment with track data calculates the disc rotations based upon the mean of the active sensor area. Thus, differences between these results are interpreted mainly as misalignment of the LAS modules on the petals and misalignment of the petals on the TEC+ discs.

Considering disc 1, both alignment methods estimate a similar correction $\Delta\phi$ in positive ϕ direction. This indicates, that the effect is due to the experimental setup of the slice test and not to a malfunction in the track-based alignment processing chain.

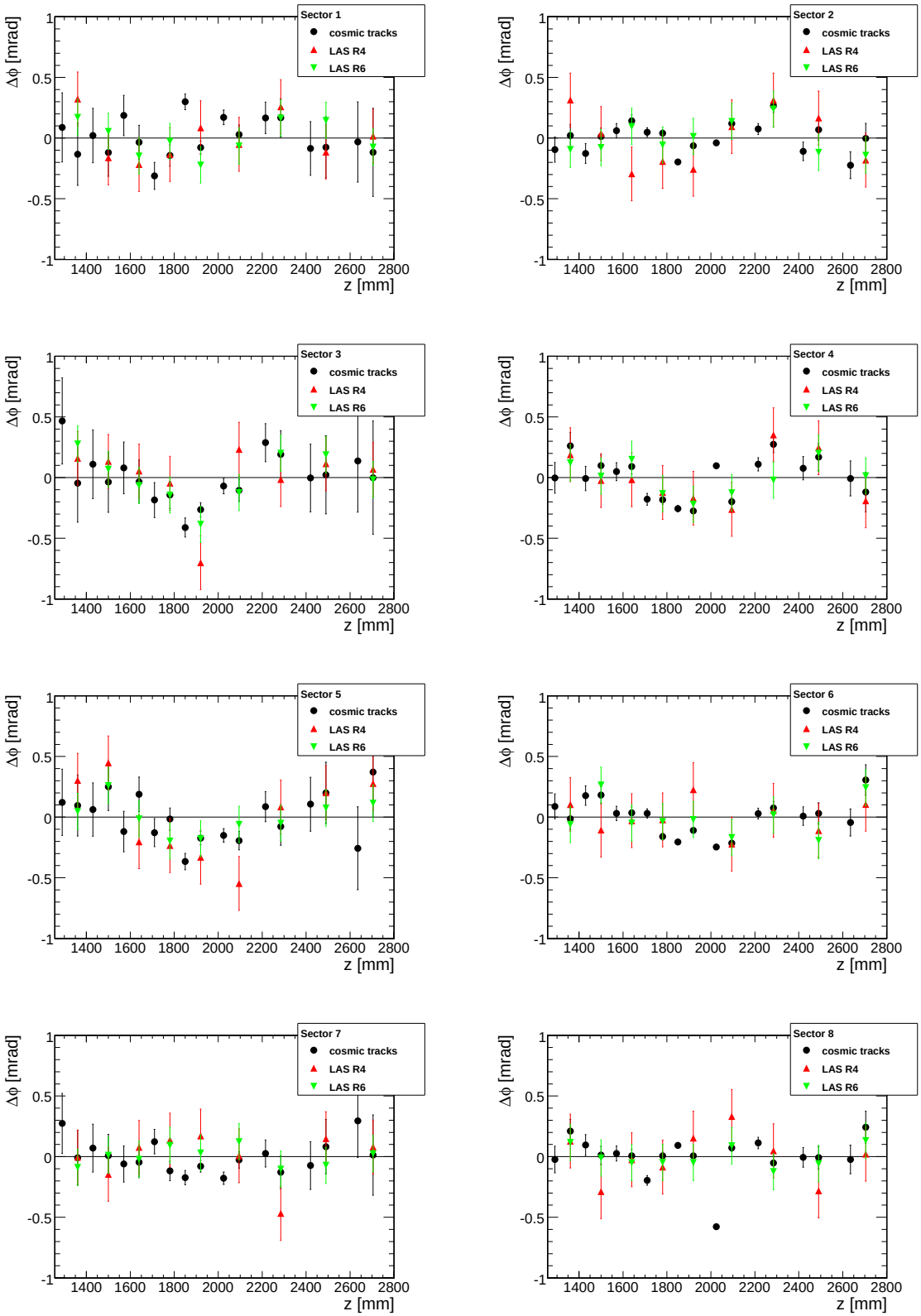


Figure 7.5: Comparison of track-based petal alignment and petal rotations estimated with LAS residuals [22].

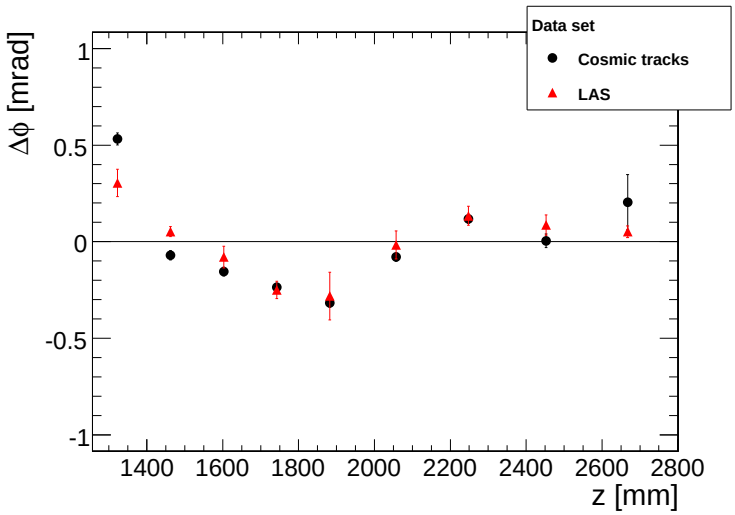


Figure 7.6: Correction to disc rotations ϕ determined with track based alignment and with the residuals of the LAS.

7.4 Comparison to Survey Measurements

A survey team determined deviations of TEC+ disc positions and rotations before integrating the petals, after their integration, and after transporting the TEC+ to CERN. Using photogrammetry, the displacements of four points at the outer circumference of each disc were measured with a precision of about 60 μm. Each measurement was done once with the TEC+ being in horizontal and once with it being in vertical orientation. Corrections to the disc positions and rotations were estimated from these measurements [23] using disc 1 as reference system.

7.4.1 Sector test disc alignment

For validation of the alignment calculated with the sector test data, a comparison to the survey measurements which were performed with the TEC+ in vertical position (discs orientated horizontally) after the petal integration is made. The survey values provide corrections for the coordinates x, y, and ϕ of the TEC+ discs. After subtracting mean and slope (Tab. 7.4), as it is done for the results of the track-based alignment, they can be compared to the disc alignment in these parameters (Fig. 7.7).

The survey measurements match the displacements estimated with the track based alignment on most discs within their errors. In general, there is a good agreement between the two results.
The determined displacements are not exactly equivalent: While the track based alignment is estimating corrections to the disc positions and rotations based upon the active silicon sensor area, the survey measurements are representing the displacements of the support structure part of the discs. Thus, differences can be interpreted as shifts of the sensor area mean with respect to the disc support structure.

7.5 Comparison to MillePede Results

The slice test data has been processed with three different alignment algorithms: HIP [24, 25], MillePede [12, 26], and Kalman Alignment Algorithm [10]. To validate

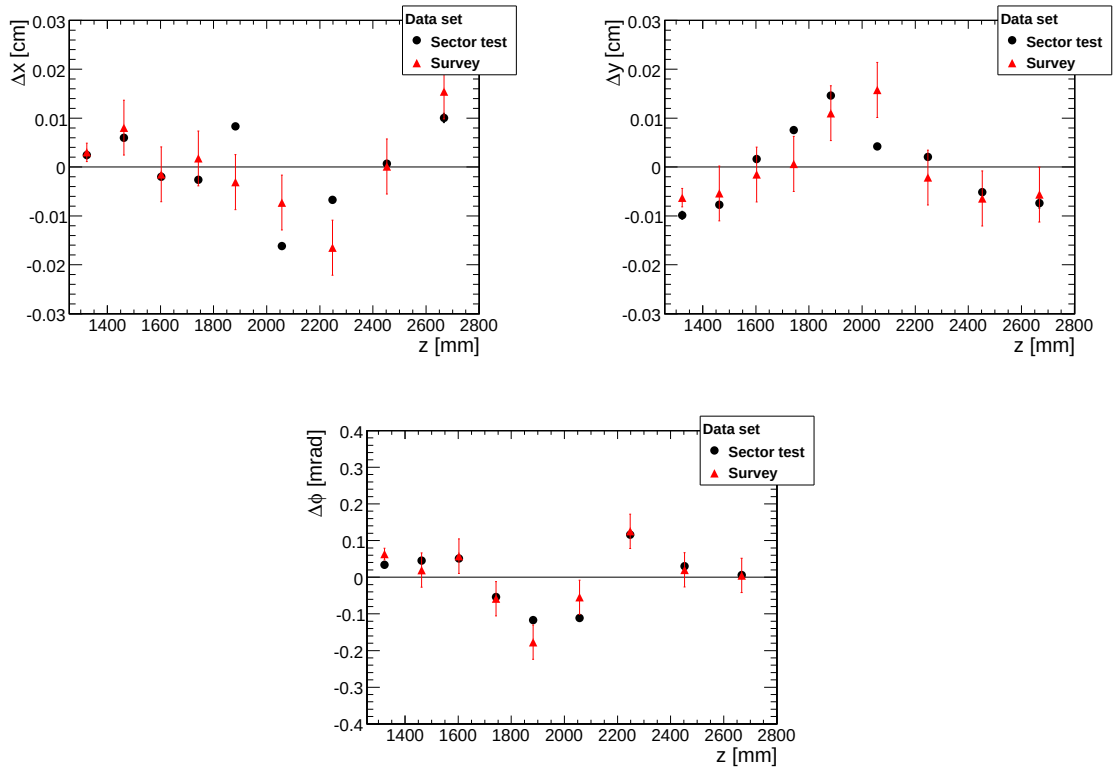


Figure 7.7: Comparison of survey [23] and track-based alignment results.

the results of the Kalman Alignment Algorithm, the estimated disc level alignment is compared to the one obtained with MillePede.

7.5.1 Slice test disc alignment

A comparison of the disc alignment in ϕ determined with MillePede [27] and the Kalman Alignment Algorithm using the slice test data is made (Fig. 7.8).

MillePede demands at least 100 hits per alignable, disc 9 is hence not included in the alignment. The two algorithms calculate corrections with discrepancies of up to 0.2 mrad. Considering the alignment uncertainties, the results show a good agreement.
There are some differences between the alignment algorithms. Therefore, slight

Table 7.4: Displacements Δx, Δy, $\Delta\phi$ of TEC+ discs determined with survey measurements

Disc number	Δx [mm]	Δy [mm]	$\Delta\phi$ [mrad]
1	0.030 ± 0.019	-0.063 ± 0.019	0.063 ± 0.016
2	0.081 ± 0.056	-0.054 ± 0.056	0.019 ± 0.047
3	-0.015 ± 0.056	-0.015 ± 0.056	0.057 ± 0.047
4	0.018 ± 0.056	0.006 ± 0.056	-0.058 ± 0.047
5	-0.031 ± 0.056	0.110 ± 0.056	-0.177 ± 0.047
6	-0.073 ± 0.056	0.158 ± 0.056	-0.055 ± 0.047
7	-0.165 ± 0.056	-0.021 ± 0.056	0.125 ± 0.047
8	0.001 ± 0.056	-0.064 ± 0.056	0.020 ± 0.047
9	0.154 ± 0.056	-0.056 ± 0.056	0.005 ± 0.047

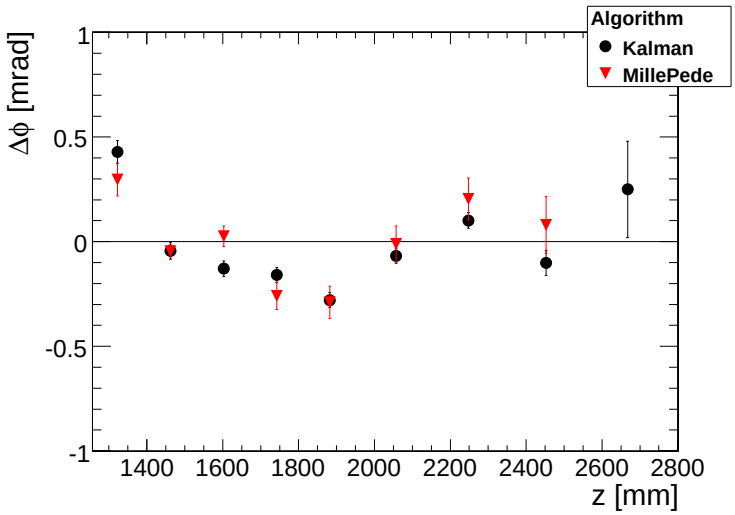


Figure 7.8: Corrections $\Delta\phi$ calculated by MillePede [27] and the Kalman Alignment Algorithm using the slice test data.

differences between the results can be explained. For example, outliers are rejected by the Kalman algorithm if they exceed certain thresholds. MillePede has a smooth transition between used and rejected tracks by assigning correspondingly lower weights to outliers. The considering of multiple scattering is also different in the regarded algorithms. Kalman takes all hit correlations into account, while MillePede neglects correlations among the track hits and just quadratically adds the multiple scattering uncertainty to the track errors. Thus, these errors are somewhat overestimated.

From the good agreement between Kalman and MillePede results, the conclusion can be drawn, that the Kalman algorithm works properly. Also, both algorithms determine a similarly large correction to the orientation of disc 1. Thus, this comparison confirmes, that the large petal corrections described in Section 6.3 are not an artefact of the alignment algorithm.

8. Summary

A Kalman filter has been used to perform multiple alignment studies of the CMS tracker endcap TEC+ on disc and on petal level with cosmic muon tracks taken in two very different configurations.
The TEC+ discs have been aligned with about 220 000 tracks to a precision of 0.01 mrad in ϕ and 10 μm in x and y. Displacements in ϕ of up to 0.12 mrad and up to 160 μm in x and y have been found. In addition to these parameters, deviations of the discs from their ideal z positions have been determined with a precision of about 50 μm and have been found to be of the order of 150 μm.
TEC+ petals have been aligned in ϕ with an accuracy between 0.01 and 0.3 mrad, depending on the number of tracks in the regarded TEC+ sector. Corrections to the petal orientation of the order of 0.25 mrad have been estimated. A petal alignment in x, y, and ϕ could not be determined with sufficient accuracy due to a low number of tracks per petal. Here, the limit of the data sets has been reached.
The weak modes $\Delta x = a_x \cdot z + b_x$, $\Delta y = a_y \cdot z + b_y$, $\Delta z = a_z \cdot z + b_z$, and $\Delta\phi = b_\phi$ cannot be determined with cosmic tracks and have hence been fixed to zero in all results. A weak sensitivity of the alignment procedure to the weak mode $\Delta\phi = a_\phi \cdot z$ has been found, and it has been determined at disc level. A global, linear torsion of the endcap of about 0.06 mrad over its full length has been estimated.
The obtained alignment results have been confirmed by optical survey measurements and results of the CMS tracker Laser Alignment System. The correct functionality of the alignment algorithm has also been validated by comparing alignments determined with independent data sets and by comparing results of a different alignment algorithm.
Alignments have been determined with data taken at different tracker temperatures. Comparing these, a good stability of the TEC+ with respect to temperature changes is found. From the data taken before and after the TEC+ has been transported from its integration position in Aachen to the Tracker Integration Facility at CERN, it can be concluded that the endcap is mechanically stable based on the comparison of alignment corrections.

With the studies described in this work the available data sets have been fully exploited. Generally, the obtained results confirm the expectations regarding alignment precision and stability of the TEC+.

An improvement of the alignment precision is possible by using larger sets of tracks. These would also allow to estimate an alignment down to module level. Including tracks to which a beam spot or mass constraint can be applied, also the weak modes of the TEC+ can be determined. These further studies will be approached as soon as the first LHC data arrives.

A. Results from Petal Alignment with Sector Test Data

Petal Alignment in ϕ

Table A.1: Alignment parameters $\Delta\phi$ for front petals of sectors 1 to 4 for petal alignment in ϕ.

Disc number	S1FP $\Delta\phi$ [mrad]	S2FP $\Delta\phi$ [mrad]	S3FP $\Delta\phi$ [mrad]	S4FP $\Delta\phi$ [mrad]
1	0.088 ± 0.103	0.274 ± 0.248	-0.024 ± 0.110	0.088 ± 0.285
2	0.178 ± 0.081	0.071 ± 0.198	0.096 ± 0.086	0.021 ± 0.225
3	0.031 ± 0.059	-0.061 ± 0.149	0.025 ± 0.062	0.187 ± 0.167
4	0.030 ± 0.038	0.124 ± 0.101	-0.195 ± 0.040	-0.312 ± 0.112
5	-0.206 ± 0.019	-0.174 ± 0.059	0.093 ± 0.019	0.299 ± 0.064
6	-0.247 ± 0.018	-0.178 ± 0.050	-0.578 ± 0.019	0.171 ± 0.061
7	0.029 ± 0.044	0.026 ± 0.111	0.113 ± 0.047	0.167 ± 0.130
8	0.008 ± 0.076	-0.073 ± 0.197	-0.006 ± 0.081	-0.086 ± 0.222
9	-0.044 ± 0.111	0.295 ± 0.302	-0.023 ± 0.118	-0.032 ± 0.330

Table A.2: Alignment parameters $\Delta\phi$ for front petals of sectors 5 to 8 for petal alignment in ϕ.

Disc number	S5FP $\Delta\phi$ [mrad]	S6FP $\Delta\phi$ [mrad]	S7FP $\Delta\phi$ [mrad]	S8FP $\Delta\phi$ [mrad]
1	-0.095 ± 0.104	0.468 ± 0.355	-0.003 ± 0.126	0.122 ± 0.273
2	-0.126 ± 0.081	0.110 ± 0.284	-0.007 ± 0.100	0.062 ± 0.220
3	0.061 ± 0.059	0.080 ± 0.214	0.049 ± 0.074	-0.119 ± 0.167
4	0.049 ± 0.037	-0.185 ± 0.144	-0.179 ± 0.049	-0.128 ± 0.115
5	-0.197 ± 0.018	-0.411 ± 0.079	-0.257 ± 0.026	-0.366 ± 0.068
6	-0.039 ± 0.018	-0.069 ± 0.064	0.098 ± 0.021	-0.151 ± 0.056
7	0.075 ± 0.045	0.289 ± 0.157	0.110 ± 0.055	0.086 ± 0.124
8	-0.109 ± 0.077	-0.003 ± 0.280	0.077 ± 0.097	0.107 ± 0.222
9	-0.224 ± 0.111	0.137 ± 0.422	-0.007 ± 0.144	-0.257 ± 0.341

Table A.3: Alignment parameters $\Delta\phi$ for back petals of sectors 1 to 4 for petal alignment in ϕ.

Disc number	S1BP $\Delta\phi$ [mrad]	S2BP $\Delta\phi$ [mrad]	S3BP $\Delta\phi$ [mrad]	S4BP $\Delta\phi$ [mrad]
1	0.088 ± 0.103	0.274 ± 0.248	-0.024 ± 0.110	0.088 ± 0.285
2	0.178 ± 0.081	0.071 ± 0.198	0.096 ± 0.086	0.021 ± 0.225
3	0.031 ± 0.059	-0.061 ± 0.149	0.025 ± 0.062	0.187 ± 0.167
4	0.030 ± 0.038	0.124 ± 0.101	-0.195 ± 0.040	-0.312 ± 0.112
5	-0.206 ± 0.019	-0.174 ± 0.059	0.093 ± 0.019	0.299 ± 0.064
6	-0.247 ± 0.018	-0.178 ± 0.050	-0.578 ± 0.019	0.171 ± 0.061
7	0.029 ± 0.044	0.026 ± 0.111	0.113 ± 0.047	0.167 ± 0.130
8	0.008 ± 0.076	-0.073 ± 0.197	-0.006 ± 0.081	-0.086 ± 0.222
9	-0.044 ± 0.111	0.295 ± 0.302	-0.023 ± 0.118	-0.032 ± 0.330

Table A.4: Alignment parameters $\Delta\phi$ for back petals of sectors 5 to 8 for petal alignment in ϕ.

Disc number	S5BP $\Delta\phi$ [mrad]	S6BP $\Delta\phi$ [mrad]	S7BP $\Delta\phi$ [mrad]	S8BP $\Delta\phi$ [mrad]
1	-0.095 ± 0.104	0.468 ± 0.355	-0.003 ± 0.126	0.122 ± 0.273
2	-0.126 ± 0.081	0.110 ± 0.284	-0.007 ± 0.100	0.062 ± 0.220
3	0.061 ± 0.059	0.080 ± 0.214	0.049 ± 0.074	-0.119 ± 0.167
4	0.049 ± 0.037	-0.185 ± 0.144	-0.179 ± 0.049	-0.128 ± 0.115
5	-0.197 ± 0.018	-0.411 ± 0.079	-0.257 ± 0.026	-0.366 ± 0.068
6	-0.039 ± 0.018	-0.069 ± 0.064	0.098 ± 0.021	-0.151 ± 0.056
7	0.075 ± 0.045	0.289 ± 0.157	0.110 ± 0.055	0.086 ± 0.124
8	-0.109 ± 0.077	-0.003 ± 0.280	0.077 ± 0.097	0.107 ± 0.222
9	-0.224 ± 0.111	0.137 ± 0.422	-0.007 ± 0.144	-0.257 ± 0.341

Petal Alignment in x, y, ϕ

In the following, results of the petal alignment in x, y, and ϕ are given for each TEC+ sector and compared to the disc alignment results in x, y, and ϕ. The disc alignment is determined with all tracks in the eight TEC+ sectors, while only the tracks in the regarded sector are available for the petal alignment.

Sector 1

In this sector, 4597 tracks have been used for alignment.

Table A.5: Alignment parameters for front petals (top) and back petals (bottom) of sector 1 for petal alignment in x, y, ϕ.

Disc number	Δx [mm]	Δy [mm]	$\Delta\phi$ [mrad]
1	0.097 ± 1.442	-0.599 ± 0.379	-0.7255 ± 0.1757
2	0.082 ± 1.126	0.045 ± 0.296	0.4630 ± 0.1369
3	-0.495 ± 0.820	-0.010 ± 0.216	0.1013 ± 0.1026
4	-0.180 ± 0.523	0.185 ± 0.137	0.2529 ± 0.0726
5	-0.082 ± 0.247	-0.110 ± 0.062	-0.6641 ± 0.0505
6	-0.124 ± 0.237	0.353 ± 0.057	0.2900 ± 0.0497
7	-0.065 ± 0.623	0.184 ± 0.160	0.4111 ± 0.0819
8	-0.356 ± 1.075	-0.114 ± 0.279	-0.2617 ± 0.1346
9	-0.075 ± 1.576	-1.249 ± 0.407	-1.0540 ± 0.2061
Disc number	Δx [mm]	Δy [mm]	$\Delta\phi$ [mrad]
1	-0.018 ± 1.287	0.239 ± 0.474	-0.4478 ± 0.4393
2	0.494 ± 0.971	-0.355 ± 0.355	0.4733 ± 0.3246
3	-0.111 ± 0.666	-0.564 ± 0.257	0.5390 ± 0.2424
4	0.074 ± 0.372	0.326 ± 0.179	-0.4937 ± 0.1891
5	0.125 ± 0.143	0.010 ± 0.141	-0.0655 ± 0.1747
6	0.018 ± 0.369	0.186 ± 0.186	-0.2243 ± 0.2124
7	0.178 ± 0.773	-0.036 ± 0.305	0.2372 ± 0.3038
8	0.408 ± 1.230	-0.349 ± 0.478	0.4448 ± 0.4608
9	0.029 ± 1.732	-0.388 ± 0.725	0.3381 ± 0.7275

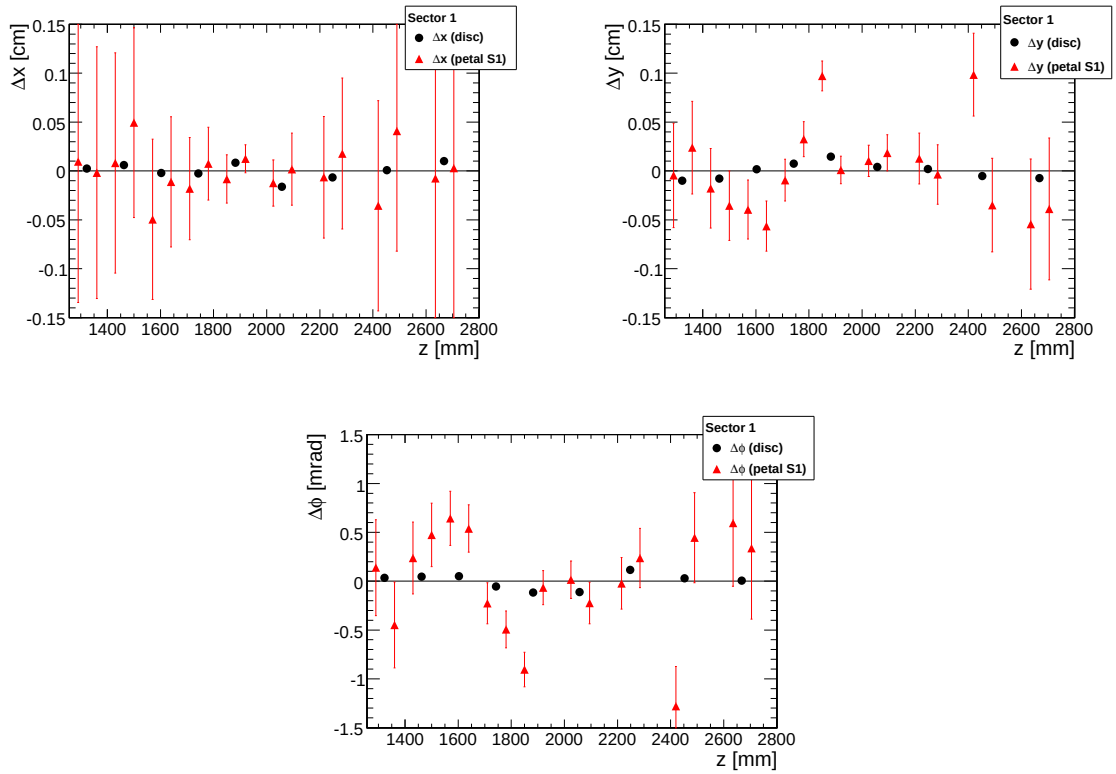


Figure A.1: Alignment parameters for petal alignment in x, y, and ϕ of TEC+ sector 1.

Sector 2

In this sector, 52 396 tracks have been used for alignment.

Table A.6: Alignment parameters for front petals (top) and back petals (bottom) of sector 2 for petal alignment in x, y, ϕ.

Disc number	Δx [mm]	Δy [mm]	$\Delta\phi$ [mrad]
1	0.532 ± 0.300	-0.599 ± 0.379	-0.7255 ± 0.1757
2	0.313 ± 0.234	0.045 ± 0.296	0.4630 ± 0.1369
3	0.332 ± 0.170	-0.010 ± 0.216	0.1013 ± 0.1026
4	-0.572 ± 0.108	0.185 ± 0.137	0.2529 ± 0.0726
5	0.168 ± 0.051	-0.110 ± 0.062	-0.6641 ± 0.0505
6	-0.180 ± 0.050	0.353 ± 0.057	0.2900 ± 0.0497
7	-0.176 ± 0.128	0.184 ± 0.160	0.4111 ± 0.0819
8	0.205 ± 0.221	-0.114 ± 0.279	-0.2617 ± 0.1346
9	-0.541 ± 0.323	-1.249 ± 0.407	-1.0540 ± 0.2061
Disc number	**Δx [mm]**	**Δy [mm]**	**$\Delta\phi$ [mrad]**
1	-0.128 ± 0.268	-0.217 ± 0.336	-0.0234 ± 0.1552
2	-0.202 ± 0.202	0.103 ± 0.255	-0.2750 ± 0.1182
3	0.081 ± 0.140	-0.111 ± 0.175	0.2846 ± 0.0866
4	-0.327 ± 0.079	0.305 ± 0.097	-0.5149 ± 0.0603
5	-0.067 ± 0.035	0.428 ± 0.034	-0.3990 ± 0.0470
6	-0.300 ± 0.078	0.312 ± 0.094	-0.4526 ± 0.0611
7	-0.244 ± 0.160	0.210 ± 0.201	-0.2127 ± 0.0999
8	0.251 ± 0.255	0.690 ± 0.320	-0.1438 ± 0.1571
9	0.854 ± 0.363	0.323 ± 0.449	0.6367 ± 0.2403

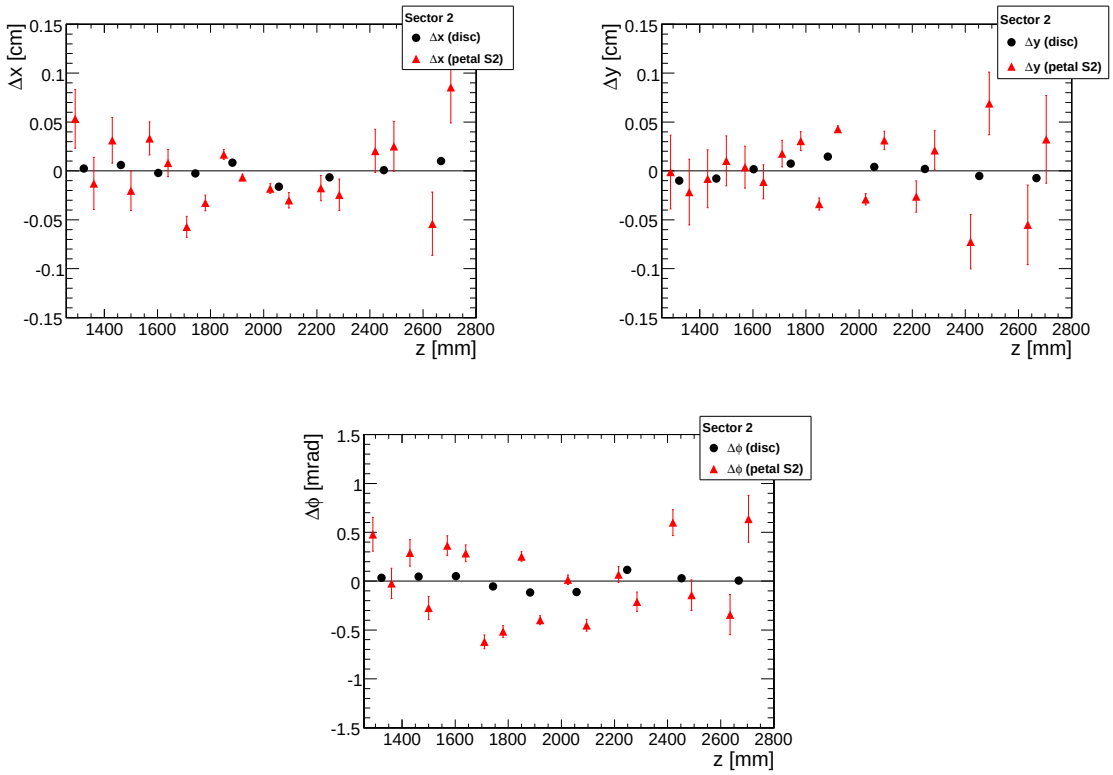


Figure A.2: Alignment parameters for petal alignment in x, y, and ϕ of TEC+ sector 2.

Sector 3

In this sector, 4264 tracks have been used for alignment.

Table A.7: Alignment parameters for front petals (top) and back petals (bottom) of sector 3 for petal alignment in x, y, ϕ.

Disc number	Δx [mm]	Δy [mm]	$\Delta\phi$ [mrad]
1	0.165 ± 0.657	-0.599 ± 0.379	-0.7255 ± 0.1757
2	-0.038 ± 0.483	0.045 ± 0.296	0.4630 ± 0.1369
3	0.537 ± 0.346	-0.010 ± 0.216	0.1013 ± 0.1026
4	0.476 ± 0.235	0.185 ± 0.137	0.2529 ± 0.0726
5	0.018 ± 0.159	-0.110 ± 0.062	-0.6641 ± 0.0505
6	0.018 ± 0.171	0.353 ± 0.057	0.2900 ± 0.0497
7	-0.486 ± 0.291	0.184 ± 0.160	0.4111 ± 0.0819
8	-0.435 ± 0.472	-0.114 ± 0.279	-0.2617 ± 0.1346
9	0.393 ± 0.721	-1.249 ± 0.407	-1.0540 ± 0.2061
Disc number	Δx [mm]	Δy [mm]	$\Delta\phi$ [mrad]
1	0.385 ± 0.587	0.333 ± 1.437	0.5581 ± 0.6319
2	-0.214 ± 0.420	-0.222 ± 1.086	-0.3652 ± 0.4482
3	-0.655 ± 0.293	-0.135 ± 0.745	-0.8481 ± 0.3208
4	-0.810 ± 0.194	-0.062 ± 0.414	-1.1279 ± 0.2297
5	0.334 ± 0.149	-0.269 ± 0.146	-0.0433 ± 0.1923
6	-0.343 ± 0.207	-0.218 ± 0.404	-0.6285 ± 0.2429
7	0.342 ± 0.345	0.009 ± 0.857	0.5437 ± 0.3759
8	0.139 ± 0.533	0.263 ± 1.365	0.2701 ± 0.5808
9	0.175 ± 0.778	0.586 ± 1.910	0.4581 ± 0.8759

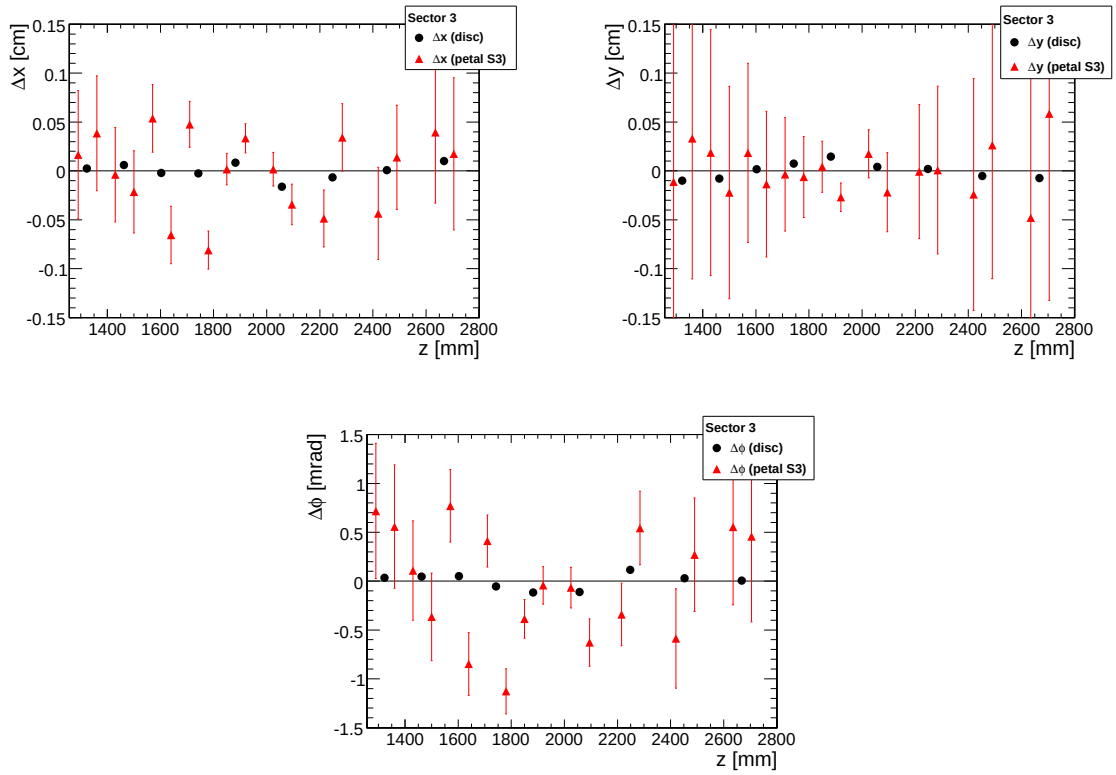


Figure A.3: Alignment parameters for petal alignment in x, y, and ϕ of TEC+ sector 3.

Sector 4

In this sector, 35 044 tracks have been used for alignment.

Table A.8: Alignment parameters for front petals (top) and back petals (bottom) of sector 4 for petal alignment in x, y, ϕ.

Disc number	Δx [mm]	Δy [mm]	$\Delta\phi$ [mrad]
1	0.386 ± 0.466	-0.599 ± 0.379	-0.7255 ± 0.1757
2	0.227 ± 0.364	0.045 ± 0.296	0.4630 ± 0.1369
3	0.007 ± 0.265	-0.010 ± 0.216	0.1013 ± 0.1026
4	0.048 ± 0.168	0.185 ± 0.137	0.2529 ± 0.0726
5	-0.013 ± 0.076	-0.110 ± 0.062	-0.6641 ± 0.0505
6	-0.331 ± 0.071	0.353 ± 0.057	0.2900 ± 0.0497
7	0.165 ± 0.196	0.184 ± 0.160	0.4111 ± 0.0819
8	-0.423 ± 0.342	-0.114 ± 0.279	-0.2617 ± 0.1346
9	0.996 ± 0.501	-1.249 ± 0.407	-1.0540 ± 0.2061

Disc number	Δx [mm]	Δy [mm]	$\Delta\phi$ [mrad]
1	0.107 ± 0.413	-0.503 ± 0.328	-0.2767 ± 0.1998
2	-0.269 ± 0.314	-0.292 ± 0.247	-0.4093 ± 0.1531
3	-0.030 ± 0.216	0.120 ± 0.169	0.1814 ± 0.1130
4	-0.255 ± 0.120	0.251 ± 0.096	-0.0741 ± 0.0802
5	0.180 ± 0.044	0.071 ± 0.044	-0.1304 ± 0.0641
6	-0.172 ± 0.116	0.360 ± 0.098	0.0837 ± 0.0819
7	-0.525 ± 0.248	-0.374 ± 0.197	-0.5985 ± 0.1312
8	-0.243 ± 0.395	-0.071 ± 0.312	-0.1282 ± 0.2091
9	0.146 ± 0.559	0.075 ± 0.448	0.0553 ± 0.3470

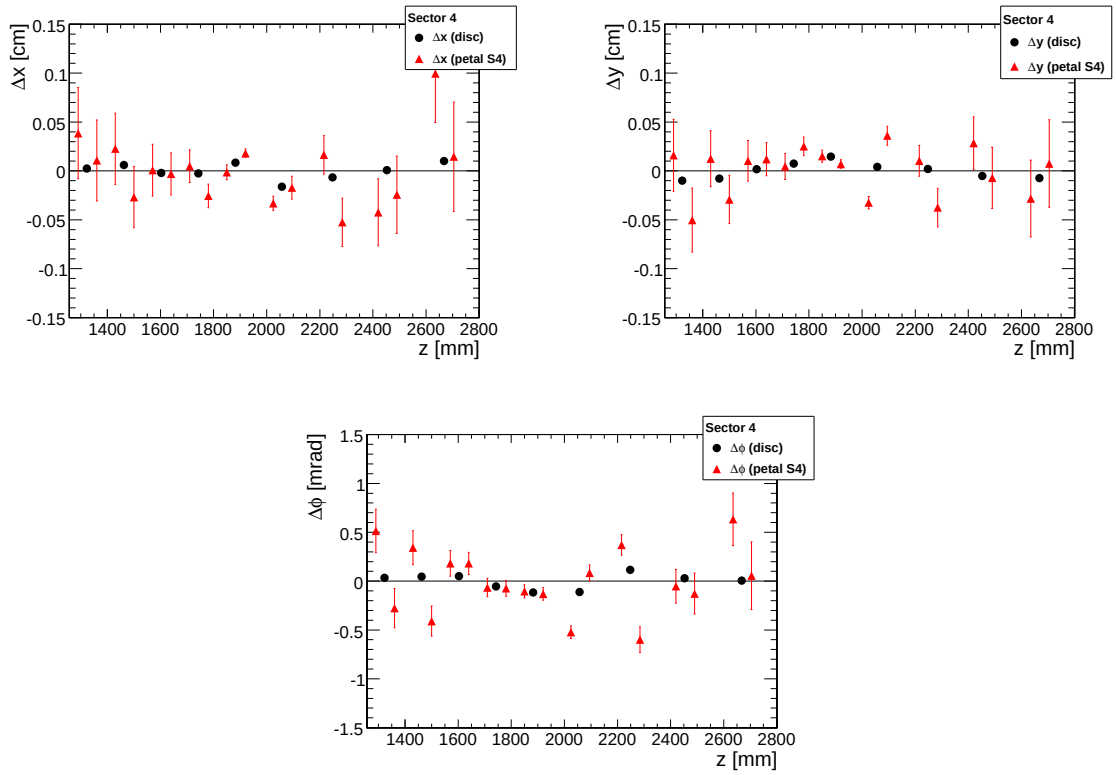


Figure A.4: Alignment parameters for petal alignment in x, y, and ϕ of TEC+ sector 4.

Sector 5

In this sector, 5120 tracks have been used for alignment.

Table A.9: Alignment parameters for front petals (top) and back petals (bottom) of sector 5 for petal alignment in x, y, ϕ.

Disc number	Δx [mm]	Δy [mm]	$\Delta\phi$ [mrad]
1	-0.216 ± 1.472	-0.579 ± 0.483	-0.4995 ± 0.4711
2	-0.437 ± 1.150	-0.404 ± 0.366	-0.3737 ± 0.3617
3	0.049 ± 0.839	-0.188 ± 0.272	-0.3255 ± 0.2761
4	0.067 ± 0.536	-0.024 ± 0.194	-0.1473 ± 0.2100
5	0.205 ± 0.259	0.674 ± 0.145	0.4328 ± 0.1728
6	0.298 ± 0.251	0.633 ± 0.153	0.5814 ± 0.1801
7	0.398 ± 0.636	-0.249 ± 0.238	-0.2581 ± 0.2541
8	0.333 ± 1.097	0.150 ± 0.384	0.2288 ± 0.4048
9	0.395 ± 1.610	-0.214 ± 0.614	-0.5673 ± 0.6692

Disc number	Δx [mm]	Δy [mm]	$\Delta\phi$ [mrad]
1	0.874 ± 1.324	0.057 ± 0.453	-0.0554 ± 0.4505
2	0.538 ± 0.997	0.068 ± 0.329	0.1588 ± 0.3295
3	-0.458 ± 0.690	-0.038 ± 0.239	0.2756 ± 0.2493
4	-0.220 ± 0.391	0.028 ± 0.174	0.0316 ± 0.1981
5	-0.336 ± 0.174	0.401 ± 0.148	0.3116 ± 0.1821
6	-1.029 ± 0.388	0.578 ± 0.183	0.7850 ± 0.2115
7	-0.417 ± 0.795	-0.315 ± 0.284	-0.3148 ± 0.3010
8	-0.099 ± 1.258	-0.106 ± 0.434	0.0187 ± 0.4575
9	0.054 ± 1.766	-0.474 ± 0.647	-0.2827 ± 0.7138

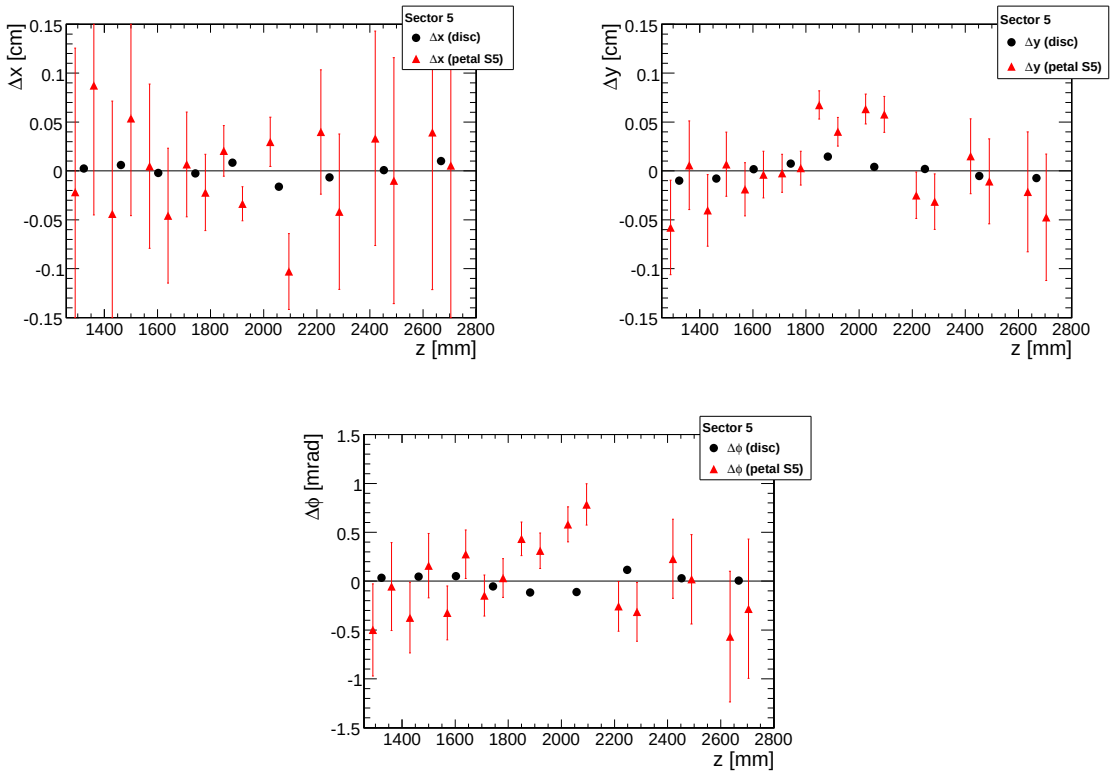


Figure A.5: Alignment parameters for petal alignment in x, y, and ϕ of TEC+ sector 5.

Sector 6

In this sector, 57 255 tracks have been used for alignment.

Table A.10: Alignment parameters for front petals (top) and back petals (bottom) of sector 6 for petal alignment in x, y, ϕ.

Disc number	Δx [mm]	Δy [mm]	$\Delta\phi$ [mrad]
1	0.379 ± 0.299	-0.599 ± 0.379	-0.7255 ± 0.1757
2	-0.244 ± 0.233	0.045 ± 0.296	0.4630 ± 0.1369
3	-0.096 ± 0.169	-0.010 ± 0.216	0.1013 ± 0.1026
4	-0.089 ± 0.107	0.185 ± 0.137	0.2529 ± 0.0726
5	0.349 ± 0.051	-0.110 ± 0.062	-0.6641 ± 0.0505
6	-0.255 ± 0.050	0.353 ± 0.057	0.2900 ± 0.0497
7	-0.216 ± 0.128	0.184 ± 0.160	0.4111 ± 0.0819
8	0.263 ± 0.220	-0.114 ± 0.279	-0.2617 ± 0.1346
9	0.030 ± 0.320	-1.249 ± 0.407	-1.0540 ± 0.2061
Disc number	Δx [mm]	Δy [mm]	$\Delta\phi$ [mrad]
1	0.082 ± 0.266	-0.489 ± 0.337	-0.4547 ± 0.1565
2	-0.490 ± 0.201	-0.193 ± 0.256	0.5977 ± 0.1196
3	-0.056 ± 0.138	0.348 ± 0.176	0.2869 ± 0.0876
4	0.093 ± 0.078	0.225 ± 0.098	-0.0945 ± 0.0613
5	0.617 ± 0.035	0.542 ± 0.035	-0.4505 ± 0.0480
6	-0.187 ± 0.078	0.663 ± 0.094	0.4913 ± 0.0622
7	-0.151 ± 0.160	0.076 ± 0.201	0.3819 ± 0.1013
8	0.111 ± 0.253	-0.229 ± 0.321	-0.2147 ± 0.1594
9	-0.139 ± 0.360	0.372 ± 0.452	0.6435 ± 0.2517

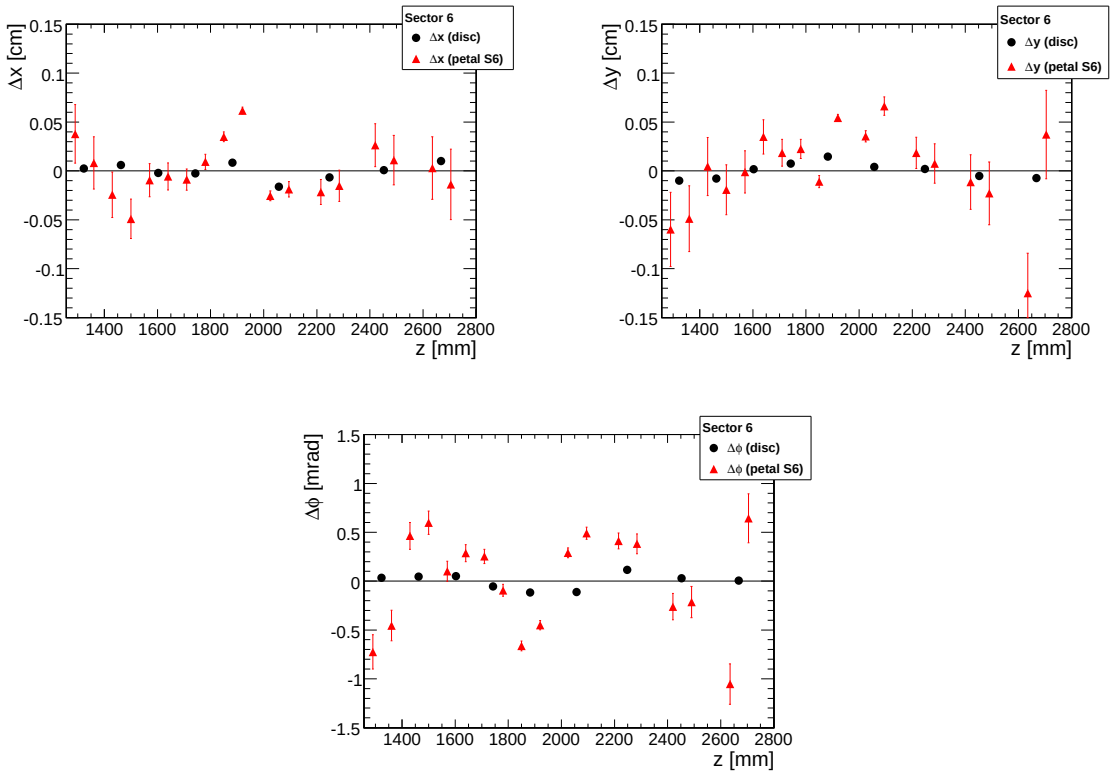


Figure A.6: Alignment parameters for petal alignment in x, y, and ϕ of TEC+ sector 6.

Sector 7

In this sector, 5364 tracks have been used for alignment.

Table A.11: Alignment parameters for front petals (top) and back petals (bottom) of sector 7 for petal alignment in x, y, ϕ.

Disc number	Δx [mm]	Δy [mm]	$\Delta\phi$ [mrad]
1	-0.291 ± 0.422	-0.425 ± 1.262	0.5507 ± 0.3987
2	-0.296 ± 0.325	-0.178 ± 0.986	0.3773 ± 0.3115
3	-0.245 ± 0.240	0.259 ± 0.717	0.1885 ± 0.2379
4	-0.024 ± 0.167	0.207 ± 0.456	0.1141 ± 0.1777
5	-0.446 ± 0.115	0.607 ± 0.220	0.3374 ± 0.1412
6	-0.576 ± 0.124	0.408 ± 0.220	0.5221 ± 0.1518
7	-0.520 ± 0.204	0.373 ± 0.545	0.6847 ± 0.2197
8	-0.698 ± 0.333	-0.088 ± 0.938	0.8352 ± 0.3464
9	-0.173 ± 0.510	-0.180 ± 1.382	0.5477 ± 0.5499

Disc number	Δx [mm]	Δy [mm]	$\Delta\phi$ [mrad]
1	0.894 ± 0.384	0.003 ± 1.129	-1.1115 ± 0.3669
2	-0.024 ± 0.286	-0.284 ± 0.852	0.1147 ± 0.2772
3	0.169 ± 0.206	-0.079 ± 0.586	-0.2025 ± 0.2094
4	0.447 ± 0.142	0.239 ± 0.332	-0.6988 ± 0.1610
5	0.232 ± 0.116	0.344 ± 0.152	-0.4643 ± 0.1461
6	0.289 ± 0.154	-0.638 ± 0.335	-0.0849 ± 0.1800
7	-0.028 ± 0.247	-0.597 ± 0.684	0.1061 ± 0.2600
8	1.016 ± 0.379	-0.198 ± 1.087	-1.1746 ± 0.3955
9	0.277 ± 0.564	0.227 ± 1.534	-0.6419 ± 0.6196

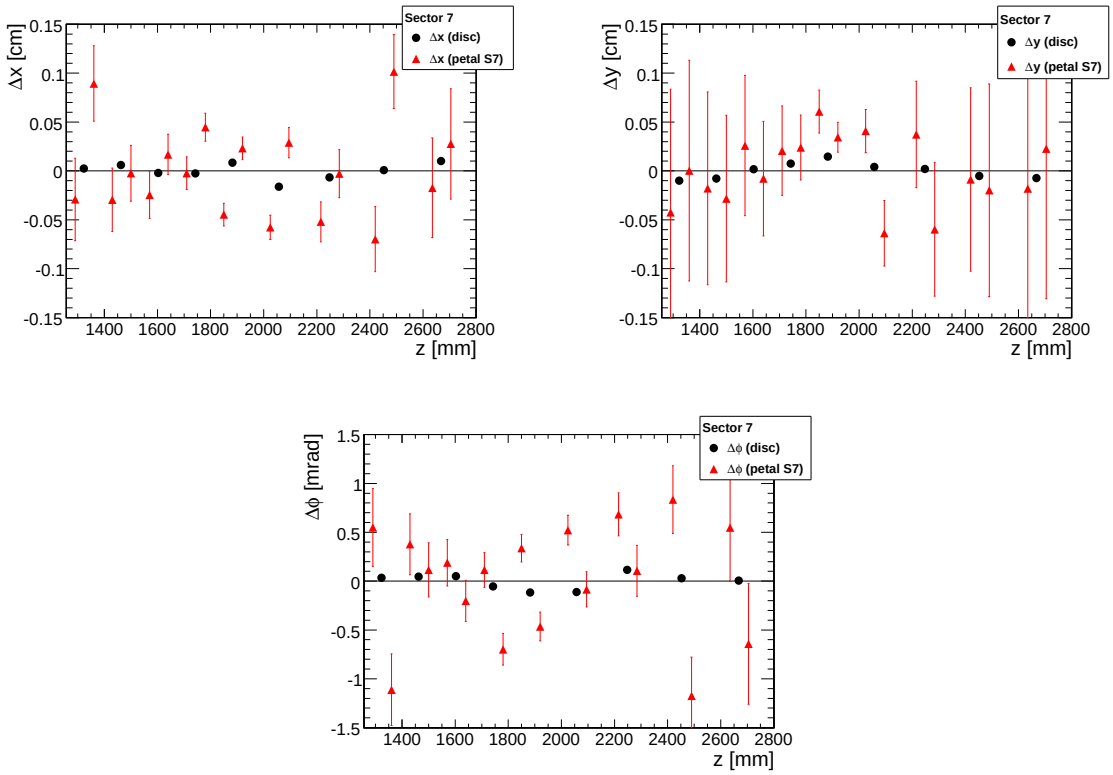


Figure A.7: Alignment parameters for petal alignment in x, y, and ϕ of TEC+ sector 7.

Sector 8

In this sector, 51 548 tracks have been used for alignment.

Table A.12: Alignment parameters for front petals (top) and back petals (bottom) of sector 8 for petal alignment in x, y, ϕ.

Disc number	Δx [mm]	Δy [mm]	$\Delta\phi$ [mrad]
1	0.012 ± 0.414	0.056 ± 0.323	-0.0362 ± 0.1851
2	-0.061 ± 0.325	-0.285 ± 0.252	0.4117 ± 0.1442
3	-0.124 ± 0.236	0.114 ± 0.183	0.0150 ± 0.1078
4	-0.312 ± 0.150	0.338 ± 0.116	-0.2686 ± 0.0759
5	-0.172 ± 0.068	0.089 ± 0.055	0.0955 ± 0.0526
6	0.114 ± 0.063	0.583 ± 0.054	-1.3005 ± 0.0520
7	-0.403 ± 0.175	0.180 ± 0.139	0.1968 ± 0.0862
8	-0.135 ± 0.304	0.348 ± 0.238	-0.2793 ± 0.1411
9	-0.032 ± 0.444	0.289 ± 0.347	-0.2854 ± 0.2146
Disc number	Δx [mm]	Δy [mm]	$\Delta\phi$ [mrad]
1	0.200 ± 0.369	0.138 ± 0.289	-0.1716 ± 0.1658
2	0.544 ± 0.280	-0.353 ± 0.218	0.0466 ± 0.1261
3	0.296 ± 0.193	-0.003 ± 0.150	-0.1937 ± 0.0919
4	0.164 ± 0.107	-0.516 ± 0.085	0.4812 ± 0.0639
5	-0.037 ± 0.039	-0.164 ± 0.038	0.2136 ± 0.0497
6	-0.851 ± 0.103	0.184 ± 0.084	0.3609 ± 0.0649
7	-0.288 ± 0.220	0.054 ± 0.172	0.0690 ± 0.1059
8	0.455 ± 0.350	-0.686 ± 0.273	0.4716 ± 0.1659
9	0.631 ± 0.492	-0.366 ± 0.387	0.1734 ± 0.2540

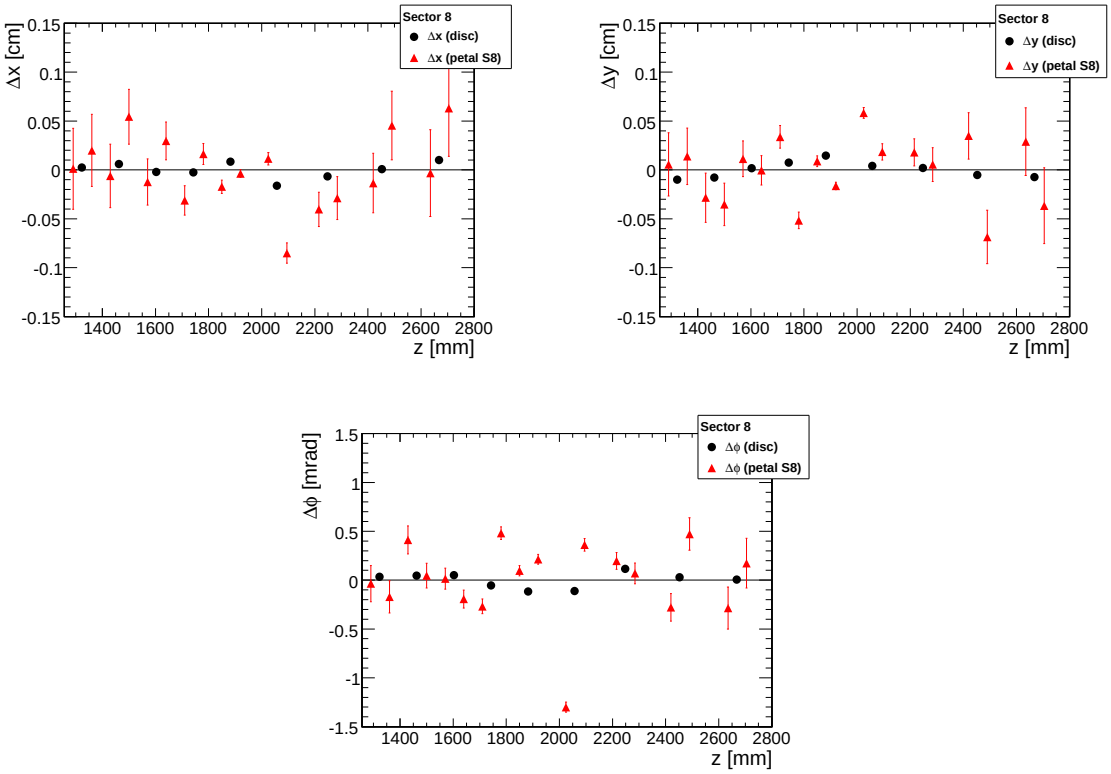


Figure A.8: Alignment parameters for petal alignment in x, y, and ϕ of TEC+ sector 8.

In this sector, a deformation of a petal mounting point on disc 6 has been found [6]. This explains the anomalous $\Delta\phi$ correction of the front petal of disc 6, which is visible in Figure A.8.

B. Configuration files

In the following, example configuration files for the ORCA and CMSSW programs are listed to detail the used configuration of the CMS software framework.

Configuration in ORCA

Listing B.1: orcarc_tracks_21713

```
# Debugging
Verbose:info=0
Verbose:debug=0
Verbose:test=0
MemoryDebug = 0
TextColor=false

# Data Input
DaqApplication:InputFile=/disk1/user/weberm/TECRawData/RU0021713_000.root
RootFileReader:StartBranch=1
RootFileReader:LastFile=109
DaqApplication:MaxEvents = 100000

# Data output
GenEventStudy:histFileName = TEC_tracks_21713.root
TECEventAnalyser:RunNumber = 21713

# Geometry
ExtraPackages = DDDInterface
TkDDDInterface:UseDDD = true
TkDDDInterface:GeometryVersion=new
DDDParserInstance = 1
DDDConfigFile = TECconfiguration.xml
#Geometry_PATH = .:/home/home4/institut_1b/weberm/ORCA_8_13_3/src/Data/TrackerTBGeometries//
    TECCosmic:${Geometry_PATH}
Geometry_PATH = .:/home/home4/institut_1b/weberm/ORCA_8_13_3/src/Data/TrackerTBGeometries//
    TECCosmic.new:${Geometry_PATH}
TkDetLayerFactory:TEC=FastTEC
TkDetLayerFactory:TID=FastTID
GenEventStudy:UseTkNumbering = true

# Magnetic field
MagneticField:Name = UniformMagneticField
UniformMagneticField:Value = 0.0

# Cabling map
SiStripDigiSetUp:DefaultPartitioner = false
SiStripConnectivity:MappingFileName = /home/home4/institut_1b/weberm/config/sector8/geometry.txt
SiStripConnectivity:XdaqFileName = /home/home4/institut_1b/weberm/config/sector8/TEC_peak.xml
SiStripConnectivity:PartitionerType = fromMapping

# Data input specific settings
SiStripDataFormatter:UseDummyFormatter = 0
SiStripDataFormatter:FedReadoutPath = VME
SiStripDataFormatter:AppendedHeaderBytes = 68
SiStripFrontEndDriver:FedReadoutMode = VIRGIN_RAW
TkDaqInitialiser:SwitchOffPixels = true

# Digi processing
TkSiStripDigitizer:DigitizerName = SiStripZSDigitizerFromApvAnalysis
ApvAnalysis:FactoryName = GeneralApvAnalysisFactory
SiStripDetPartitioner:ZeroSuppressedFEDs = false
StripDaqCmsRawFormatterInitializer:formatterTB2004 = true
```

```
52
53 # Zero suppression
54 SiStripPartitioner:ZeroSuppressedFEDs = 0
55 GeneralApvAnalysisFactory:zeroSuppressor = Reference
56
57 # Calibration (pedestals, noise, strip mask)
58 GenEventStudy:calibFileName = /home/home4/institut_1b/weberm/data/21713/../21707/TEC_calib_21707/
       .root
59 SiStripDigitizerFromApvAnalysis:doAnyCalibration = false
60 TECEventAnalyser:Alignment = true
61 # possible choices for Endcap: TECLayers, TECWedges, TECDets
62 TECEventAnalyser:SelectedAlignables=TECLayers
63 # choose the parameters which are going to be aligned
64 TECEventAnalyser:AlignX = true
65 TECEventAnalyser:AlignY = true
66 TECEventAnalyser:AlignZ = false
67 TECEventAnalyser:AlignAlpha = false
68 TECEventAnalyser:AlignBeta = false
69 TECEventAnalyser:AlignGamma = true
70
71 KalmanFilterAlignment:AlignmentFileName=TEC_align_21713.root
72 GeneralApvAnalysisFactory:saveCalibrationData = false
73 GeneralApvAnalysisFactory:readCalibrationData = false
74
75 GeneralApvAnalysisFactory:pedestalCalculator = TT6
76 PedestalCalculator:eventsRequiredToCalibrate = 50000
77 PedestalCalculator:eventsRequiredToUpdate    = 50000
78 PedestalCalculator:cutToAvoidSignal          = 5.
79
80 GeneralApvAnalysisFactory:noiseCalculator    = TT6
81 NoiseCalculator:eventsRequiredToCalibrate    = 50000
82 NoiseCalculator:eventsRequiredToUpdate       = 50000
83 NoiseCalculator:cutToAvoidSignal             = 5.
84
85 GeneralApvAnalysisFactory:cmnCalculator = MedianTT6
86 GeneralApvAnalysisFactory:theNumCMstripsInGroup = 128
87
88 GeneralApvAnalysisFactory:maskAlgorithm = TT6
89 TT6ApvMask:noisyStripDefinition = 1
90 # sigma cut for noisy strips
91 TT6ApvMask:cutForNoisyStrips    = 5.
92 # sigma cut for dead strips
93 TT6ApvMask:cutForDeadStrips     = 5.
94 # ignore this number of strips on left and right of APV
95 TT6ApvMask::cutForSideStrips    = 1
96 # ignore 5 lowest and 5 highest values after sorting
97 TT6ApvMask:cutForTruncation     = 0.04
98
99 # Cluster finding
100 StripClusterizerBuilder:StripThreshold = 3.
101 StripClusterizerBuilder:SeedThreshold = 5.
102 StripClusterizerBuilder:ClusterThreshold = 8.
103
104 # TEC Navigation
105 CombinatorialTrajectoryBuilder:NavigationSchool = TBNavigationSchool
106
107 # Track seeding
108 CombinatorialTrajectoryBuilder:minimumNumberOfHits = 4
109 TBSeedGeneratorFromNFarLayers:SeedLayers = 1
110 TBSeedGeneratorFromNFarLayers:minimumNumberOfHits = 9
111 TBSeedGeneratorFromNFarLayers:TrajectoryDirection = 3
112 TBSeedGeneratorFromNLayers:TrajectoryDirection = 3
113 TBSeedGeneratorFromNFarLayers:ParticleMomentum = 1.3
114
115 # Track reconstruction
116 CombinatorialTrajectoryBuilder:chiSquarCut = 100.
117 TrajectoryCleanerBySharedHits:MaximumSharedHitFraction = 0.
118 TransientCombinatorialTrackFinder:SeedGenerator = TBSeedGeneratorFromNFarLayers
119 TransientCombinatorialTrackFinder:seedCleaning = false
120 #TransientCombinatorialTrackFinder:Smoother:Fitter = KFSplittingFitter
```

Configuration in CMSSW v1.3.6

The job submisson is done by a bash script, that handles the insertion of reasonable logfile, output file, and source file names.

Listing B.2: Alignment/KalmanAlignmentAlgorithm/test/alignment.cfg

```
process Alignment = {
# Initialize  MessageLogger
#=========================
    service = MessageLogger {
        # note: LOGFILE will be replaced by bash script
        untracked vstring destinations = { "LOGFILE" }# {, "cout" }
        untracked vstring statistics = { "LOGFILE" } #{, "cout" }
        untracked vstring categories = { "Alignment", "LogicError", "FwkReport", "TrackProducer"/
            }

        untracked PSet cout    = {
            untracked string threshold = "DEBUG" # "ERROR"
            untracked PSet FwkReport = {
                untracked string threshold = "INFO"
            }
            untracked PSet TrackProducer = {
                untracked string threshold = "INFO"
            }
            # untracked bool noLineBreaks = true
        }
        untracked PSet LOGFILE  = {
            untracked string threshold = "INFO"
            untracked PSet INFO = { untracked int32 limit = 10 }
            untracked PSet WARNING = { untracked int32 limit = 10 }
            untracked PSet ERROR = { untracked int32 limit = -1 }
            untracked PSet DEBUG = { untracked int32 limit = -1 }
            untracked PSet Alignment = { untracked int32 limit = -1}
            untracked PSet LogicError = { untracked int32 limit = -1}
            # untracked bool noLineBreaks = true
        }
    }

# ideal geometry and interface
    include "Geometry/CMSCommonData/data/cmsIdealGeometryXML.cfi"
    include "Geometry/TrackerNumberingBuilder/data/trackerNumberingGeometry.cfi"


# Track selection for alignment
#==============================
    module AlignmentTracks = AlignmentTrackSelectorModule {
        InputTag src = ctfWithMaterialTracksTIF # cosmictrackfinderTIFTIBTOB
        bool filter = false

        bool applyBasicCuts = true
        double ptMin   = 0
        double ptMax   = 999.
        double etaMin  = -2.4
        double etaMax  =  2.4
        double phiMin  = -3.1416
        double phiMax  =  3.1416
        double nHitMin = 5
        double nHitMax = 99
        double chi2nMax= 999999.

        bool applyNHighestPt = false
        int32 nHighestPt = 2

        bool applyMultiplicityFilter = true
        int32 minMultiplicity = 1
    }

    # Alignment producer
    include "Alignment/CommonAlignmentProducer/data/AlignmentProducer.cff"
    replace AlignmentProducer.applyDbAlignment = false #true
    #replace AlignmentProducer.tjTkAssociationMapTag = cosmictrackfinder # default is /
        TrackRefitter
    # MisalignmentScenarioSettings is a block from Scenario.cff from AlignmentProducer.cff:
    #replace MisalignmentScenarioSettings.setError = false # no APE!


# AlignmentProducer - Setting the Alignables
#===========================================
# First string: Specifies the alignable
#   Possible values for TEC: "TECDets", "TECPetals", "TECLayers", "TECs"
#
# Second string: determines which of the (rigid body) parameters are active,
#   the order is u, v, w, alpha, beta, gamma.
#   Other letters than 0 and 1 also select the parameter, but may be interpreted
#   in a special way, e.g. f and c in millepede.

    replace AlignmentProducer.ParameterBuilder.Selector = {
        vstring alignParams = {
            "TECLayers,000001,selTECplus"
#            "TECLayers,110001,selTECplus"
#            "TECLayers,010001,selTECplus"
#            "TECLayers,100001,selTECplus"
#            "TECLayers,111111,selTECplus"

#            "TECPetals,000001,selTECplus"
#            "TECPetals,010001,selTECplus"
```

```
89 #             "TECPetals,100001,selTECplus"
90 #             "TECPetals,110001,selTECplus"
91         }
92         PSet selTECplus = {
93               vdouble etaRanges = {}
94               vdouble rRanges = {}
95
96               # disks 1 to 9
97               vdouble zRanges = {0,300}
98
99               # disks 1 to 7
100              #vdouble zRanges = {0,230}
101
102              # all sectors (for layer level alignment)
103              vdouble phiRanges = {}
104
105              # sector 2 and 3 (3pi/16, 11pi/16)
106              #vdouble phiRanges = {0.5890, 2.1599}
107
108              # sector 2 and 3, back petals (5pi/16, 7pi/16), (9pi/16, 11pi/16)
109              #vdouble phiRanges = {0.9817, 1.3744, 1.7671, 2.1598}
110
111              # sector 2 and 3, front petals (3pi/16, 5pi/16), (7pi/16, 9pi/16)
112              #vdouble phiRanges = {0.5890, 0.9817, 1.3744, 1.7671}
113
114              # sector 3, front petals
115              #vdouble phiRanges = {1.3744, 1.7671}
116
117              # sector 3, back petals (9pi/16, 11pi/16)
118              #vdouble phiRanges = {1.7671, 2.1598}
119        }
120    }
121
122
123 ## ----------------write/read from DB----------------------------------
124 ##    replace AlignmentProducer.saveToDB = false
125 ##    replace AlignmentProducer.applyDbAlignment =false #remember to set doMisalignmentScenario /
       = false
126 ##    include "Alignment/MillePedeAlignmentAlgorithm/data/DBConfiguration.cff"
127 ## --------------------------------------------------------------------
128
129 # Misalignment tools
130 #====================
131     replace AlignmentProducer.doMisalignmentScenario = false
132
133     include "Alignment/KalmanACAlignmentAlgorithm/data/MisalignmentScenarios.cff"
134     replace AlignmentProducer.MisalignmentScenario = {
135         using DiskTestScenario6
136     }
137
138     #double AlignmentProducer.MisalignmentScenario.TECs.scale = 1.0
139
140
141 # Configuration of KalmanACAlignmentAlgorithm
142 #=============================================
143     replace AlignmentProducer.algoConfig = {
144         using KalmanACAlignmentAlgorithm
145     }
146     include "Alignment/KalmanACAlignmentAlgorithm/data/KalmanACAlignmentAlgorithm.cfi"
147     replace KalmanACAlignmentAlgorithm.fileDir = ""
148     # note: ROOTFILE will be replaced by bash script
149     replace KalmanACAlignmentAlgorithm.alignmentFileName="ROOTFILE"
150     replace KalmanACAlignmentAlgorithm.skipInvalidHits=true
151     replace KalmanACAlignmentAlgorithm.minNumberOfHits = 5
152     replace KalmanACAlignmentAlgorithm.multipleScattering = true
153
154
155 # Configuration of magnetic field
156 #================================
157     include "MagneticField/Engine/data/uniformMagneticField.cfi"
158     replace UniformMagneticFieldESProducer.ZFieldInTesla = 0
159     es_prefer = UniformMagneticFieldESProducer{}
160
161
162 # refitting for normal tracks...
163     include "RecoTracker/TrackProducer/data/RefitterWithMaterial.cff"
164     include "RecoTracker/TransientTrackingRecHit/data/TransientTrackingRecHitBuilderWithoutRefit/
          .cfi"
165     replace TrackRefitter.src = "AlignmentTracks" //"beamTrackproducer"
166     replace TrackRefitter.TrajectoryInEvent = true
167     replace TrackRefitter.TTRHBuilder = "WithoutRefit"# TransientTrackingRecHitBuilder: no refit/
            of hits...
168     replace ttrhbwor.Matcher = "StandardMatcher" # ... but with matching for strip stereo!
169
170 #     ...or new cosmic track reco for cosmics:
171 ##    include "Alignment/MillePedeAlignmentAlgorithm/test/AlignmentProducerFittingCosmics.cff"
172 ##    replace cosmictrackfinder.TrajInEvents=true # is already default?
173 #     include "RecoLocalTracker/Configuration/data/RecoLocalTracker.cff"
174 #     include "RecoTracker/Configuration/data/RecoTracker.cff"
175 #     include "RecoTracker/SingleTrackPattern/data/CosmicTrackFinderP5.cff"
176
177
178 # Specifying input file
179 #======================
180     source = PoolSource {
181         untracked vstring fileNames = {
182         # INSERTING POSITION FOR SOURCE FILES BY BASHSCRIPT
183
184         #"rfio:/castor/cern.ch/cms/store/trkalign/TIF/TIF-PASS3-SKIM-20070825/run00010215_1.root/
              "
```

```
185           #"rfio:/castor/cern.ch/cms/testbeam/TAC/TIFCosmicMC_13x/ScintillatorPositionC//
                  TIFCosmicMC_ConfC_1.root"
186           "rfio:/castor/cern.ch/cms/store/trkalign/TIF/TIF-PASS3-SKIM-20070825/run00010681_1.root"
187           }
188           untracked int32 maxEvents   = -1
189           untracked uint32 skipEvents = 0
190       }
191
192   path p = { AlignmentTracks, TrackRefitter }
193 }
```

Configuration in CMSSW v1.7.5

The job submisson is done by a bash script, that handles the insertion of reasonable logfile, output file, and source file names.

Listing B.3: Alignment/KalmanAlignmentAlgorithm/test/alignment.cfg

```
process Alignment = {
    # initialize  MessageLogger
    # include "FWCore/MessageLogger/data/MessageLogger.cfi"
    service = MessageLogger {
        # note: LOGFILE will be replaced by bash script
        untracked vstring destinations = { "LOGFILE" }# {, "cout" }
        untracked vstring statistics = { "LOGFILE" } #{, "cout" }
        untracked vstring categories = { "Alignment", "LogicError", "FwkReport", "TrackProducer"/
            }

        untracked PSet cout    = {
            untracked string threshold = "DEBUG" # "ERROR"
            untracked PSet FwkReport = {
                untracked string threshold = "INFO"
            }
            untracked PSet TrackProducer = {
                untracked string threshold = "INFO"
            }
            # untracked bool noLineBreaks = true
        }
        untracked PSet LOGFILE  = {
            untracked string threshold = "INFO"
            untracked PSet INFO = { untracked int32 limit = 10 }
            untracked PSet WARNING = { untracked int32 limit = 10 }
            untracked PSet ERROR = { untracked int32 limit = -1 }
            untracked PSet DEBUG = { untracked int32 limit = -1 }
            untracked PSet Alignment = { untracked int32 limit = -1}
            untracked PSet LogicError = { untracked int32 limit = -1}
            # untracked bool noLineBreaks = true
        }
    }


# Configuration of magnetic field
#=================================
#    include "MagneticField/Engine/data/volumeBasedMagneticField.cfi"
    include "MagneticField/Engine/data/uniformMagneticField.cfi"

    es_prefer magfield = XMLIdealGeometryESSource {}
    es_prefer = UniformMagneticFieldESProducer{}
    replace UniformMagneticFieldESProducer.ZFieldInTesla = 0.0


# ideal geometry and interface
    include "Geometry/CMSCommonData/data/cmsIdealGeometryXML.cfi"
    include "Geometry/TrackerNumberingBuilder/data/trackerNumberingGeometry.cfi"


# Track selection for alignment
#===============================
    include "Alignment/CommonAlignmentProducer/data/AlignmentTrackSelector.cfi"

    replace AlignmentTracks.src = ctfWithMaterialTracksTIF # cosmictrackfinderTIFTIBTOB

    # basic cuts for configuration C
    replace AlignmentTracks.applyBasicCuts = true
    replace AlignmentTracks.ptMin   = 0.0
    replace AlignmentTracks.ptMax   = 999.
    replace AlignmentTracks.etaMin  = -1.5 # -2.4
    replace AlignmentTracks.etaMax  =  0.6 #  2.4
    replace AlignmentTracks.phiMin  = -1.8 # -3.1415
    replace AlignmentTracks.phiMax  = -1.2 #  3.1415
    replace AlignmentTracks.nHitMin = 5
    #replace AlignmentTracks.nHitMin2D = 2
    replace AlignmentTracks.nHitMax = 99
    replace AlignmentTracks.chi2nMax= 4 # 999999.

    # min hits in TEC
    replace AlignmentTracks.minHitsPerSubDet.inTEC = 5

    # only one-track-events
    replace AlignmentTracks.applyMultiplicityFilter = true
    replace AlignmentTracks.minMultiplicity = 1
    replace AlignmentTracks.maxMultiplicity = 1
    replace AlignmentTracks.multiplicityOnInput = true


    # Alignment producer
    include "Alignment/CommonAlignmentProducer/data/AlignmentProducer.cff"
    #replace AlignmentProducer.applyDbAlignment = false #true
    #replace AlignmentProducer.tjTkAssociationMapTag = cosmictrackfinder # default is /
        TrackRefitter
    # MisalignmentScenarioSettings is a block from Scenario.cff from AlignmentProducer.cff:
    #replace MisalignmentScenarioSettings.setError = false # no APE!


    #PASS3 object
    #-------------
#// for normal reconstruction:
# replace TrackerDigiGeometryESModule.applyAlignment = true
```

```
#// running AlignmentProducer
 replace AlignmentProducer.applyDbAlignment = false

include "CondCore/DBCommon/data/CondDBSetup.cfi"

es_source trackerAlignment = PoolDBESSource {
    using CondDBSetup
    string connect="frontier://Frontier/CMS_COND_18X_ALIGNMENT"
    string timetype = "runnumber"
    VPSet toGet =
        {
            { string record = "TrackerAlignmentRcd"      string tag = "TIFpass4" },
            { string record = "TrackerAlignmentErrorRcd" string tag = "TIFpass4APE" }
        }
}

# To get APE=0  uncomment the following and comment
# the lines marked 'for APE' above.

#es_source setAPEtoZero = PoolDBESSource {
#   using CondDBSetup
#   VPSet toGet = {
#      { string record = "TrackerAlignmentErrorRcd"
#           string tag = "TrackerIdealGeometryErrors170" } # zero APE
#   }
#   string timetype = "runnumber"
#   string connect = "frontier://FrontierDev/CMS_COND_ALIGNMENT"
#}


# AlignmentProducer - Setting the Alignables
#=========================================
# First string: Specifies the alignable
#   Possible values for TEC: "TECDets", "TECPetals", "TECLayers", "TECs"
#
# Second string: determines which of the (rigid body) parameters are active,
#   the order is u, v, w, alpha, beta, gamma.
#   Other letters than 0 and 1 also select the parameter, but may be interpreted
#   in a special way, e.g. f and c in millepede.

    replace AlignmentProducer.ParameterBuilder.Selector = {
        vstring alignParams = {
            "TECLayers,000001,selTECplus"
#            "TECLayers,110001,selTECplus"
#            "TECLayers,010001,selTECplus"
#            "TECLayers,100001,selTECplus"
#            "TECLayers,111111,selTECplus"

#            "TECPetals,000001,selTECplus"
#            "TECPetals,010001,selTECplus"
#            "TECPetals,100001,selTECplus"
#            "TECPetals,110001,selTECplus"
        }
        PSet selTECplus = {
             vdouble etaRanges = {}
             vdouble rRanges = {}
             vdouble xRanges = {}
             vdouble yRanges = {}

             # disks 1 to 9
             vdouble zRanges = {0,300}

             # disks 1 to 7
             #vdouble zRanges = {0,230}

             # for debugging: disks 2, 3, 5, 6, 7, 8, 9
             #vdouble zRanges = {140, 175, 182, 300}

             # all sectors (for layer level alignment)
             vdouble phiRanges = {}

             # sector 2 and 3 (3pi/16, 11pi/16)
             #vdouble phiRanges = {0.5890, 2.1599}

             # sector 2 and 3, back petals (5pi/16, 7pi/16), (9pi/16, 11pi/16)
             #vdouble phiRanges = {0.9817, 1.3744, 1.7671, 2.1598}

             # sector 2 and 3, front petals (3pi/16, 5pi/16), (7pi/16, 9pi/16)
             #vdouble phiRanges = {0.5890, 0.9817, 1.3744, 1.7671}

             # sector 3, front petals
             #vdouble phiRanges = {1.3744, 1.7671}

             # sector 3, back petals (9pi/16, 11pi/16)
             #vdouble phiRanges = {1.7671, 2.1598}
        }
    }

    # Misalignment
    replace AlignmentProducer.doMisalignmentScenario =false #true


# Configuration of KalmanACAlignmentAlgorithm
#============================================
    replace AlignmentProducer.algoConfig = {
        using KalmanACAlignmentAlgorithm
    }
    include "Alignment/KalmanACAlignmentAlgorithm/data/KalmanACAlignmentAlgorithm.cfi"
    replace KalmanACAlignmentAlgorithm.fileDir = ""
    # note: ROOTFILE will be replaced by bash script
```

```
189     replace KalmanACAlignmentAlgorithm.alignmentFileName="ROOTFILE"
190     replace KalmanACAlignmentAlgorithm.skipInvalidHits=true
191     replace KalmanACAlignmentAlgorithm.minNumberOfHits = 5
192     replace KalmanACAlignmentAlgorithm.useMultipleScattering = true
193
194
195
196 # refitting for normal tracks...
197     include "RecoTracker/TrackProducer/data/RefitterWithMaterial.cff"
198     include "RecoTracker/TransientTrackingRecHit/data/TransientTrackingRecHitBuilderWithoutRefit/
          .cfi"
199     replace TrackRefitter.src = "AlignmentTracks" #"beamTrackproducer"
200     replace TrackRefitter.TrajectoryInEvent = true
201     replace TrackRefitter.TTRHBuilder = "WithoutRefit"# TransientTrackingRecHitBuilder: no refit/
          of hits...
202     replace ttrhbwor.Matcher = "StandardMatcher" # ... but with matching for strip stereo!
203
204
205 # Specifying input file
206 #======================
207     source = PoolSource {
208         untracked vstring fileNames = {
209         # INSERTING POSITION FOR SOURCE FILES BY BASHSCRIPT
210
211         # DO NOT USE UNLESS STAGE_SVCLASS=wan: "rfio:/castor/cern.ch/cms/store/trkalign/TIF/TIF-/
              MC/CMSSW_1_7_5/TIF-CONF_C-SKIM/mc-TIFconfC_1.root"
212         # DO NOT USE UNLESS STAGE_SVCLASS=cmscaf: "rfio:/castor/cern.ch/cms/store/cmscaf/alca//
              alignment/TIF/TIF-PASS4-SKIM-20080115/run_10681_1.root"
213         }
214         untracked uint32 skipEvents = -1
215     }
216     untracked PSet maxEvents = {untracked int32 input = -1}
217
218  path p = { AlignmentTracks, TrackRefitter }
219 }
```

Bibliography

[1] CMS Collaboration. The CMS experiment at the CERN LHC, 2008.

[2] CMS Collaboration. Muon Technical Design Report, CMS Technical Design Report 3. *CERN/LHCC 97-32*, 1997.

[3] CMS Collaboration. The Hadron Calorimeter, CMS Technical Design Report 2. *CERN/LHCC 97-31*, 1997.

[4] CMS Collaboration. CMS Electromagnetic Calorimeter, CMS Technical Design Report 4. *CERN/LHCC 97-33*, 1997.

[5] Richard Bremer né Brauer. *Integration of the End Cap TEC+ of the CMS Silicon Strip Tracker*. PhD thesis, RWTH Aachen University, 2008.

[6] M. Weber. Private communication.

[7] A. Ostaptchouk, S. Schael, R. Siedling, B. Wittmer. The Alignment System of the CMS Tracker. *CMS Note 2001/053*, 2001.

[8] CMS Collaboration. CMS High Level Trigger. *CERN/LHCC 2007-021*, 2007.

[9] CMS Collaboration. The Trigger Systems, CMS Technical Design Report 6.1. *CERN/LHCC 2000-38*, 2000.

[10] E. Widl, R. Frühwirth, W. Adam. A Kalman Filter for Track-based Alignment. *CMS Note 2006/022*, 2006.

[11] R. Frühwirt, T. Todorov, M. Winkler. Estimation of detector alignment parameters using the Kalman filter with annealing. *J. Phys. G: Nucl. Part. Phys.*, 029, 2003.

[12] G. Flucke, P. Schleper, G. Steinbrück, M. Stoye. A Study of Full Scale CMS Tracker Alignment using High Momentum Muons and Cosmics. *CMS Note 2008/008*, 2008.

[13] R. Barret et al. *Templates for the Solution of Linear Systems: Building Blocks for Iterative Methods*. Society for Industrial and Applied Mathematics, 1994.

[14] W.-M. Yao et al. Review of Particle Physics. *Journal of Physics G*, 33:1+, 2006.

[15] CMS Tracker Collaboration. Silicon Strip Tracker Detector Performance with Cosmic Ray Data at the Tracker Integration Facility. *CMS NOTE (in preparation)*, 2008.

[16] V. Innocente and D. Stickland. The design, implementation and deployment of a functional prototype OO reconstruction software for CMS. Proocedings of the conference on Computing in High Energy Physics (CHEP), Padova (Italy), 2000.

[17] C.-D. Jones et al. The New CMS Data Model and Framework. Proocedings of the conference on Computing in High Energy Physics (CHEP), Mumbai (India), 2006.

[18] R. Brun, F. Rademakers. ROOT - An Object Oriented Data Analysis Framework. Proceedings AIHENP'96 Workshop, Lausanne, Sep. 1996, Nucl. Inst. & Meth. in Phys. Res. A 389 (1997) 81-86. See also http://root.cern.ch/.

[19] C. Noeding. Track Reconstruction and Experience with Cosmic Ray Data in CMS. *CMS CR-2008/006*, 2008.

[20] W. Adam. Private communication.

[21] CMS Tracker Alignment Team. CMS Tracker Alignment at Integration Facility. *CMS NOTE (in preparation)*, 2008.

[22] B. Wittmer. Private communication.

[23] A. Ostaptchouk. Private communication.

[24] V. Karimäki, A. Heikkinen, T. Lampén, T. Linden. Sensor Alignment by Tracks. *arXiv:physics/0306034v2*, 2003.

[25] V. Karimäki, T. Lampén, F.-P. Schilling. The HIP Algorithm for Track Based Alignment and its Application to the CMS Pixel Detector. *CMS NOTE 2006/018*, 2008.

[26] V. Blobel. MillePede2 (Draft). http://www.desy.de/~blobel/mptalks.html, 2007.

[27] R. Castello. Private communication.

[28] CMS Collaboration. CMS Physics, Volume II: Physics Performance, CMS Technical Design Report 8.2. *CERN/LHCC/2006-021*, 2006.

Danksagung

Meinen herzlichen Dank möchte ich Prof. Dr. Lutz Feld für das Ermöglichen dieser Diplomarbeit aussprechen. Außerdem danke ich ihm für die gute Zusammenarbeit während des letzten Jahres und die Gelegenheit Zeit am CERN zu verbringen.

Weiterhin bedanke ich mich bei Prof. Dr. Stefan Schael dafür, dass er sich als Zweitkorrektor zur Verfügung gestellt hat.

Dr. Martin Weber hat viel Zeit für sehr hilfreiche Betreuung aufgewendet. Vielen Dank für die konstruktive Kritik an meiner Arbeit, das gründliche Korrekturlesen meines Manuskripts und das unermüdliche Kontern meiner Probleme mit ausgesprochen wertvollen Ratschlägen!

Darüber hinaus gilt mein Dank Martin, Matthias, Niklas und Richard, sowie den neuen Diplomanden, Albert und Klaus, für die produktive und doch ungezwungene Atmosphäre in unserem Büro (aka "RWTH KiTa"). Ihnen und Prof. Dr. Lutz Feld, Dr. Katja Klein, Rüdiger Jussen, Jennifer Merz und Jan Sammeth danke ich zudem für die Hilfsbereitschaft und angenehme Stimmung in der Arbeitsgruppe.

For providing feedback to results, answers to questions and help concerning problems especially with the CMS software framework, I would like to thank the CMS tracker alignment group. Especially Nhan Tran's help with the English language was very appreciated.

Many thanks to Roberto Castello, Andrei Ostaptchouk, and Bruno Wittmer, who offered results for comparison studies!

Bei meinen Mitbewohnern der "Alignment Villa", Matthias und Martin, möchte ich mich für das kurzweilige und unkomplizierte Zusammenleben in den letzten Monaten bedanken.

Meinen Freunden danke ich dafür, dass sie mir durch ihre Gesellschaft das Studium angenehmer gestaltet haben und mir halfen auch aus Schlechtem das Beste zu machen. Besonderer Dank gilt Jenni, Konstantin, Sebastian und speziell Matthias für gemeinsam bewältigte Übungen, Vorlesungen, Praktika, Klausuren und die vielen Diskussion über Physik und die Welt.

Der JuJutsu Hochschulsportgruppe möchte in meinen Dank für sportliche und gesellschaftliche Aktivitäten aussprechen, die während der letzten Jahre eine willkommene Abwechselung zur geistigen Arbeit des Studiums boten.

Meine Familie hat einen entscheidenden Beitrag zu meinem bisherigen Werdegang geleistet. Ich danke meinen Eltern, Ina und Bernd, die mir mit ihrer finanziellen Unterstützung das Physik-Studium ermöglicht haben, sowie meinen Brüdern, Christoph und Georg.

Erklärung

Hiermit versichere ich, dass ich die vorliegende Arbeit selbständig verfasst und keine anderen als die angegebenen Quellen und Hilfsmittel verwendet habe.

Aachen, den 29.07.2008